MOLECULAR MODELING OF POTENTIAL ANTI-TB AGENTS ACTIVE AGAINST *M.TUBERCULOSIS* INHA AND GYRB

NARUEDON PHUSI

A THESIS SUBMITTED IN PARTIAL FULFILLMENT OF THE REQUIREMENTS FOR THE DEGREE OF MASTER OF SCIENCE MAJOR IN CHEMISTRY FACULTY OF SCIENCE UBON RATCHATHANI UNIVERSITY ACADEMIC YEAR 2017

UBON RATCHATHANI UNIVERSITY

THESIS APPROVAL

MASTER OF SCIENCE

MAJOR IN CHEMISTRY FACULTY OF SCIENCE

TITLE MOLECULAR MODELING OF POTENTIAL ANTI-TB AGENTS ACTIVE AGAINST *M.TUBERCULOSIS* INHA AND GYRB

AUTHOR MR NARUEDON PHUSI

EXAMINATION COMMITTEE

ASST. PROF. DR. PATCHAREENART SAPARPAKORN	CHAIRPERSON
ASSOC. PROF. DR. PORNPAN PUNGPO	MEMBER
ASST. PROF. DR. CHAN INNTAM	MEMBER

ADVISOR Pornpan Pungpo .....

(ASSOC. PROF. DR. PORNPAN PUNGPO)

.....

(ASST. PROF. DR. CHARIDA PUKAHUTA)

DEAN, FACULTY OF SCIENCE

A. Pongrat .....

(ASSOC. PROF. DR. ARIYAPORN PONGRAT)

VICE PRESIDENT FOR ACADEMIC AFFAIRS

ACADEMIC YEAR 2017

ACKNOWLEDGEMENT

I would like to express my deepest gratitude to my advisor, Associate Professor Dr. Pornpan Pungpo for her continuous support, encouragement, and guidance throughout in my study from initial to the final level enable me to develop an understanding of the subject. I would like to thank my thesis committees, Assistant Professor Dr. Patchareenart Saparpakorn and Assistant Professor Dr. Chan Inntam for their helpful suggestion. I would like to thank Assistant Professor Dr. Auradee Punkvang, Dr. Pharit Kamsri and Miss Chayanin Hanwarinroj for their help and suggestion in a part of this project.

I would like to thank Center for Innovation in Chemistry (PERCH-CIC), Thailand Research Fund and Faculty of Science, Ubon Ratchathani University, are gratefully acknowledged for partially financial supports for the study. Furthermore, I would like to thank department of Chemistry, Faculty of Science, Ubon Ratchathani University, the Laboratory for Computational and Applied Chemistry (LCAC) at Kasetsart University, Centre for Computational Chemistry (CCC), School of Chemistry, University of Bristol, United Kingdom, the High Performance Computing Center of the National Electronics and Computer Technology (NECTEC) are gratefully acknowledged for computational resource and software facilities.

Finally, I would like to thank my family, who always love and understand whatever I am. They always encourage and unconditional support me throughout in my study.

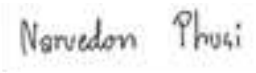

Naruedon Phusi

Researcher

บทคัดย่อ

เรื่อง : การจำลองแบบสารต้านโรควัณโรคที่มีศักยภาพในการยับยั้งเอนไซม์ *M. tuberculosis* InhA และ GyrB

ผู้วิจัย : นฤดล ภูศรี

ชื่อปริญญา : วิทยาศาสตรมหาบัณฑิต

สาขาวิชา : เคมี

อาจารย์ที่ปรึกษา : รองศาสตราจารย์ ดร.พรพรรณ พึ่งโพธิ์

คำสำคัญ : ตัวยับยั้งเอนไซม์ไอเอ็นเอชเอ, ตัวยับยั้งเอนไซม์จีวายอาร์บี, การคำนวณโมเลคิวลาร์ด๊อกกิ้ง, การจำลองแบบพลวัตเชิงโมเลกุล, การศึกษาความสัมพันธ์ระหว่างโครงสร้างกับค่ากัมมันตภาพในเชิงสามมิติ

ในงานวิจัยนี้ได้นำเอาระเบียบวิธีทางด้านการออกแบบโมเลกุลด้วยการคำนวณมาประยุกต์ใช้ในการศึกษาความต้องการทางโครงสร้างสารยับยั้งชนิดใหม่ที่มีศักยภาพสูงในการยับยั้งโรควัณโรค เอนไซม์เป้าหมายแรกคือ เอนไซม์อีโนอิลเอซีพีรีดักเตส หรือเอนไซม์ไอเอ็นเอชเอ ของเชื้อไมโคแบคทีเรียม ทูเบอร์คูโลซิส ซึ่งเป็นเอนไซม์เป้าหมายในการออกฤทธิ์ยับยั้งของตัวยาหลักในการรักษาโรควัณโรคอย่างยาไอโซไนอาซิด จากปัญหาการดื้อยาไอโซไนอาซิดที่เกิดจากการกลายพันธุ์ของเอนไซม์คะตะเลสเปอร์ออกซิเดส สารอนุพันธ์เฮทเทอโรเอริล เบนซาไมด์ ถูกพัฒนาเพื่อใช้เป็นสารยับยั้งเอนไซม์ไอเอ็นเอชเอโดยตรง ระเบียบวิธีการคำนวณโมเลคิวลาร์ด๊อกกิ้ง การจำลองแบบพลวัตเชิงโมเลกุล และการศึกษาความสัมพันธ์ระหว่างโครงสร้างกับค่ากัมมันตภาพในเชิงสามมิติถูกประยุกต์ใช้เพื่อศึกษาข้อมูลที่สำคัญของตัวยับยั้งเอนไซม์ไอเอ็นเอชเอ เพื่อพัฒนาและเพิ่มประสิทธิภาพในการยับยั้งเอนไซม์ไอเอ็นเอชเอของเชื้อไมโคแบคทีเรียม ทูเบอร์คูโลซิส เอนไซม์เป้าหมายที่สองคือ เอนไซม์ดีเอ็นเอไจเรส หน่วยย่อย บี หรือเอนไซม์จีวายอาร์บี ซึ่งเป็นเอนไซม์นี้ที่ทำหน้าที่ตัดและคลายเกลียวของสายดีเอ็นเอของเชื้อไมโคแบคทีเรียม ทูเบอร์คูโลซิสและพบว่ามีการดื้อยาที่รุนแรงในกลุ่มยาฟลูออโรควิโนโลนจากการกลายพันธุ์ของเอนไซม์จีวายอาร์บี การคำนวณโมเลคิวลาร์ด๊อกกิ้งและการจำลองแบบพลวัตเชิงโมเลกุลถูกประยุกต์ใช้ในการทำนายรูปแบบการจับและอันตรกิริยาที่เกิดขึ้นของสารอนุพันธ์ 4-อะมิโนควิโนลิน การศึกษาความสัมพันธ์ระหว่างโครงสร้างกับค่ากัมมันตภาพในเชิงสามมิติถูกใช้ในการศึกษาความต้องการทางโครงสร้างของสารอนุพันธ์ 4-อะมิโนควิโนลิน เพื่อออกแบบสารยับยั้งเอนไซม์จีวายอาร์บี ชนิดใหม่ที่มีศักยภาพในการยับยั้งสูง ดังนั้น ข้อมูลที่ได้จากการศึกษา ทำให้ทราบถึงรูปแบบการวางตัวในโพรงการจับของตัวยับยั้ง อันตรกิริยาที่สำคัญที่เกิดขึ้นในโพรงการจับและความต้องการทางโครงสร้างของสารอนุพันธ์เฮทเทอโรเอริล เบนซาไมด์ ที่เป็น

ตัวยับยั้งเอนไซม์ไอเอ็นเอชเอ และสารอนุพันธ์ 4-อะมิโนควิโนลิน ที่เป็นตัวยับยั้งเอนไซม์จีวายอาร์บี ซึ่งเป็นแนวทางในการออกแบบตัวยับยั้งเอนไซม์ไอเอ็นเอชเอ และตัวยับยั้งเอนไซม์จีวายอาร์บี มีศักยภาพสูงขึ้นและแก้ไขปัญหาในการดื้อยาของเชื้อไมโคแบคทีเรียม ทูเบอร์คูโลซิส

ABSTRACT

TITLE : MOLECULAR MODELING OF POTENTIAL ANTI-TB AGENTS ACTIVE AGAINST *M.TUBERCULOSIS* INHA AND GYRB
AUTHOR : NARUEDON PHUSI
DEGREE : MASTER OF SCIENCE
MAJOR : CHEMISTRY
ADVISOR : ASSOC. PROF. PORNPAN PUNGPO, Ph.D
KEYWORDS : INHA INHIBITOR, GYRB INHIBITOR, MOLECULAR DOCKING CALCULATIONS, MOLECULAR DYNAMICS SIMULATIONS, THREE DIMENSIONAL QUANTITATIVE STRUCTURE ACTIVITY RELATIONSHIP

In this research, computer aided molecular design (CAMD) approaches were applied to investigate the structural requirements of novel inhibitors as highly potent anti-tuberculosis. The first enzyme target, enoyl-ACP reductase (InhA) of *M. tuberculosis* has been shown to be the primary target of the isoniazid. Because of the isoniazid resistance associated with catalase-peroxidase mutations, heteroaryl benzamide derivatives were developed as the novel direct InhA inhibitors. Molecular docking calculations, molecular dynamics (MD) simulations and three dimensional quantitative structure activity relationships (3D-QSAR) were applied to elucidate the important information and develop more potent InhA inhibitor. The second enzyme target is DNA gyrase subunit B (GyrB). The function of this enzyme is causes supercoiling of DNA which relieves strain during the DNA unwinding for *M. tuberculosis*. The fluoroquinolone resistance arises from the mutations of GyrB enzyme. Molecular docking calculations and MD simulations were applied to predict binding mode and binding interactions of 4-aminoquinoline derivatives. 3D-QSAR studies were used to investigate the structural requirements of 4-aminoquinoline derivatives to rational design new potent GyrB inhibitors. Therefore, the important information from this study were applied to understand the binding mode of inhibitors in binding pocket, the crucial interactions of inhibitors in binding pocket and the structure requirements of heteroaryl benzamide derivatives as InhA inhibitors and

4-aminoquinoline derivatives as GyrB inhibitors provided guidelines for the design of new and more potent InhA and GyrB inhibitors, and solve drug resistant problem of *M. tuberculosis*.

CONTENTS

CONTENTS (CONTINUED)

LIST OF TABLES

LIST OF TABLES (CONTINUED)

LIST OF FIGURES

LIST OF FIGURES (CONTINUED)

LIST OF FIGURES (CONTINUED)

LIST OF FIGURES (CONTINUED)

FIGURES **PAGE**

LIST OF FIGURES (CONTINUED)

FIGURES **PAGE**

LIST OF ABBREVIATIONS

ABBREVIATIONS FULL WORDS

Å	Ångström
Ala	Alanine
Am	Amikacine
ASP	The Astex Statistical Potential
BTZ	1,3-benzothiazin-4-ones
CAMD	Computer Aided Molecular Design
Cfz	Clofazimine
Clr	Clarithromycin
Cm	Capreomycin
CoMFA	Comparative Molecular Field Analysis
CoMSIA	Comparative Molecular Similarity Index Analysis
CS	Cycloserine
CV	Cross-validation
E	Ethambutol
Eto	Ethionamide
FAS	Fatty acid synthase
FAS-I	Type I fatty acid synthase
FAS-II	Type II fatty acid synthase
fs	Femto second
GA	Genetic algorithm
Glu	Glutamine
Gly	Glycine
GOLD	Genetic Optimization for Ligand Docking
GyrB	Gyras subunit B
His	Histidine
IC_{50}	50% inhibitory concentration
Ile	Isoleucine

LIST OF ABBREVIATIONS (CONTINUED)

ABBREVIATIONS FULL WORDS

InhA	Enoyl-ACP reductase
Ipm	Imipenem
INH-NAD	Isonicotinic-acetyl-nicotinamide-adenine dinucleotide
INH	Isoniazid
K	Kelvin
KatG	Catalase peroxidase
kcal/mol	Kilocalories per mole
LBDD	Ligand based drug design
LCAO	Linear combination of atomic orbitals
Leu	Leucine
Lfx	Levofloxacin
LGA	Lamarckian genetic algorithm
LIE	Linear interaction energy
LOO	Leave-one-out
Lys	Lysine
Lzd	Linezolid
MD	Molecular dynamics
MDR-TB	Multidrug resistance tuberculosis
Met	Methionine
Mfx	Moxifloxacin
mg	Milligram
MIC	Minimum inhibitory concentration
MM	Molecular mechanics
MM-PBSA	Molecular Mechanics Poisson-Boltzmann Surface Area
MO	Molecular orbital
M. tuberculosis	*Mycobacterium tuberculosis*

LIST OF ABBREVIATIONS (CONTINUED)

ABBREVIATIONS FULL WORDS

M. tuberculosis $H_{37}R_v$	*Mycobacterium tuberculosis* strain $H_{37}R_v$
M. smegmatis	*Mycobacterium smegmatis*
Na^+	Sodium ion
NAD^+	Nicotinamide adenine dinucleotide
nM	Nanomolar
ns	nanosecond
µM	Micromolar
mM	Millimolar
Ofx	Ofloxacin
Pas	*para*-Aminosalicylic
PDB	Protein data bank
Phe	Phenylalanine
PLP	Piecewise linear potential
PLS	Partial least squares
PRESS	Prediction Error Sum of Squares
Pro	Proline
Pto	Protionamide
ps	Picosecond
QSAR	Quantitative Structure-Activity Relationship
R	Rifampicin
r^2	Non-cross-validated correlation coefficient
r_{cv}^2	Cross- validated correlation coefficient, predictive ability
RESP	Restrained electrostatic potential
RMSD	Root mean square deviations
S	Streptomycin

LIST OF ABBREVIATIONS (CONTINUED)

ABBREVIATIONS FULL WORDS

SBDD	Structure based drug design
SEE	Standard Error of Estimates
Ser	Serine
S_{PRESS}	The Standard of Error of Prediction
TB	Tuberculosis
TDR-TB	Totally drug resistant tuberculosis
Thr	Threonine
Thz	Thioacetazone
Trd	Terizidone
Tyr	Tyrosine
Val	Valine
WHO	World Health Organization
XDR-TB	Extensively drug resistant tuberculosis
ΔG_{Bind}	Binding Free Energies
3D-QSAR	Three-dimensional quantitative structure activity relationship

CHAPTER 1
INTRODUCTION

1.1 Tuberculosis

Tuberculosis (TB) is caused by *Mycobacterium tuberculosis* (*M. tuberculosis*) and has been a major problem for global health. In 2017, there were an estimated 10.4 million new TB patients worldwide, and the high mortality rate of TB is caused by its HIV co-infection as well as strong drug resistance of *M. tuberculosis* (WHO, 2017). TB is a chronic infectious disease which most commonly affects the lungs. However, the infection can spread via blood from the lungs to all organs in the body. This means that TB may also affect the bones, the urinary tract and sexual organs, the intestines and even the skin. When TB bacilli are inhaled, they rapidly pass through the mouth and nose and pass into the lowest and smallest parts of the airways. They move into the terminal bronchiole and alveoli of the lung. The terminal bronchioles are the smallest part of the bronchi, the structure that guides air from the upper airways (nose, mouth and trachea) into the lung tissue. Alveoli are part of the lung tissue and are the place where the oxygen from the inhaled air is usually used by the body, and transferred into the blood to be carried to the organs that need it. Pulmonary TB, or TB of the lungs, is the most common form of the disease. If the immune system is weak, the lymphocytes cannot contain the TB bacteria and it rapidly spreads. TB infection happens in 4 stages: the initial macrophage response, the growth stage, the immune control stage, and the lung cavitation stage. These four stages happen over roughly one month (Kenneth, 2018). Stage one, the first stage takes place in the first week after the inhalation of the TB bacillus. After the bacillus reaches the alveoli in the lung, it gets picked up by special cells of the immune system, called macrophages. These macrophages usually sit within the tissue of the alveoli; their duty is to swallow and inactivate any foreign object entering the alveolar space. The macrophages swallow the TB bacillus. The events that follow largely depend on the amount of TB bacilli and the strength of the macrophage. If the amount of TB bacilli is too large, or if the macrophage is not strong enough to resist, the bacilli can reproduce

in the macrophage. This ultimately leads to the destruction of the macrophage and the infection of new, nearby macrophages that try to swallow emerging TB bacilli. Stage two, if the macrophage cannot contain the TB bacillus, TB infection enters its second stage after about a week. The TB bacilli start reproducing exponentially, that mean for every initial bacillus two new ones emerge. These two then produce two each, etc. This leads to a rapid expansion of the initial TB bacillus, and the macrophages cannot contain the spread anymore. This stage lasts until the third week after initial infection. Stage three, after the third week, the bacilli do not grow exponentially anymore, and the infection enters its third stage it seems that at that stage, bacilli growth and destruction by macrophages are balanced. The body brings in more immune cells to stabilize the site, and the infection is under control. At least nine of ten patients infected with *M. tuberculosis* stop at stage 3 and do not develop symptoms or physical signs of active disease. The TB bacilli are shielded from the lung tissue; however, they can survive for years in the macrophages. Patients in this stage are not contagious, because the TB bacilli cannot enter the airways and cannot be coughed out or exhaled. If the immune system is strong, the primary complex heals and leaves nothing more but a small cavity and a scar in the tissue. This scar can later be seen on X-rays and is a sign that the person has had an infection with *M. tuberculosis*. Stage Four, in about 5% of cases, the primary complex does not heal and the TB bacilli become reactivated after a period of 12 to 24 months after the initial infection: this is stage 4 of the infection. The reactivated TB bacilli reproduce quickly and form a cavity in the tissue, where the body's immune system cannot reach them. From this cavity, the TB bacilli quickly spread through the tissue and the person develops signs and symptoms of active TB such as coughing. In this stage, the person is highly contagious because his or her sputum contains active TB bacteria. Reactivation is more likely to happen if the immune system is weakened, such as with HIV infection or malnutrition.

Reactivation TB results from proliferation of a previously dormant bacterium seeded at the time of the primary infection. Among individuals with latent infection and no underlying medical problems, reactivation disease occurs in 5 to 10 per cent (Comstock, 1982). Immunosuppression is associated with reactivation TB, although it is not clear what specific host factors maintain the infection in a latent state and what triggers the latent infection to become overt. For immunosuppressive conditions

associated with reactivation TB. The disease process in reactivation TB tends to be localized (in contrast to primary disease): there is little regional lymph node involvement and less caseation. The lesion typically occurs at the lung apices, and disseminated disease is unusual unless the host is severely immunosuppressed. It is generally believed that successfully contained latent TB confers protection against subsequent TB exposure.

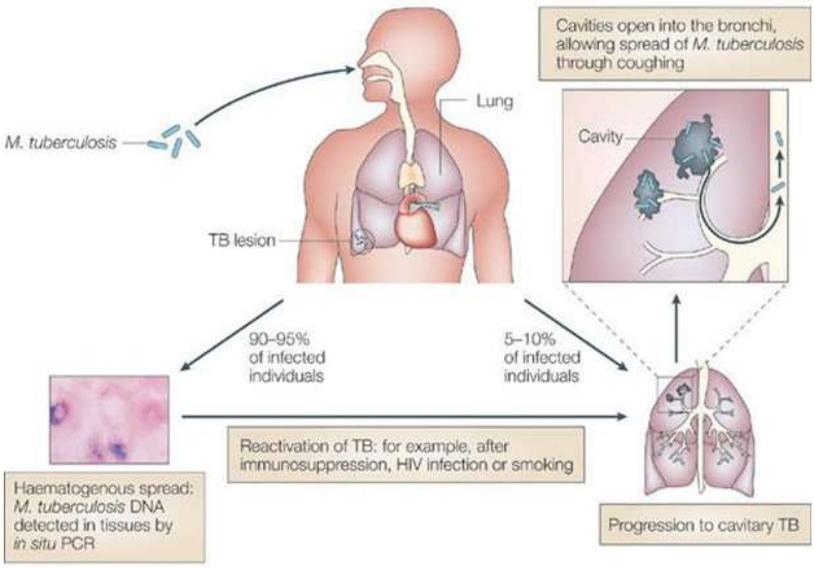

Figure 1.1 Pathophysiology of tuberculosis.

Source: Soolingen et al. (1997)

1.2 Tuberculosis drugs in current uses

Currently, anti-tuberculosis drugs are classified into two groups of first-line drugs and second-line drugs were shown in Figure 1.2 and Figure 1.3. There are 10 drugs approved by the United States Food and Drug Administration (FDA) including isoniazid (INH), rifampicin (R), rifapentine (Rpt), ethambutol (E), pyrazinamide (Z), cycloserine (Cs), ethionamide (Eth), p-aminosalicylic acid (Pas), streptomycin (S/Stm) and capreomycin (Cm) (Graham et al., 2005). Isoniazid, rifampin, ethambutol and pyrazinamide are considered first line anti-tuberculosis agents and form the core of initial treatment regimens. Rifabutin (Rfb) and rifapentine may also be considered first-line agents under the specific situations such as drug intolerance or resistance.

Streptomycin was formerly considered to be a first-line agent and is still used in initial treatment in some instances. However, an increasing prevalence of resistance to Stm in many parts of the world has decreased its overall usefulness. All approved second-line drugs and all not approved drugs are used relatively commonly to treat tuberculosis caused by drug-resistant organisms or for patients who are intolerant of some of the first-line drugs.

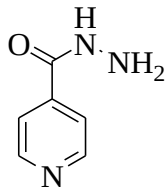

Isoniazid

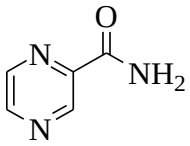

Pyrazinamide

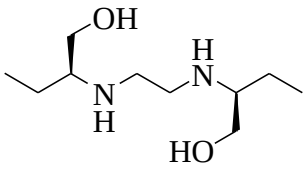

Ethambutol

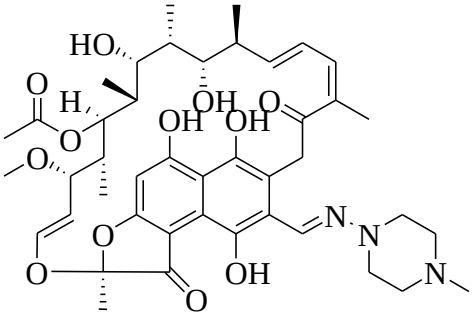

Rifampicin

Figure 1.2 First-line anti-TB agents.

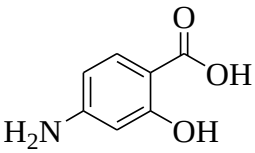

Para-amino salicylic acid

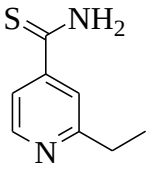

Ethionamide

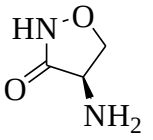

Cycloserine

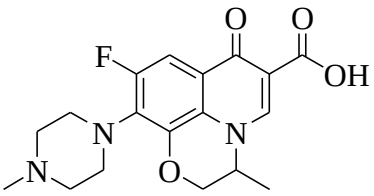

Ofloxacin

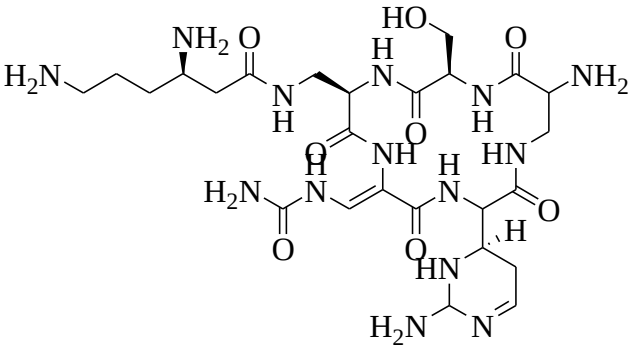

Capreomycin

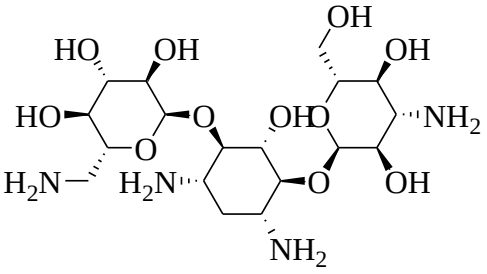

Kanamycin

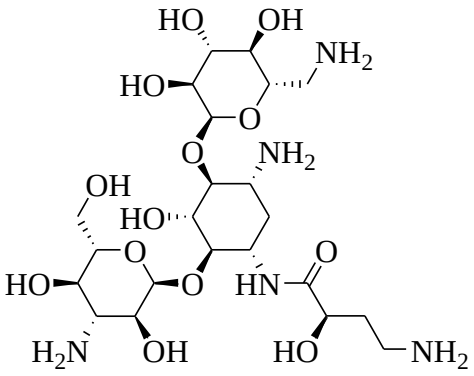

Amikacin

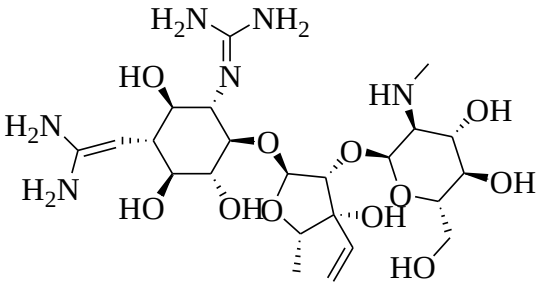

Streptomycin

Figure 1.3 Second-line anti-TB agents.

1.3 The treatment and problem of tuberculosis treatment

The goals of tuberculosis treatment are to ensure cure without relapse, to prevent death, to stop transmission and to prevent the emergence of drug resistance. To accomplish these goals, long-term treatment with a combination of drugs is required. The new World Health Organization (WHO) guideline for the treatment on tuberculosis is reported in Table 1.1 (WHO, 2010). Major progress in global TB control follows the wide spread implementation of directly observed treatment (DOTs) strategy. DOT in which a trained observer personally observes each dose of medication being swallowed by the patient can ensure high rates of treatment completion reduce development of acquired drug resistance and prevent relapse. People living with HIV are 20 to 30 times more likely to develop active TB disease than people without HIV. HIV and TB form a lethal combination, each speeding the other's progress. 0.4 million people died of HIV-associated TB. About 40% of deaths among HIV-positive people were due to TB. There were an estimated 1.4 million new cases of TB amongst people who were HIV-positive, 74% of whom were living in Africa. WHO recommends a 12-component approach of collaborative TB-HIV activities, including actions for prevention and treatment of infection and disease, to reduce deaths.

Anti-TB medicines have been used for decades and strains that are resistant to 1 or more of the medicines have been documented in every country surveyed. Drug resistance emerges when anti-TB medicines are used inappropriately, through incorrect prescription by health care providers, poor quality drugs, and patients stopping treatment prematurely. Multidrug-resistant tuberculosis (MDR-TB) is a form of TB caused by bacteria that do not respond to isoniazid and rifampicin, the 2 most powerful, first-line anti-TB drugs (Raviglione and Uplekar, 2006). MDR-TB is treatable and curable by using second-line drugs. However, second-line treatment options are limited and require extensive chemotherapy (up to 2 years of treatment) with medicines that are expensive and toxic. In some cases, more severe drug resistance can develop. Extensively drug-resistant TB (XDR-TB) is a more serious form of MDR-TB caused by bacteria that do not respond to the most effective second-line anti-TB drugs, often leaving patients without any further treatment options. MDR-TB remains a public health crisis and a health security threat. WHO estimates that there were 600,000 new cases with resistance to rifampicin the most effective

first-line drug of which 490,000 had MDR-TB. The MDR-TB burden largely falls on 3 countries; India, China and the Russian Federation which together account for nearly half of the global cases. About 6.2% of MDR-TB cases had XDR-TB. Worldwide, only 54% of MDR-TB patients and 30% of XDR-TB are currently successfully treated. WHO approved the use of a short, standardised regimen for MDR-TB patients who do not have strains that are resistant to second-line TB medicines. This regimen takes 9-12 months and is much less expensive than the conventional treatment for MDR-TB, which can take up to 2 years. Patients with XDR-TB or resistance to second-line anti-TB drugs cannot use this regimen, however, and need to be put on longer MDR-TB regimens to which 1 of the new drugs (bedquiline and delamanid) may be added (Ahmad, Sharma, and Khuller, 2005; Ahmad et al., 2006; Ahmad, Sharma and Khuller, 2006; Ahmad, Sharma and Khuller, 2006).

Table 1.1 Groups of drugs to treatment tuberculosis

Group	Drugs (abbreviations)
Group 1: First-line oral agents	- pyrazinamide (Z) - ethambutol (E) - rifabutin (Rfb)
Group 2: Injectable agents	- amikacin (Am) - capreomycin (Cm) - streptomycin (S)
Group 3	- levofloxacin (Lfx) - moxifloxacin (Mfx) - ofloxacin (Ofx)

Table 1.1 Groups of drugs to treatment tuberculosis (Continued)

Group	Drugs (abbreviations)
Group 4: Oral bacteriostatic second-line agents	- para-aminosalicylic acid (Pas) - cycloserine (Cs) - terizidone (Trd) - ethionamide (Eto) - protionamide (Pto)
Group 5: Agents with unclear role in treatment of drug resistant-TB	- clofazimine (Cfz) - linezolid (Lzd) - amoxicillin/clavulanate (Amx/Clv) - thioacetazone (Thz) - imipenem/cilastatin (lpm/Cln) - high-dose isoniazid (high-dose H)b - clarithromycin (Clr)

1.4 *Mycobacterium tuberculosis* InhA inhibitors

A 2-trans-enoyl acyl-carrier-protein (ACP) reductase (InhA) of *M. tuberculosis* was shown to be a primary target of the isoniazid frontline drugs, had been discovered in 1952 (Rozwarski et al., 1998; Mario et al., 2007). It took more than 50 years of investigations to uncover its mechanism of action. However, the high levels of isoniazid (INH) resistance of InhA arise from the mutations in both InhA and catalase-peroxidase (KatG) enzymes. The *M. tuberculosis* InhA catalyzes the nicotinamide adenine dinucleotide (NAD^+)-specific reduction of the 2-trans-enoyl-ACP in the elongation cycle of the fatty acid synthase (FAS)-II pathway as shone in Figure 1.4. This enzyme is NAD^+-specific and reduces the trans double bond between the positions C2 and C3 of a fatty acyl chain linked to the acyl carrier protein (Annaik et al., 1996). Especially, InhA has been identified as a target of the most effective first-line drugs (De and Morbidoni, 2006). INH is a prodrug requiring the activation function of catalase-peroxidase (KatG) to generate the isonicotinoyl radical as shown in Figure 1.5 (Saint-Joanis et al., 1999; Lei, Wei and Tu, 2000). The isonicotinoyl radical generated from the activation process then forms a covalent adducts with NAD^+ to generate INH-

NAD adduct, a potent inhibitor of InhA (Zhao et al., 2006). Based on inhibition mechanism, isoniazid could be called as an indirect inhibitor of InhA. To simplify the drug design process and elucidate the mechanism of an InhA reaction, the characterization of the key interactions and structural requirements of the active site of InhA is underway now. However, high potency of INH for the TB treatment was reduced by drug resistance, which is caused from the mutations in KatG enzymes (Rozwarski et al., 1999; Baulard et al., 2000; Ramaswamy et al., 2003). To overcome the drug resistance against INH, new derivatives, which directly inhibit the InhA enzyme without affecting on the activation by KatG, are expected to be promising agents against TB (Kai and Peter, 1994).

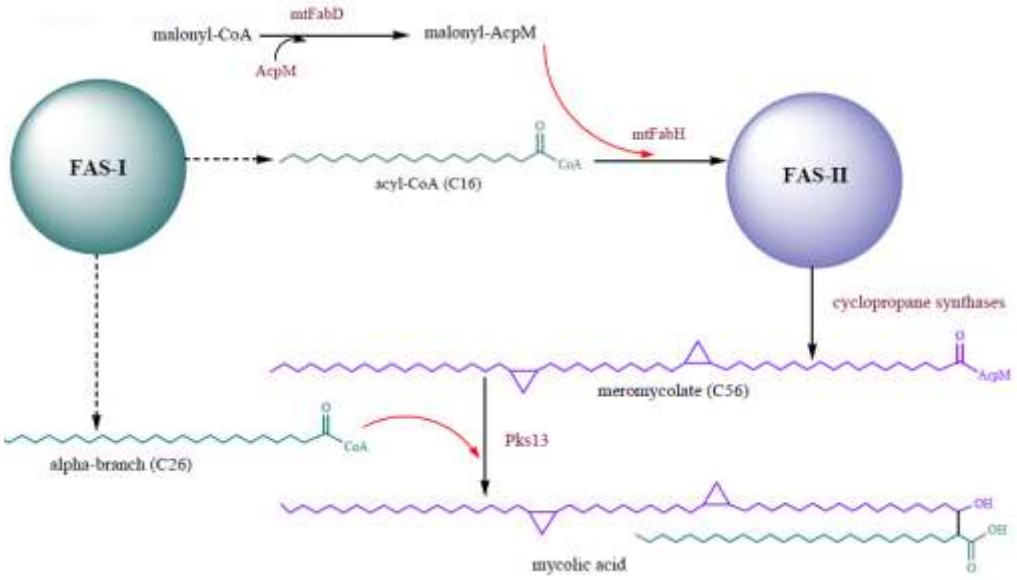

Figure 1.4 Fatty acid/mycolic acid biosynthesis in mycobacteria.

Source: Punkvang (2010)

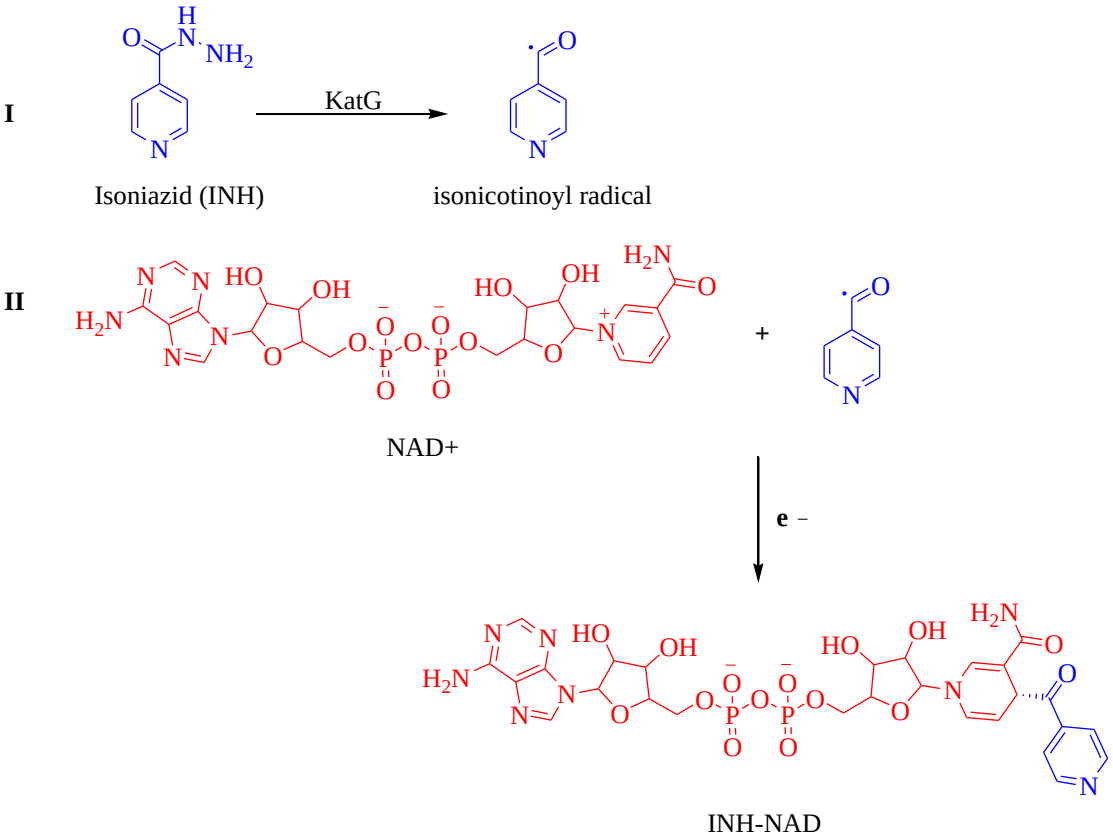

Figure 1.5 Formation of INH-NAD adduct, a potent inhibitor of InhA.

Direct InhA Inhibitors

The major mechanism of INH resistance arises from mutations in KatG (Banerjee et al., 1994; De La Iglesia and Morbidoni, 2006). To overcome the INH resistance associated with mutations in KatG, compounds which directly inhibit the InhA enzyme without requiring activation of KatG called direct InhA inhibitors are new promising agents against tuberculosis. Because of the remarkable properties of direct InhA inhibitors, many research groups have been attempting to develop direct InhA inhibitors, triclosan was reported as the first direct InhA inhibitors at the acyl substrate-binding pocket (Freundlich et al., 2009). The first generation of alkyl substituted diphenyl ether was prepared to improve affinity towards InhA (Boyne et al., 2007; am Ende et al., 2008). Pyrrolidine carboxamide derivatives (Sullivan et al., 2006) and similar high-throughput experimental design published led to arylamide derivatives is a novel direct InhA inhibitors (He, X. et al., 2006; He, Alian and Ortiz de Montellano, 2007). 2-(4-oxoquinazolin-3(4H)-yl)acetamide derivatives and

benzo[d]oxazol-2(3H)-one derivatives were identified from virtual screening followed by biological evaluation (Ganesh et al., 2014; Ganesh et al., 2014). N-Benzyl-4-((heteroaryl)methyl) benzamide derivatives were identified by high throughput screening against InhA (Guardia et al., 2016). The specificity is determined by a loop of the binding region of InhA, called the substrate-binding loop, which has been shown to be flexible (Rozwarski et al., 1998; Kuo et al., 2003). Superposition of the crystal structure of *Escherichia coli* (*E. coli*) FabI (ecFabI) with InhA demonstrates that there is a significant difference between these two enzyme with respect to the location of their substrate-binding loops. In InhA, the loop creates a substance-binding crevice with more depth than loop of ecFabI. The intrinsic specificity observed in the substrate-binding loop is consistent with the size and shape of the conserved hydrophobic pocket adjacent to the active site of InhA (Lu, Huang and You, 2011).

1.5 *Mycobacterium tuberculosis* GyrB inhibitor

The clinical efficacy of fluoroquinolone drugs demonstrated over the past 20-30 years has validated DNA gyrase as a target in the area of broad-spectrum antibacterials (Zhao et al., 1999). Gyrase A subunit, GyrA has been facing a major hurdle of their resistance developed by *M. tuberculosis* which makes gyrase B subunit a drug able target for discovery of potent anti-tuberculosis agents. DNA gyrase (topoisomerase type II) of *M. tuberculosis* can be an attractive target in this prospect due to the uniqueness of the *M. tuberculosis* genome which codes for only two types of topoisomerases (type I and II) unlike other pathogens. DNA gyrase, a crucial enzyme, causes negative supercoiling of DNA which relieves strain during the DNA unwinding (Medapi et al., 2015). Functional DNA gyrase usually exists as a heterotetramer (A_2B_2) with two A subunits and two B subunits (Jeankumar et al., 2016). Fluoroquinolones which target gyrase A subunit have been facing a major hurdle of their resistance developed by *M. tuberculosis* which makes gyrase B subunit a druggable target for discovery of potent anti-tubercular agents. DNA gyrase B subunit is involved in the process of ATP hydrolysis which in turn provides energy to gyrase A subunit for maintaining the DNA topological state. Novobiocin and coumermycin are the reported *M. tuberculosis* GyrB inhibitors.

DNA gyrase is unique among the topoisomerase family in being the only enzyme capable of catalyzing the negative supercoiling of DNA. It has been suggested that a negative supercoiling activity exists within *Xenopus* oocytes (Ryoji and Worcel; 1984; Glikin, Ruberti and Worcel, 1984), but these reports have not been substantiated with further evidence. Recently, a factor from the posterior silk gland of *Bombyx mori* has been described that is thought to complement eukaryotic topoisomerase II to produce a supercoiling activity (Ohta and Hirose, 1990); this factor is required in considerable molar excess over the DNA before the supercoiling reaction can be observed. It is not clear how supercoiling is achieved by this factor, but one proposal is that it may dictate the coiling of DNA around topoisomerase II (Ohta and Hirose, 1990). It is likely that the observations of these activities in eukaryote cells represent "passive" supercoiling, as distinct from the active supercoiling of DNA gyrase.

All topoisomerase reactions involve the binding of the protein to DNA, DNA cleavage, strand passage, DNA reunion, and in a number of cases ATP hydrolysis, and the enzymes are likely to share a similar mechanism of action to gyrase (Maxwell and Gellert, 1986). Although DNA gyrase conforms to the general topoisomerase mechanism, it must also possess unique mechanistic features that determine its ability to actively supercoil DNA. The observed reactions of DNA gyrase are listed below:

(1) ATP-dependent negative supercoiling of closed-circular double-stranded DNA
(2) ATP-independent relaxation of negatively supercoiled DNA
(3) Nucleotide-dependent relaxation of positively supercoiled DNA
(4) Formation and resolution of catenated DNA
(5) Resolution of knotted DNA
(6) Quinolone or calcium ion-induced double stranded breakage of DNA
(7) DNA-dependent ATP hydrolysis

It is likely that each of the above reactions is an aspect of a single reaction mechanism occurring with different substrates, or under different conditions. Therefore, we shall consider the mechanism of the negative supercoiling reaction by gyrase (about which most is known) and attempt to explain the other reactions in terms of this mechanism. DNA gyrase B subunit, GyrB is involved in the process of ATP hydrolysis

which in turn provides energy to gyrase A subunit for maintaining the DNA topological state (White, Cozzarelli and Bauer, 1988). So, GyrB has been genetically demonstrated to be a bactericidal drug target in *M. tuberculosis*, but there have not been any effective therapeutics developed against this target for TB (Richard and Anthony, 1991).

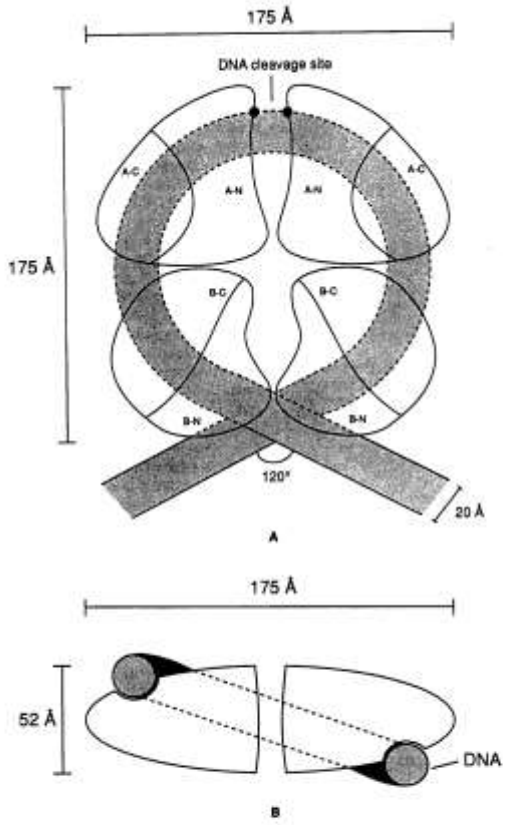

Figure 1.6 Proposed structure of the DNA gyrase-DNA complex. (A) The DNA is shown as a shaded loop wrapped around the A and B subunits. The A proteins are in the upper part of the model and the B proteins in the lower. - N and - C indicate the amino- and carboy terminal domains of the proteins. The black dots represent the sites of covalent attachment between the enzyme and the DNA. (B) A transverse section of the model indicating the DNA around the protein complex.

Source: Rhoda and Mug (1980)

Figure 1.6 shows a proposed model of the gyrase-DNA complex. It is based on those of Kirchhausen, et al. (Kirchhausen, Wang and Harrison, 1985) and Krueger, et al. (Krueger et al., 1990) and can be regarded as an update of those earlier models. This model is intended to emphasize certain features of the gyrase-DNA complex: the wrapping of DNA around the protein, the presence of solvent-filled channels, and the possible domain organization. It can be regarded as a slice through the center of the oblate particle; no significance should necessarily be attached to the shapes of the A and B subunits in this model.

In the gyrase-DNA complex about 120 bp of DNA are wrapped around the protein. The DNA entry and exit points are located close together, and the DNA tails are thought to be at an angle of 120° (Rau et al., 1987). A 120-bp segment of B-form DNA should have a length of approximately 410 Å. If assume that the DNA is smoothly wrapped around gyrase, then the diameter of the resulting circle, at the outside edge of the DNA, will be about 150 Å. The size of the gyrase particle has been estimated to be 175 Å by 52 Å (Lebeau et al., 1990). Therefore, the DNA is likely to be embedded into the protein structure, which will extend beyond the wrapped DNA. The shape of the subunits shown is arbitrary, but the B protein has been drawn as bean shaped, as suggested by Lebeau, et a1. (Shen, Baranowski and Pernet, 1989).

The N-terminal two thirds of the A protein has been shown to be involved in the cleavage and reunion of DNA is capable of interacting with the B protein and has the ability to dimerize (our unpublished observations). The C-terminal third of the molecule seems able to contribute to the stability of the DNA-protein complex (Brown, Peebles and Cozzarelli, 1979). The N-terminal half of the B protein possesses an ATPase activity, and is probably able to form dirners, while the C-terminal half of the protein interacts with both the A protein and with DNA (Gellert, Fisher, and O'Dea, 1979; Abdel-Meguid, Murthy and Steitz, 1986). Both electric dichroism and small-angle neutron scattering data have suggested that gyrase contains cavities or channels within its structure that could be around 15 Å wide (Rau et al., 1987; Abdel-Meguid, Murthy and Steitz, 1986). These have been represented in Figure 1.6 as inter subunit channels. Such structures would provide a route for the trans located DNA to pass through the protein structure.

Recently, thiazol-aminopiperidine derivatives was a new class of compounds that target selectively the mycobacterial DNA gyrase enzyme with promising attributes of synthetic accessibility and anti-tuberculosis activity. (Variam et al., 2013). Benzofuran derivatives and benzo[*d*]isothiazole derivatives were identified by high throughput screening against GyrB (Kummetha et al., 2014). Aminopiperidine derivatives were identified from virtual screening followed by biological evaluation (Variam et al., 2014), 2-amino-5-phenylthiophene-3-carboxamide derivatives was found to be the most active compound with IC_{50} of 0.86 µM in *M. smegmatis* GyrB as well as *M. tuberculosis* supercoiling IC_{50} of 0.76 µM. The compound also inhibited drug sensitive *M. tuberculosis* with MIC of 4.84 µM and was non-cytotoxic at 100 µM. Though this derivatives is showing good activity in *M. tuberculosis* GyrB, so it would be a potential lead for rational drug design against *M. tuberculosis* from pharmaceutical point of view (Shalini et al.,2015). Carboxamide derivatives and hydroxamic acid derivatives were novel structural class of DNA gyrase inhibitors provides valuable information for the discovery of improved DNA gyrase B inhibitors (Ziga et al., 2017). 4,5-dibromo-N-(thiazol-2-yl)-1H-pyrrole-2-carboxamide derivatives was novel structural class of DNA gyrase inhibitors provides valuable information for the discovery of improved DNA gyrase B inhibitors (Tihomir et al., 2017). Aminopyrazinamides derivatives were a novel class of inhibitors, aminopyrazinamides, which target the mycobacterial GyrB ATPase with chemical tractability and potent anti-tuberculosis activity (Pravin et al., 2013).

4-aminoquinoline derivatives were selected in this study. These compounds show high potency for inhibit the GyrB enzyme. The highest GyrB inhibitory activity with IC_{50} of 0.86 µM could be observed. On the other hand it has to be taken into account that the majority of 4-aminoquinoline derivatives exhibit a lower *M. tuberculosis* growth inhibition with IC_{50} against *M. tuberculosis* strain above values below 1 µM against *M. tuberculosis* GyrB and were found to be non-cytotoxic at 50 µM concentration. However, it can be reasonably assumed that these compounds are extruded out of the bacterial cell by efflux pumps. The above given data, especially the GyrB inhibitor property of 4-aminoquinoline derivatives justifies a more detailed examination of the structural basis to improve antimycobacterial activity (Medapi et al., 2015).

1.6 Computational approaches for development for anti-tuberculosis agents

Computer-aided molecular design approaches (CAMD) are becoming useful tools for developing novel and more potent anti-tuberculosis agents. This approach can divide into two approaches including structure based drug design and ligand based drug design. In this study, structure based drug design approach molecular docking calculations and molecular dynamic simulations have been applied to elucidate the potential binding modes and binding interactions of *M. tuberculosis* InhA inhibitors and GyrB inhibitors. Moreover, ligand based drug design approach QSAR CoMSIA studies was performed to investigate the structural requirements of InhA inhibitors and GyrB inhibitors. Therefore, the obtained results should aid in the rational design new compounds of *M. tuberculosis* InhA inhibitors and GyrB inhibitors with more potent anti-tuberculosis activity.

1.7 Objectives

In this work, computer-aided molecular design approaches have been applied to elucidate anti-tuberculosis agents targeting *M. tuberculosis* InhA inhibitors and GyrB inhibitors with the aim

1.7.1 To investigate binding mode and important interactions of heteroaryl benzamides derivatives in InhA binding pocket using molecular docking calculations.

1.7.2 To elucidate dynamic behavior, binding energy and crucial interactions of heteroaryl benzamides derivatives using molecular dynamics simulations.

1.7.3 To investigate the structural requirements of heteroaryl benzamides derivatives using 3D-QSAR CoMSIA approach.

1.7.4 To obtain structural requirements of heteroaryl benzamides derivatives based on the integrated results from molecular dynamics simulations and 3D-QSAR CoMSIA model.

1.7.5 To evaluate binding mode and important interactions of 4-aminoquinoline derivatives in GyrB binding pocket using molecular docking calculations.

1.7.6 To gain insight into crucial interactions of 4-aminoquinoline derivatives using molecular dynamics simulations.

1.7.7 To investigate the structural requirements of 4-aminoquinoline derivatives using 3D-QSAR CoMSIA approach.

1.7.8 To obtain structural requirements of 4-aminoquinoline derivatives based on the integrated results from molecular dynamics simulations and 3D-QSAR CoMSIA model.

CHAPTER 2
LITTERATURE REVIEWS

2.1 Molecular modeling for anti-tuberculosis agents

Nayyar, A. et al. (2006) performed synthesis, evaluation of anti-tuberculosis activity, and 3D-QSAR study of ring-substituted-2/4-quinolinecarbaldehyde derivatives. The study resulted in the identification of compounds **4a**, **7c**, and **8a** as promising inhibitors of *M. tuberculosis*. It is also clear that placement of a fluorine and its inductive and resonance effects on the basicity of ring-substituted quinolines led to a significant change in biological activity. All compounds were synthesized in good yield using inexpensive starting materials in 1–2 overall steps thereby indicating their importance as the lead compounds in anti-tuberculosis drug discovery and development due to the poor demographic profile of the TB-patients. In an attempt to understand the essential structural requirements for anti-tuberculosis activity. Molecular modeling studies have thrown some insight into the observed SAR profile. For the present quinoline dataset, the similarity index based on electrostatic and steric features of the molecules combined with PCA and SDA are able to classify them as active or inactive within the limits of statistical significance. This strategy represents a promising approach for the discovery and development of the new ring-substituted quinoline compounds effective for the treatment of TB.

Coutinhob, E. et al. (2006) investigated the 3D-QSAR study of ring-substituted quinoline class of anti-tuberculosis agents. The result indicated that 3D-QSAR analysis of a novel class of anti-tuberculosis agents was carried out using CoMFA alone, CoMFA in conjunction with a hydrophobic field evaluated using HINT and CoMSIA, to map the structural features contributing to the inhibitory activity of these molecules. Inclusion of the HINT hydropathic field to the CoMFA models does not improve the quality of the models. The CoMSIA models are comparable to the CoMFA model but lack good predictive power. The database alignment of molecules produced models with better statistics than those with field fit alignment. Out of the various models evaluated, the CoMFA model based on database alignment produced a

statistically sound model with a good correlation and predictive power. Analysis of the CoMFA contours provide detail on the fine relationship linking structure and activity, and provide clues for structural modifications that can improve the activity. This study also discloses several new derivatives of quinolines with activity higher than that of the molecules in this study. Attempts are currently underway in our laboratory to synthesize and evaluate the anti-tuberculosis activities of the newly proposed structures.

Wahab, H. A. et al. (2008) performed molecular docking and MD simulation to study the binding of isoniazid onto the active site of InhA of *M. tuberculosis* in an attempt to address the mycobacterial resistance against isoniazid. The results show that isonicotinic acyl-NADH (INH-NAD) has an extremely high binding affinity toward the wild type InhA by forming stronger interactions compared to the parent drug (isoniazid) (INH). Due to the increase of hydrophobicity and reduction in the side chain's volume of **A94** of mutant type InhA, both INH-NAD and the mutated protein become more mobile. Due to this reason, the molecular interactions of INH-NAD with mutant type are weaker than that observed with the wild type. However, the reduced interaction caused by the fluctuation of INH-NAD and the mutant protein only inflected minor resistance in the mutant strain as inferred from free energy calculation. MD results also showed there exists a water-mediated hydrogen bond between INH-NAD and InhA. However, the bridged water molecule is only present in the INH-NAD-wild type complex reflecting the putative role of the water molecule in the binding of INH-NAD to the wild type protein. The results support the assumption that the conversion of prodrug isoniazid into its active form INH-NAD is mediated by KatG as a necessary step prior to target binding on InhA. Our findings also contribute to a better understanding of INH resistance in mutant type.

Xiao-Yun, L. et al. (2009) performed develops an efficient approach for discovering new InhA direct inhibitors in theory. The InhA bound conformation of a pyrrolidine carboxamide inhibitor was used to build a pharmacophore model. This model with feature-shape query was successfully used to identify and align the bioactive conformations of pyrrolidine carboxamide analogues and screen SPECS database. A statistically valid 3D-QSAR with good results (r^2_{cv} = 0.66 and r^2 = 0.96) was obtained. From database screening, 30 hits were selected and identified as

potential leads, which exhibit good estimated activities by 3D-QSAR model. Docking studies were carried out on two representative hits to analyze their interactions with InhA. Also, the interactions between existing pyrazole inhibitors and InhA were explored based on the pharmacophore model.

Patrice, L. J. et al. (2009) applied 3D-QSAR studies CoMFA and CoMSIA were carried out on 26 structurally diverse subcutaneous pentylenetetrazol (scPTZ) active enaminone analogues, previously synthesized in our laboratory. CoMFA and CoMSIA were employed to generate models to define the specific structural and electrostatic features essential for enhanced binding to the putative GABA receptor. The 3D-QSAR models demonstrated a reliable ability to predict the CLogP of the active anticonvulsant enaminones, resulting in a q^2 of 0.56 for CoMFA, and a q^2 of 0.70 for CoMSIA. The outcomes from the contour maps have provided insight for the design of a novel series of anticonvulsant agents that will have greater activity by identifying significant regions for steric, electrostatic, hydrophobic, hydrogen bond donor and hydrogen bond acceptor interactions. The outcomes of the contour maps for both models provide detailed insight for the structural design of novel enaminone derivatives as potential anticonvulsant agents.

Punkvang, A. et. al. (2010) applied molecular docking calculations and QSAR approaches to find a sound binding conformation for the different arylamide analogs. The results thus obtained are perfectly consistent (rmsd = 0.73 Å) with the results from X-ray analysis. A thorough investigation of the arylamide binding modes with InhA provided ample information about structural requirements for appropriate inhibitor-enzyme interactions. Three different QSAR models were established using two three-dimensional (CoMFA and CoMSIA) and one two-dimensional (HQSAR) techniques. With statistically ensured models, the QSAR results obtained had high correlation coefficients between molecular structure properties of **28** arylamide derivatives and their biological activity. Molecular fragment contributions to the biological activity of arylamides could be obtained from the HQSAR model. Finally, a graphic interpretation designed in different contour maps provided coincident information about the ligand–receptor interaction thus offering guidelines for syntheses of novel analogs with enhanced biological activity.

Krishna, K. M. et al. (2014) performed 1,2,4-triazole derivatives comprising of diphenyl amine moiety were synthesized and evaluated for *in vitro* anti-tuberculosis activity against *M. tuberculosis* H_{37}Rv. The Mannich bases **4a**, **4d** and **4e** were found to be the most potent molecules with MIC value in the range of 0.20-3.12 µM. The cytotoxicity analysis of the most active compounds have carried out by MTT assay for Vero and HepG2 cell lines, none of the tested compounds were found toxic. Hence, activities of the tested compounds were not due to cytotoxicity. All the compounds were subjected for CoMFA and CoMSIA analysis to understand the structural requirement for anti-tubercular activity. The Mannich bases **4a-l** were relatively more active than the triazolothiazolidinones **5a-f** and triazoloquinazolines **6a-f**. The significant anti-tubercular activity of Mannich bases **4a-l** may be due to the presence of the structural resemblance with the lead compound triclosan. The hydrogen bond acceptor like morpholino group and the bulker aryl imino group on 4^{th} nitrogen of the triazole can be considered essential for the anti-tuberculosis activity. Both CoMFA (q^2= 0.43, r^2= 0.90) and CoMSIA (q^2= 0.51, r^2= 0.95) models have good internal and external validation results when studied along with Polar Surface Area, and provided significant insights that could be used in further design of novel and potent anti-tuberculosis agents. Studies on the mechanism of action of the most active compounds are in progress and will be reported in future.

More, U. A. et al. (2014) performed synthesis of novel derivatives of N0-(1-(4-(2,5-disubstituted-1H-pyrrol-1-yl)phenyl)ethylidene)-substitutedaroylhydrazides (**4a-j** and **5a-j**), N0-(1-(4-(2,5-disubstituted-1H-pyrrol-1-yl)phenyl)ethylidene)-2-(aroyloxy) acetohydrazides (**4k-s** and **5k-s**), N0-(1-(4-(2,5-disubstituted-1Hpyrrol-1-yl) phenyl) ethylidene)-4-substitutedbenzenesulfonohydrazides (**4t-v** and **5t-v**), 1-(4-(1-(2-(substitutedphenyl)hydrazono) ethyl)phenyl)-2,5-disubstituted-1*H*-pyrroles (**4w**, **x** and **5w**, **x**) and 2-(1-(4-(2,5-disubstituted-1Hpyrrol-1-yl)phenyl)ethylidene)hydrazine carbothioamide /xamides (**4y**, **z** and **5y**, **z**). These pyrrole hydrazones were explored as a new entry in the search for new tuberculostatics, identifying several hydrazones with reasonable inhibitory activities against *M. tuberculosis*. Among all the compounds **4r-u**, **5k** and **r-u** displayed significant activity (0.2-0.8 µg/mL) against *M. tuberculosis* H_{37}Rv strain. The 3D-QSAR studies, CoMFA and CoMSIA models showed high correlative and predictive abilities. A high bootstrapped r^2 value and a small standard

deviation indicated that a similar relationship exists in all the compounds. For comparison, two different alignment rules including docked alignment and database alignment were used to obtain the 3D-QSAR models that were obtained from the database alignment, which showed better correlation with anti-tuberculosis activity and improved predictability.

Zhipeng, K. et al. (2014) using 3D-QSAR modeling and molecular docking investigation of 2,4-diaminopyrimidines and 2,7-disubstituted-pyrrolo[2,1-f][1,2,4]triazine-based compounds. Three favorable 3D-QSAR models (CoMFA with q^2 = 0.55, r^2 = 0.94, CoMSIA with q^2 = 0.62, r^2 = 0.97, Topomer CoMFA with q^2 = 0.56, r^2 = 0.76) have been developed to predict the biological activity of novel compounds. Topomer Search was utilized for virtual screening to obtain suitable fragments. The novel compounds generated by molecular fragment replacement (MFR) were evaluated by Topomer CoMFA prediction, Glide (docking) and further evaluated with CoMFA and CoMSIA prediction. 25 novel 2,7-disubstituted-pyrrolo[2,1-f][1,2,4]triazine derivatives as potential ALK inhibitors were finally obtained. In this paper, a combination of CoMFA, CoMSIA and Topomer CoMFA could obtain favorable 3D-QSAR models and suitable fragments for ALK inhibitors optimization. The work flow which comprised 3D-QSAR modeling, Topomer Search, MFR, molecular docking and evaluating criteria could be applied to de novo drug design and the resulted compounds initiate us to further optimize and design new potential ALK inhibitors.

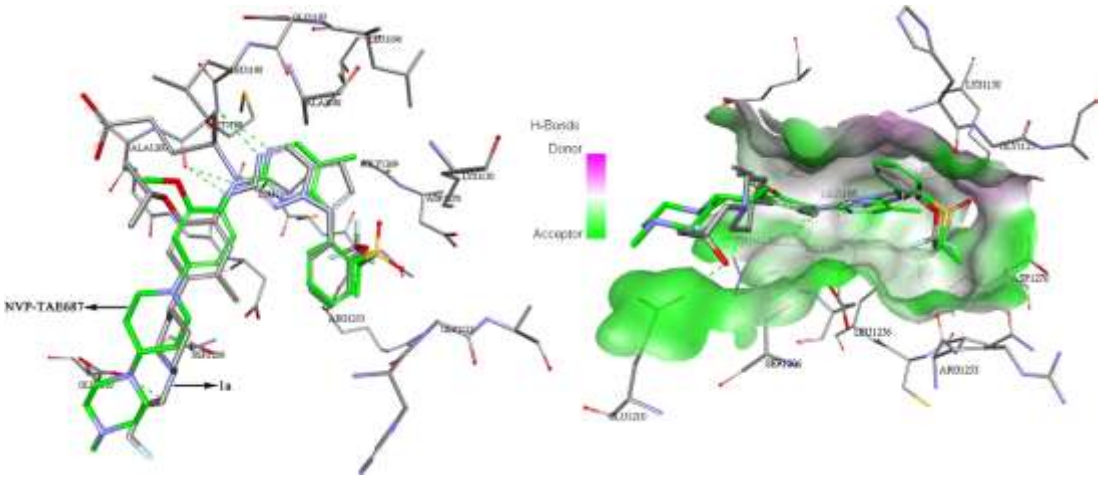

Figure 2.1 Docking interactions of designed compound 1a and NVP-TAE684 in the active site.

Source: Zhipeng et al. (2014)

Akib, M. K. et al. (2017) performed multiple conformers using molecular dynamics simulations for Mycobacterium Enoyl ACP Reductase (InhA) with ethionamide and fluorinedirected modified drugs. In addition, 20 crystallographic structures that retrieved from protein data bank of this receptor are also considered for the conformational study. Our study discloses that different conformations of InhA shown difference in binding affinity and binding interactions and help to find amino acid residues that play major role in drug-receptor interaction. For instance, the binding energies of **EN** and **N1** drugs after the molecule dynamics significantly improved to -15.0 and -17.5 kcal/mol from -10.1 and -11.7 kcal/mol, respectively. Overall, **N1** shows enhanced binding affinity compared to **EN** with all conformers generated from MD simulations as well as retrieved from crystallographic structures. Addition to trifluoromethyl, trifluoroacetyl groups and single fluorine atoms can increase thermodynamic stability of the drugs but likely to shown little or no change in chemical reactivity and kinetic stability. Addition to fluorinated groups to ethionamide increases its binding affinity with InhA. Relatively small radial volume of trifluoromethyl group allows it to bury deeper into hydrophobic pocket of protein and form fluorine mediated hydrogen bonds. Fluorine modifications are also likely to improve pharmacokinetic properties.

Adib G. et al. (2017) using 3D-QSAR to explore the structure-activity relationship of novel 2,5 disubstituted 1,3,4-oxadiazoles analogues as anti-fungal agents. The excellent predictive ability of CoMFA model (q^2 and r^2 as 0.52 and 0.92, respectively) and CoMSIA model (q^2 and r^2 as 0.51 and 0.92, respectively) observed for test set of compounds indicate that these models can be successfully used for predicting the MIC values. Furthermore, the CoMFA and CoMSIA contour maps results offered enough information to understand the structure activity relationship and identified structural features influencing the activity. A number of novel derivatives were designed by utilizing the structure activity relationship taken from present study, based on the excellent performance of the external validation, the predicted activities of these newly designed molecules may be trustworthy.

Fangfang, W. et al. (2018) formulated the 3D-QSAR modeling of a series of compounds possessing Protein tyrosine phosphatase 1B (PTP1B) inhibitory activities using CoMFA and CoMSIA techniques. The optimum template ligand-based models are statistically significant with great CoMFA (R^2_{cv} = 0.60, R^2_{pred} = 0.676) and CoMSIA (R^2_{cv} = 0.62, R^2_{pred} = 0.807) values. Molecular docking was employed to elucidate the inhibitory mechanisms of this series of compounds against PTP1B. In addition, the CoMSIA field contour maps of compound **46** agree well with the structural characteristics of the binding pocket of PTP1B active site as shown in Figure 2.2. The knowledge of structure activity relationship and ligand-receptor interactions from 3D-QSAR model and molecular docking will be useful for better understanding the mechanism of ligand-receptor interaction and facilitating development of novel compounds as potent PTP1B inhibitors.

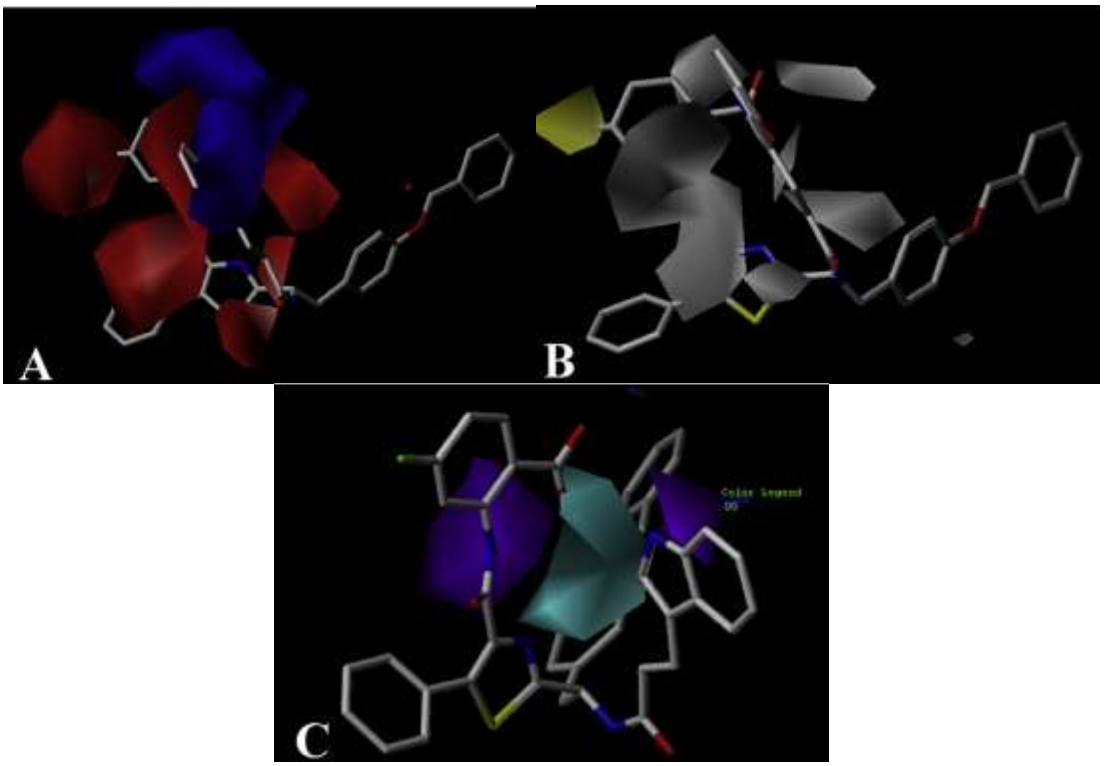

Figure 2.2 CoMSIA StDev*Coeff contour plots for PTP1B inhibitors in combination of compound 46. (A) The electrostatic contour map, (B) The hydrophobic contour map and (C) The hydrogen bond donor contour map.
Source: Fangfang et al. (2018)

Amit, P. et al. (2018) applied 3D-QSAR CoMFA models on 58 urea based GCPII inhibitors were generated, and the best correlation was obtained in Gast-Huck charge assigning method with q^2, r^2 and r^2_{pred} values as 0.59, 0.99 and 0.84 respectively. Moreover, steric, electrostatic, and hydrogen bond donor field contribution analysis provided best statistical values from CoMSIA model (q^2, r^2 and r^2_{pred} as 0.53, 0.98 and 0.71, respectively). Contour maps (as shown in Figure 2.3) study revealed that electrostatic field contribution is the major factor for discovering better binding affinity ligands. Further molecular dynamic assisted molecular docking was also performed on GCPII receptor and most active GCPII inhibitor, DCIBzL. 4NGM cocrystallised ligand, JB7 was used to validate the docking procedure and the amino acid interactions present in JB7 are compared with DCIBzL. The results

suggest that Arg210, Asn257, Gly518, Tyr552, Lys699, and Tyr700 amino acid residues may play a crucial role in GCPII inhibition. Molecular Dynamics Simulation provides information about docked pose stability of DCIBzL. By combination of CoMFA, CoMSIA field analysis and docking interaction analysis studies, conclusive SAR was generated for urea based derivatives based on which GCPII inhibitor 7 was designed and chemically synthesized in their laboratory. Evaluation of GCPII inhibitory activity of 7 by performing NAALADase assay provided IC_{50} value of 113 nM which is in close agreement with in *silico* predicted value (119 nM). Thus they have successfully validated our 3D-QSAR and molecular docking based designing of GCPII inhibitors methodology through biological experiments. This conclusive SAR would be helpful to generate novel and more potent GCPII inhibitors for drug delivery applications.

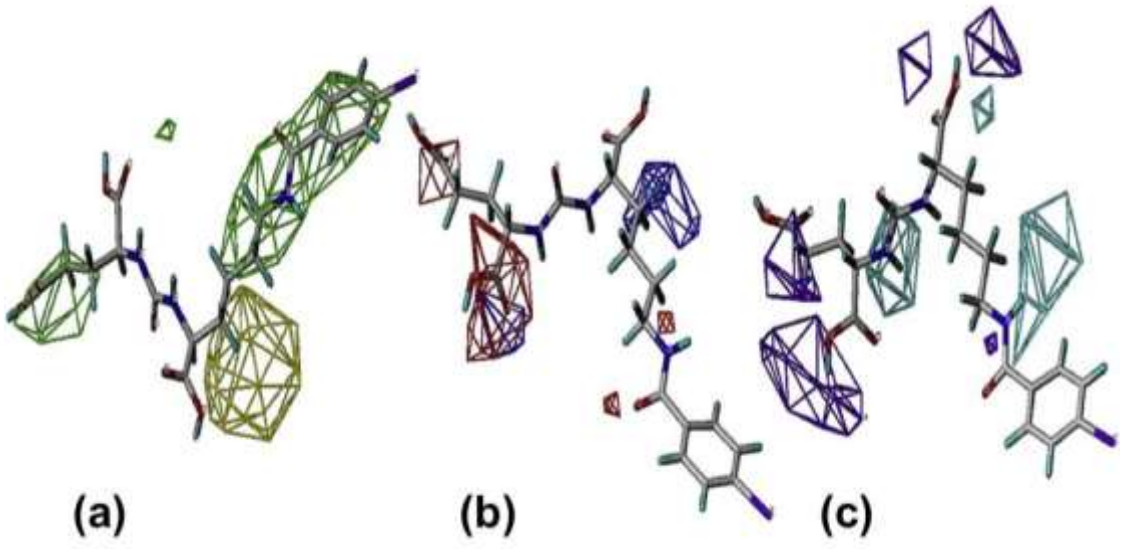

Figure 2.3 Contour maps for CoMSIA. (A) Steric map-Green and yellow colors denotes favourable and unfavourable steric areas. (B) Electrostatic map-Red and blue colors denotes favourable negative and positive electrostatic areas. (C) Hydrogen bond donor map-Cyan and purple colors denotes favourable and unfavourable hydrogen bond donors respectively.

Source: Amit et al. (2018)

Srilata, B. et al. (2018) combined studies of 3D-QSAR, molecular docking which are validated by molecular dynamics simulations and in *silico* ADME prediction on isothiazoloquinolones inhibitors against methicillin resistance staphylococcus aureus. 3D-QSAR study was applied using CoMFA with q^2 of 0.58, r^2 of 0.99, and CoMSIA with q^2 of 0.55, r^2 of 0.97. The predictive ability of these model was determined using a test set of molecules that gave acceptable predictive correlation (r^2_{pred}) values 0.55 and 0.57 of CoMFA and CoMSIA respectively. Figure 2.4 presented the structural requirements for improving the binding and inhibitory activity of isothiazoloquinolones. Docking, simulations were employed to position the inhibitors into protein active site to find out the most probable binding mode and most reliable conformations. Developed models and docking methods provide guidance to design molecules with enhanced activity.

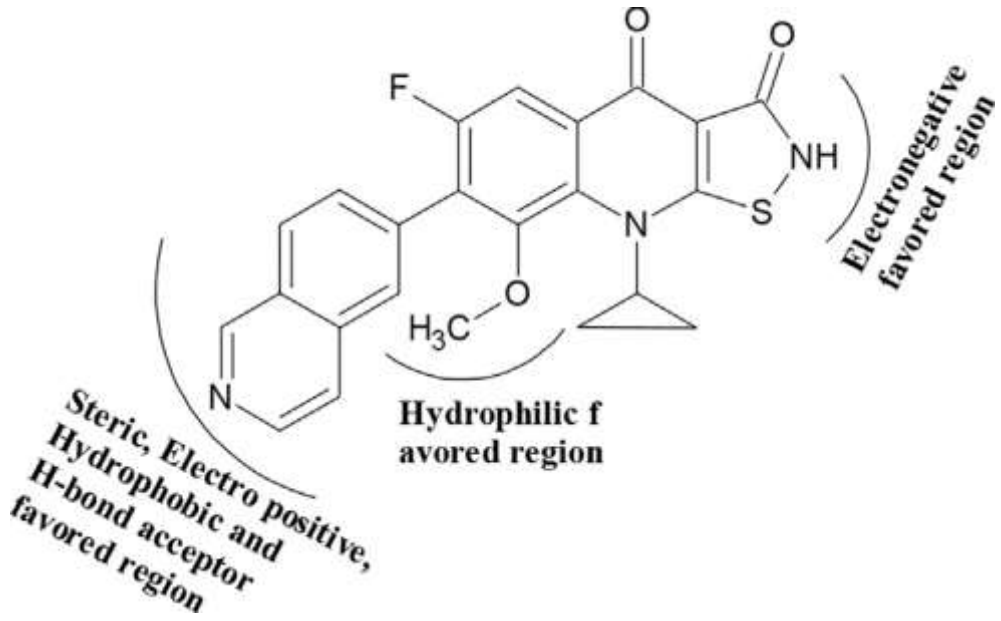

Figure 2.4 Structural requirements for improving the binding and inhibitory activity of isothiazoloquinolones.
Source: Srilata et al. (2018)

2.2 InhA inhibitors

Guardia, A. et al. (2016) performed synthesis, evaluation of anti-tuberculosis activity of heteroaryl benzamides derivatives. The study resulted in the identification a series of N-benzyl-4-((heteroaryl)methyl)-benzamides as a novel class of direct InhA inhibitors by highthroughput screening. These compounds demonstrated potent activity against *M. tuberculosis*, maintaining activity versus KatG mutant clinical strains and emerging as a potential tool against MDR-TB and XDR-TB. Despite the thorough SAR investigation around the hit, no compounds were obtained with significantly improved potency against *M. tuberculosis* $H_{37}R_v$ relative to compound **1**. However, several derivatives were obtained with similar InhA inhibitory and antibacterial activity. Compound **1** is a potent direct InhA inhibitor with moderate whole cell activity and an encouraging safety profile, but unfortunately it was not efficacious in an *in vivo* murine model of TB infection. The SAR information presented for this new anti-tuberculosis compound series, rationalized by interactions observed in a co-crystal structure with InhA should serve as a valuable guide in the design of new molecules toward the goals of improved levels of InhA inhibition and anti-tuberculosis whole cell activity.

Christophe, M. et al. (2012) studies a series of triazoles which have been prepared and evaluated as inhibitors of InhA as well as inhibitors of *M. tuberculosis* $H_{37}R_v$. Several of these new compounds possess a good activity against InhA, particularly compounds **17** and **18** for which molecular docking has been performed. Concerning their activities against *M. tuberculosis* $H_{37}R_v$ strain, two of them, **3** and **12**, were found to be good inhibitors with MIC values of 0.50 and 0.25 mg/mL, respectively. Particularly, compound **12** presenting the best MIC value of all compounds tested (0.60 mM) is totally inactive against InhA.

Ganesh S. P. et al. (2014) performed synthesis, anti-tuberculosis activity of a series of twenty seven substituted 2-(2-oxobenzo[d]oxazol-3(2H)-yl)acetamide derivatives were designed based on our earlier reported *M. tuberculosis* enoyl-acyl carrier protein reductase (InhA) lead. Compounds were evaluated for *M. tuberculosis* InhA inhibition study, *in vitro* activity against drug sensitive and resistant *M. tuberculosis* strains, and cytotoxicity against RAW 264.7 cell line. Among the compounds tested, 2-(6-nitro-2-oxobenzo[d]oxazol-3(2H)-yl)-N-(5-nitrothiazol-2-yl)

acetamide (**30**) was found to be the most promising compound with IC_{50} of 5.12 ± 0.44 µM against *M. tuberculosis* InhA, inhibited drug sensitive *M. tuberculosis* with MIC 17.11 µM and was non-cytotoxic at 100 µM. The interaction with protein and enhancement of protein stability in complex with compound **30** was further confirmed biophysically by differential scanning fluorimetry.

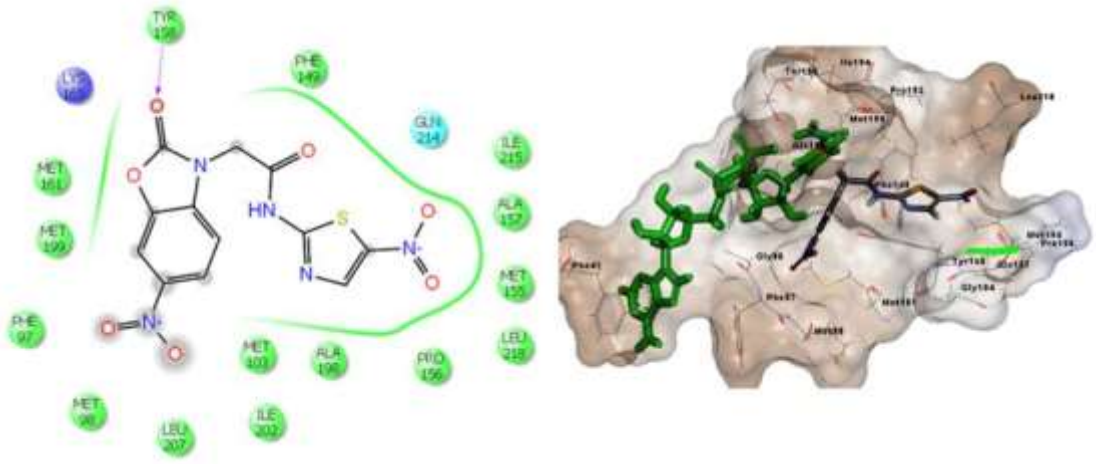

Figure 2.5 Binding pose and its interaction pattern of the compounds 30.
Source: Ganesh et al. (2014)

Ganesh, S. P. et al. (2014) synthesized and evaluated twenty eight 2-(4-oxoquinazolin-3(4H)-yl)acetamide derivatives for their *in vitro M. tuberculosis* InhA inhibition. Compounds were further evaluated for their *in vitro* activity against drug sensitive and resistant *M. tuberculosis* strains and cytotoxicity against RAW 264.7 cell line. Compounds were docked at the active site of InhA to understand their binding mode and differential scanning fluorimetry was performed to ascertain their protein interaction and stability. The synthesis and screening results of twenty eight substituted 2-(4-oxoquinazolin-3(4H)-yl)acetamide derivatives against *M. tuberculosis* InhA as well as drug sensitive and resistant *M. tuberculosis* strains. All the synthesized compounds showed better InhA inhibition as compared to lead molecule, and compound **21** emerged as the most active compound exhibiting 88.12% inhibition of InhA at 10 µM with an IC_{50} of 3.12 µM. It inhibited drug sensitive *M. tuberculosis* with MIC of 4.76 µM and was non-cytotoxic at 100 µM.

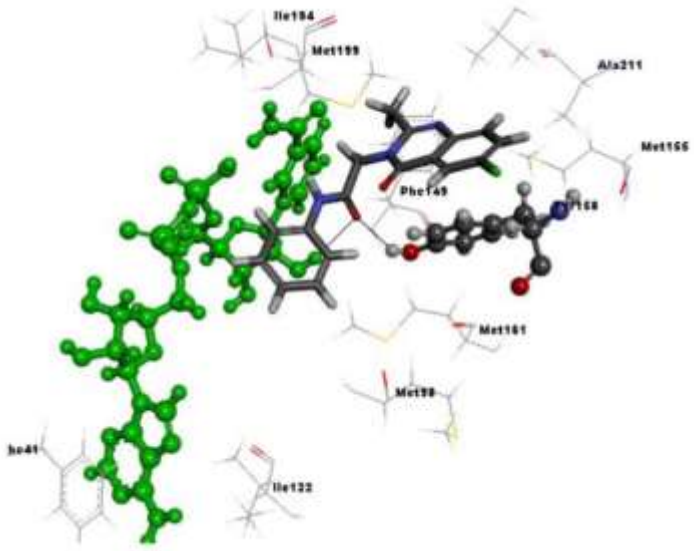

Figure 2.6 Interacting pattern of the compound 21 at the active site of the InhA protein.

Source: Ganesh et al. (2016)

Stane, P. et al. (2016) performed synthesis, evaluation of anti-tuberculosis activity of the tetrahydropyran compound **1** which was identified in a high throughput screen of the GlaxoSmithKline collection, and it showed good InhA inhibitory potency (IC_{50} = 0.02 mM), moderate *in vitro* antimycobacterial activity (MIC = 11.70 mM), modest hERG inhibition, and low cytotoxicity against the HepG2 human cell line. Following initial *in vitro* profiling, a SAR study was initiated and a series of 18 analogs was synthesized and evaluated. Based on the SAR data generated, it appears that rings C and D can be modified in further optimization efforts. The best compound **42** in this series demonstrated InhA inhibitory potency in the nanomolar range (IC_{50} = 36 nM), anti-mycobacterial potency comparable to compound **1** (MIC = 5.00 mM), and a reasonable SI. Additionally, the crystalstructure of compound **1** bound into InhA provided information on the binding mode, rationalised the SARs, and provided insight into the opportunities for further structure-based optimization of InhA inhibitors as shown in Figure 2.7.

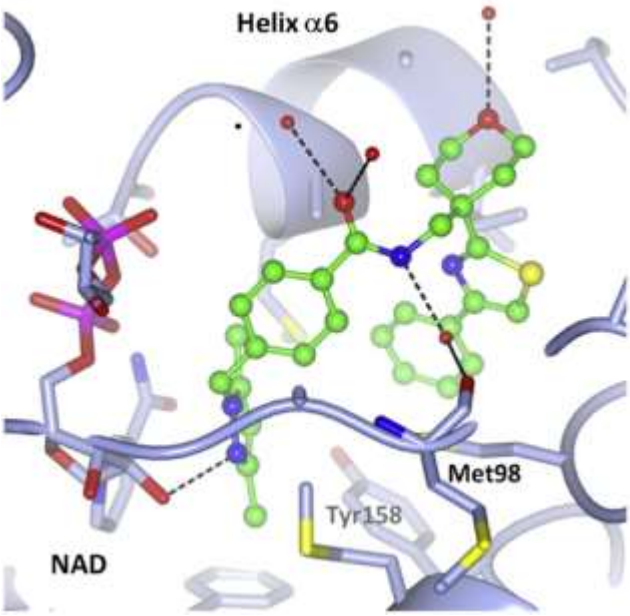

Figure 2.7 Compound 1 bound to the active site of InhA. Compound 1 is shown in green ball-and-sticks, NAD in thick gray lines, and hydrogen bonds in dashed lines. Helix a6 is ordered in the structure, with Met98 and Tyr158 highlighted. Tyr158 adopts an apo orientation.
Source: Stane et al. (2016)

Bruno, C. G. et al. (2017) performed synthesis, evaluation of anti-tuberculosis activity of a new series of 2-(quinolin-4-yloxy)acetamides and their *in vitro* anti-tuberculosis activities. The compounds were obtained with well-established synthetic protocols using accessible reactants and reagents that produced the molecules in reasonable yields. In addition, the synthesized compounds showed potent and selective activity against drug-sensitive and drug-resistant *M. tuberculosis* strains with no apparent cytotoxicity to mammalian cells, and exhibited intracellular activities similar to those of the first-line drugs isoniazid and rifampin. The combined effectiveness of the evaluated 2-(quinolin-4-yloxy) acetamides (**12l** and **12n**) and rifampin may be useful for further novel anti-tuberculosis regimens, especially when patients cannot use the current available treatments because of drug-resistant infection, toxicity events or drug-drug interactions. Finally, the submicromolar anti-tuberculosis activity elicited by 2-(quinolin-4-yloxy) acetamides coupled with some drug-like parameters suggests that this class of compounds may yield candidates for the future

development of novel drugs for tuberculosis treatment. Studies evaluating the *in vivo* oral bioavailability of the lead compounds (a possible attrition point for this chemical class) and to assess their efficacy in a murine model of *M. tuberculosis* infection are in progress.

Shrinivas D. J. et al. (2017) efforts design and develop new anti-tuberculosis agents, report the synthesis of a series of novel pyrrole hydrazine derivatives. The molecules were evaluated against inhibitors of InhA, which is one of the key enzymes involved in type II fatty acid biosynthetic pathway of the mycobacterial cell wall as well as inhibitors of *M. tuberculosis* $H_{37}R_v$. The binding mode of compounds at the active site of enoyl-ACP reductase was explored using the surflex-docking method. The model suggests one or two hydrogen bonding interactions between the compounds and the InhA enzyme. Some compounds exhibited good activities against InhA in addition to promising activities against *M. tuberculosis*.

Manaf, A. M. et al. (2018) studies the complications in translating potent on-target activity into anti-tubercular action with the demanding challenges of growing and continuous TB drug resistance stand in the way of prosperous anti-tuberculosis agents design. Isoniazid, which is considered as one of the first anti-tuberculosis agents, remains the most given drug for prophylaxis and tuberculosis treatment. Resistance to isoniazid described as one of the hallmarks of MDR clinical strains. The compounds discussed in this article comprise InhA inhibitors which have new binding modes of action, display solid evidence of successful target engagement with activity in *silico*. For the predictable future, *M. tuberculosis* appears to be treated with multidrug combinations. However, the emerging data support the fact that InhA inhibitor is a considerable choice to attain new drugs for use in drug combinations in future treatments. This communication will encourage the research community in both academia and industry to target InhA with novel agent discovery methods.

2.3 GyrB inhibitors

Medapi, B. et al. (2015) performed synthesis, evaluation of anti-tuberculosis activity of 4-aminoquinoline derivatives. The study resulted in the identification structural optimization of the reported GyrB inhibitor resulting in synthesis of a series of 46 novel quinoline derivatives. These compounds were evaluated for their *in vitro*

M. smegmatis GyrB inhibitory ability and *M. tuberculosis* DNA supercoiling inhibitory activity. The anti-tuberculosis activity of these compounds were tested over *M. tuberculosis* $H_{37}Rv$ strain and their safety profile was checked against mouse macrophage RAW 264.7 cell line. Among all, three compounds (**23**, **28**, and **53**) emerged to be active displaying IC_{50} values below 1.00 µM against *M. smegmatis* GyrB and were found to be non-cytotoxic at 50 µM concentration. Compound **53** was identified to be potent GyrB inhibitor with 0.86 ± 0.16 µM and an MIC (minimum inhibitory concentration) of 3.30 µM. The binding affinity of this compound towards GyrB protein was analysed by differential scanning fluorimetry which resulted in a positive shift of 3.30 ^{o}C in melting temperature when compared to the native protein thereby reacertaining the stabilization effect of the compound over protein.

Variam, U. J. et al. (2013) designing by molecular hybridization and synthesizing from aryl thioamides in five steps of a series of ethyl-4-(4-((substituted benzyl)amino) piperidin-1-yl)-2-(phenyl/pyridyl) thiazole-5-carboxy lates. The compounds were evaluated for their *in vitro M. smegmatis* GyrB ATPase assay, *M. tuberculosis* DNA gyrase super coiling assay, anti-tuberculosis activity and cytotoxicity. Among the twenty four compounds studied, ethyl-4-(4-((4-fluorobenzyl)amino)piperidin-1-yl)-2-phenylthiazole-5-carboxylate (**14**) was found to be the promising compound and interaction profile with GyrB ATPase domain of *M. smegmatis* as shown in Figure 2.8 which showed activity against all test with *M. smegmatis* GyrB IC_{50} of 24.0 ± 2.1 µM, 79% inhibition of *M. tuberculosis* DNA gyrase at 50 µM, *M. tuberculosis* MIC of 28.44 µM, and not cytotoxic at 50 µM.

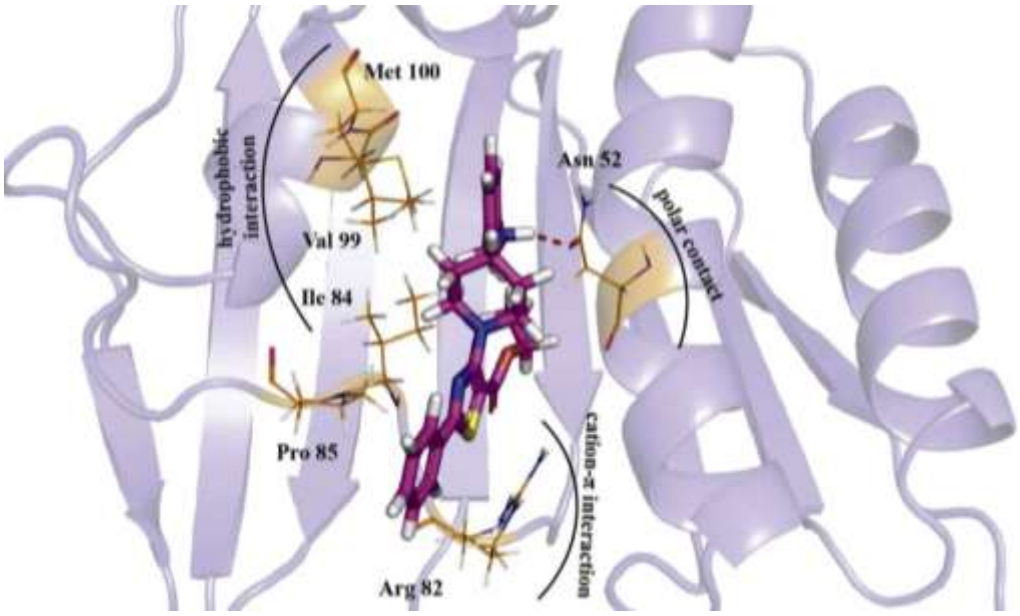

Figure 2.8 Compound 14 interaction profile with GyrB ATPase domain of *M. smegmatis*. The various polar contacts, cation-p interaction and the hydrophobic interaction with compound 14 are marked.
Source: Variam et al. (2013)

Kummetha, I. R. et al. (2014) designed a series of twenty eight molecules of ethyl 5-(piperazin-1-yl)benzofuran-2-carboxylate and 3-(piperazin-1-yl) benzo[*d*] isothiazole by molecular hybridization of thiazole aminopiperidine core and carbamide side chain in eight steps and screened there *in vitro M. smegmatis* GyrB ATPase assay, *M. tuberculosis* DNA gyrase super coiling assay, anti-tuberculosis activity, cytotoxicity and protein–inhibitor interaction assay through differential scanning fluorimetry. Also the orientation and the ligand–protein interactions of the top hit molecules with *M. smegmatis* DNA gyrase B subunit active site were investigated applying extra precision mode (XP) of Glide. Among the compounds studied, 4-(benzo[d]isothiazol-3-yl)-N-(4-chlorophenyl)piperazine-1-carboxamide (**26**) was found to be the most promising inhibitor with an *M. smegmatis* GyrB IC_{50} of 1.77 ± 0.23 µM, 0.42 ± 0.23 against *M. tuberculosis* DNA gyrase, *M. tuberculosis* MIC of 3.64 µM, and was not cytotoxic in eukaryotic cells at 100 µM. Moreover the interaction of protein–ligand complex was stable and showed a positive shift of 3.50 °C in differential scanning fluorimetric evaluations.

Variam, U. J. et al. (2014) DNA gyrase of *M. tuberculosis* is a type II topoisomerase that ensures the regu-lation of DNA topology and has been genetically demonstrated to be a bactericidal drug target. The discovery and optimisation of a novel series of mycobacterial DNA gyrase inhibitors with a high degree of specificity towards the mycobacterial ATPase domain. Compound 5-fluoro-1-(2-(4-(4-(trifluoromethyl)benzylamino)piperidin-1-yl)ethyl) indoline-2,3-dione (**17**) emerged as the most potentlead, exhibiting inhibition of *M. tuberculosis* DNA gyrase supercoiling assay with an IC_{50} of 3.60 ± 0.16 µM, a *M. smegmatis* GyrB IC_{50} of 10.60 ± 0.60 µM, and *M. tuberculosis* minimum inhibitory concentrations of 6.95 µM and 10 µM against drug-sensitive (*M. tuberculosis* $H_{37}R_v$) and extensively drug-resistant strains, respectively.

Shalini, S. et al. (2015) developing twenty eight derivatives and experimentally characterized novel class of mycobacterial DNA GyrB inhibitors. Most of the synthesized compounds showed good GyrB inhibition, however 2-benzamido-5-phenylthiophene-3-carboxamide (compound **23**) (Figure 2.9) was found to be the most active compound with IC_{50} of 0.86 ± 0.81 µM in *M. smegmatis* GyrB as well as *M. tuberculosis* supercoiling IC_{50} of 0.76 ± 0.25 µM. The compound also inhibited drug sensitive *M. tuberculosis* with MIC of 4.84 µM and was non-cytotoxic at 100 µM. Though compound **23** is showing good activity in *M. tuberculosis* GyrB, so it would be a potential lead for rational drug design against *M. tuberculosis* from pharmaceutical point of view. Furthermore, the binding affinity and thermal stability of the most active compound **23** was explored with the GyrB protein by DSF experiments. Altogether these studies have highlighted few possibilities for further optimization of the hit series to increase the inhibitory activity of selected compounds.

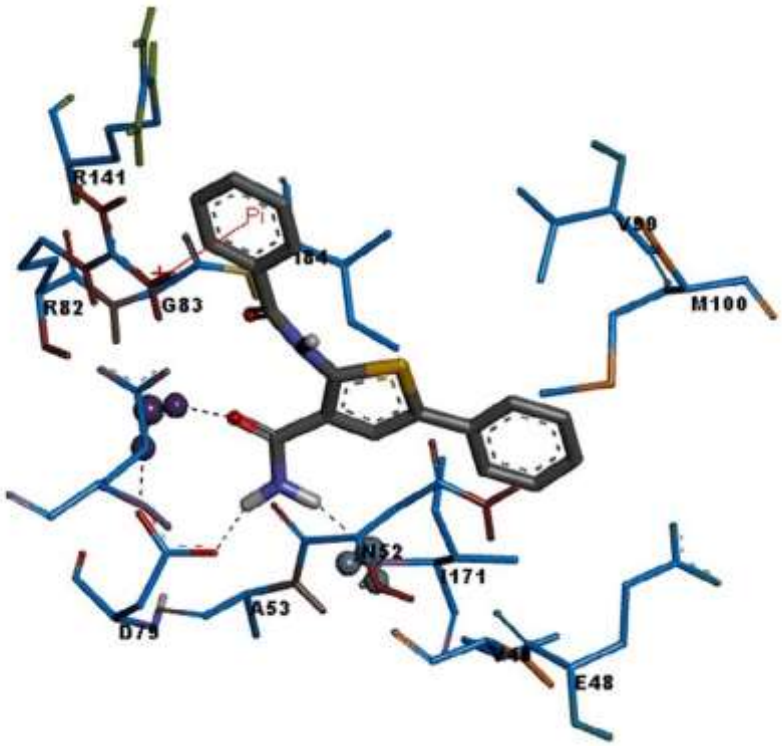

Figure 2.9 Interaction profile diagram of compound 23 with GyrB active site residues. Hydrogen bonds are shown as black dashed lines; the cation–pi interactions are colored red line; water molecule is shown as a round sphere.
Source: Shalini et al. (2015)

Ziga, J. et al. (2017) designed and synthesized a series of substituted oxadiazoles as potential DNA gyrase inhibitors. Structure-based optimization resulted in the identification of compound **35**, displaying an IC_{50} of 1.20 µM for *E. coli* DNA gyrase, while also exhibiting a balanced low micromolar inhibition of *E. coli* topoisomerase IV and of the respective staphylococcus aureus homologues. The most promising inhibitors identified from each series were ultimately evaluated against selected Grampositive and Gram-negative bacterial strains, of which compound **35** inhibited Enterococcus faecalis with a MIC_{90} of 75 µM. Overall, the results offer a valuable insight into the structural requirements of substituted oxadiazoles for DNA gyrase inhibition and thus provide a good foundation for further research in this field.

Tihomir, T. et al. (2017) designed and synthesized two new series of *E. coli* DNA gyrase inhibitors bearing the 4,5-dibromopyrrolamide moiety. 4,5,6,7-Tetrahydrobenzo[1,2-d]thiazole-2,6-diamine derivatives inhibited *E. coli* DNA gyrase in the submicromolar to low micromolar range (IC_{50} values between 0.89 and 10.40 μM). Their ‘‘ring-opened” analogues, based on the 2-(2-aminothiazol-4-yl) acetic acid scaffold, displayed weaker DNA gyrase inhibition with IC_{50} values between 15.90 and 169.00 μM. Molecular docking experiments were conducted to study the binding modes of inhibitors.

CHAPTER 3
MATERIAL AND METHODS

3.1 Biological activity data

3.1.1 InhA inhibitor

Structures and biological activities of heteroaryl benzamides derivatives against *M. tuberculosis* were taken from literatures (Guardia et al., 2016) as shown in Table 3.1. The biological activities of these compounds in term of 50 % inhibitory concentration (IC_{50}) were used and converted to log ($1/IC_{50}$) for linear relationship and for decreasing the large range of biological data.

Table 3.1 Structures and biological activities of heteroaryl benzamides derivatives

Cpd.	structure	IC_{50} (µM)	log($1/IC_{50}$)
01	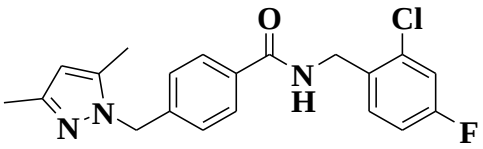	0.05	7.30
02	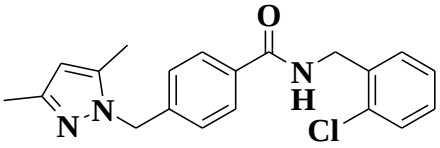	1.26	5.90
03	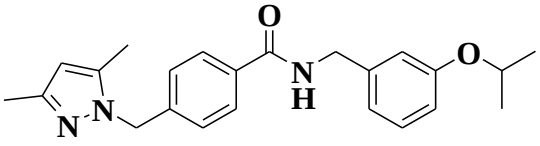	1.58	5.80
04	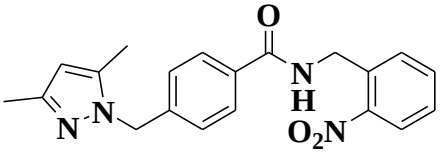	2.51	5.60
05	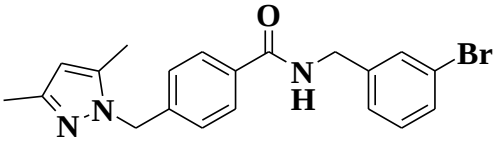	1.58	5.80

Table 3.1 Structures and biological activities of heteroaryl benzamides derivatives (Continued)

Cpd.	structure	IC_{50} (μM)	$\log(1/IC_{50})$
06	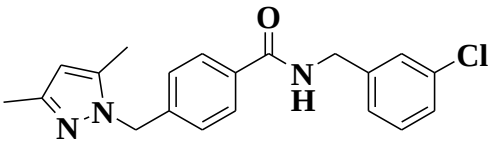	1.58	5.80
07	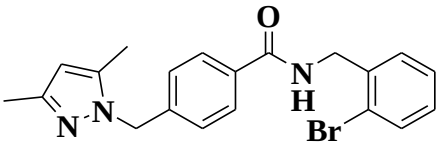	0.54	6.27
08	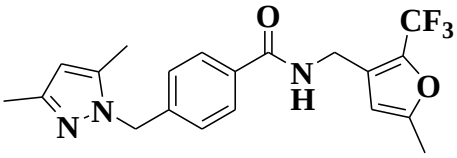	0.12	6.92
09	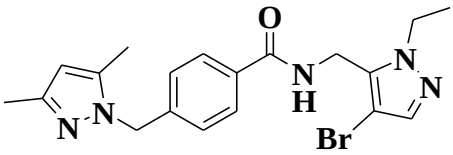	0.09	7.05
10	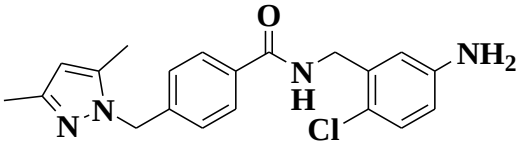	0.35	6.46
11	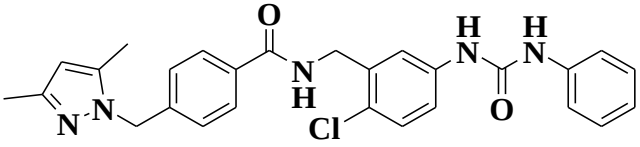	0.09	7.05
12	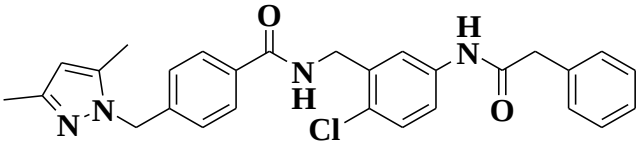	0.08	7.10
13	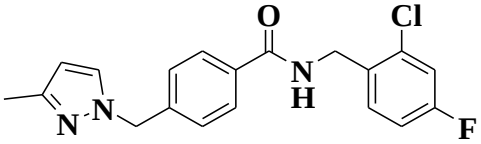	0.50	6.30
14	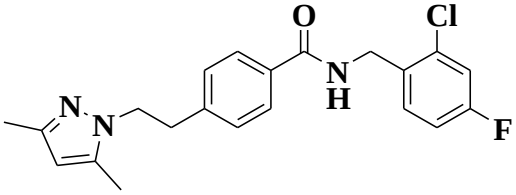	0.32	6.49

Table 3.1 Structures and biological activities of heteroaryl benzamides derivatives (Continued)

Cpd.	structure	IC_{50} (μM)	$\log(1/IC_{50})$
15	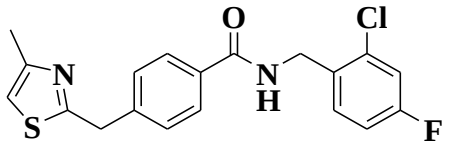	0.06	7.22
16	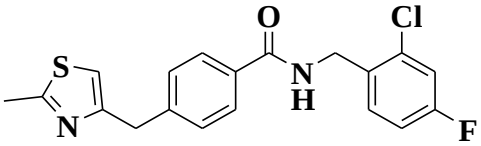	0.09	7.05
17	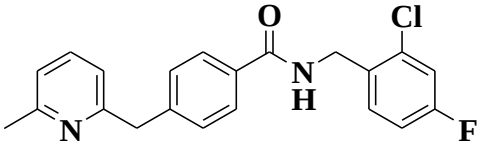	0.05	7.30
18	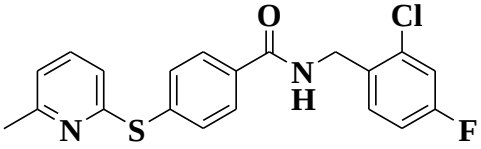	0.06	7.22
19	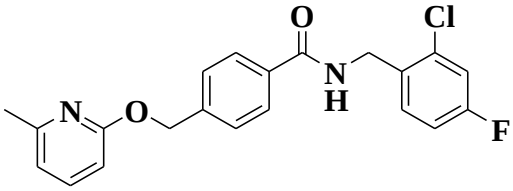	0.02	7.70
20	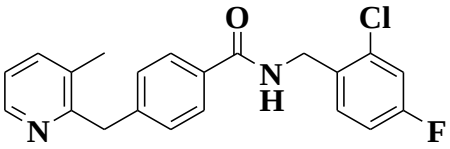	0.55	6.26
21	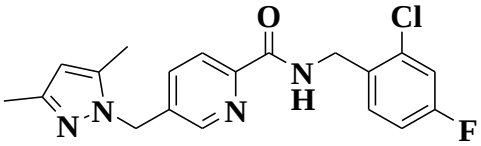	0.19	6.72
22	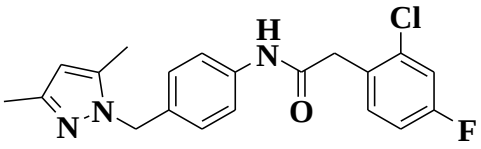	0.04	7.40
23	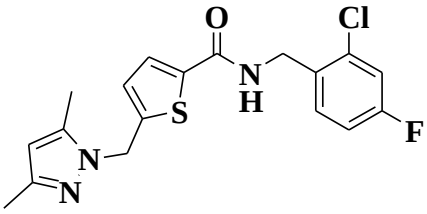	1.20	5.92

Table 3.1 Structures and biological activities of heteroaryl benzamides derivatives (Continued)

Cpd.	structure	IC_{50} (μM)	$\log(1/IC_{50})$
24	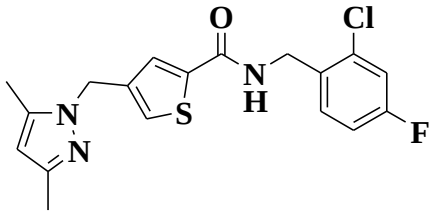	1.20	5.92
25	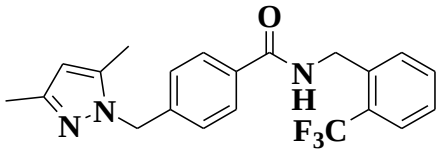	1.00	6.00
26	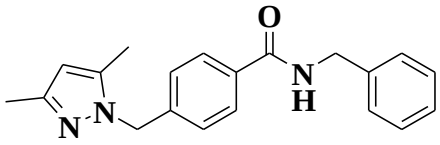	5.93	5.23
27	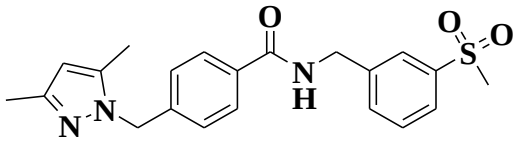	2.51	5.60
28	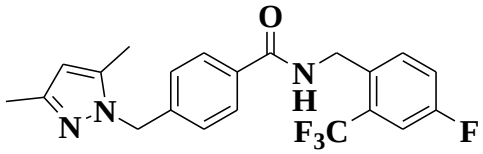	0.25	6.60
29	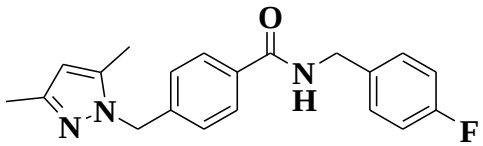	3.10	5.51
30	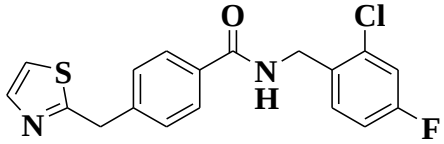	3.25	5.49
31	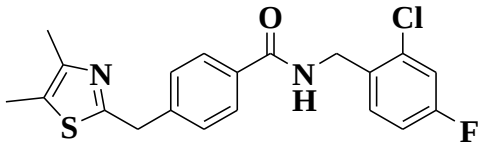	1.40	5.85
32	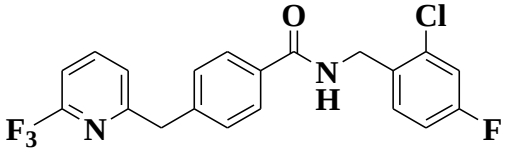	0.25	6.60

Table 3.1 Structures and biological activities of heteroaryl benzamides derivatives (Continued)

Cpd.	structure	IC_{50} (μM)	$log(1/IC_{50})$
33	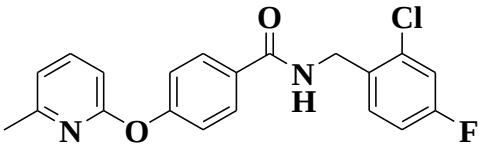	3.40	5.47
34	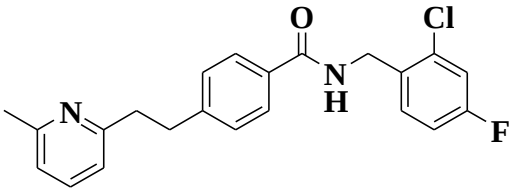	1.55	5.81
35	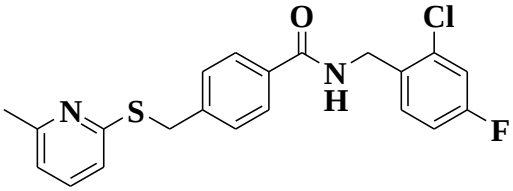	0.26	6.59
36	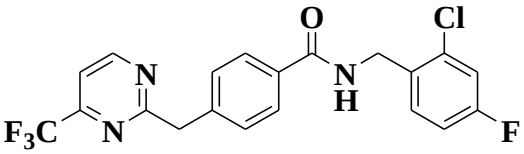	0.57	6.24
37	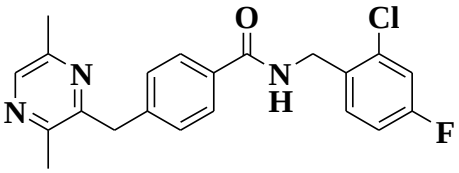	5.00	5.30
38	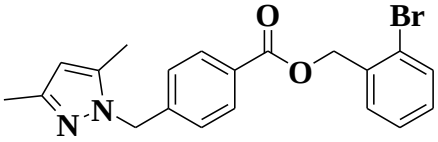	6.10	5.21
39	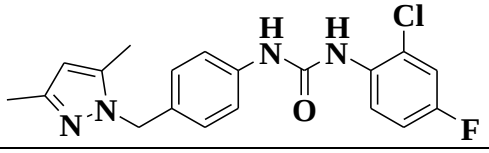	1.70	5.77

Source: Guardia et al. (2016)

3.1.2 GyrB inhibitor

Structures and biological activities of 4-aminoquinoline derivatives against *M. tuberculosis* were taken from literatures (Medapi et al., 2015) as shown in Table 3.2. The biological activities of these compounds in term of 50 % inhibitory

concentration (IC_{50}) were used and converted to log ($1/IC_{50}$) for linear relationship and for decreasing the large range of biological data.

Table 3.2 The chemical structures and their *Msm*Gyr B assay (IC_{50} in µM) values of 4-aminoquinoline derivatives

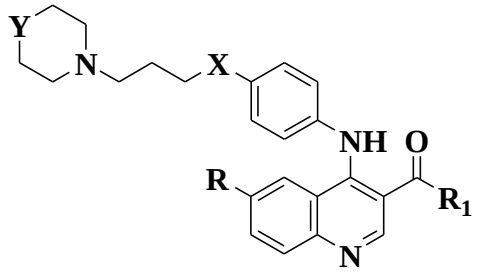

The general structure of 4-aminoquinoline derivatives

Cpd.	R	R_1	X	Y	*Msm*Gyr B assay (IC_{50} in µM)	log($1/IC_{50}$)
01	H	OC_2H_5	O	O	22.83	4.64
02	OCH_3	OC_2H_5	O	O	14.92	4.83
03	F	OC_2H_5	O	O	16.87	4.77
04	CF_3	OC_2H_5	O	O	38.84	4.41
05	H	OC_2H_5	NH	O	17.92	4.75
06	OCH_3	OC_2H_5	NH	O	22.31	4.65
07	F	OC_2H_5	NH	O	11.34	4.95
08	CF_3	OC_2H_5	NH	O	6.62	5.18
09	OCH_3	OC_2H_5	O	NC_2H_5	15.92	4.80
10	F	OC_2H_5	O	NC_2H_5	23.61	4.63
11	CF_3	OC_2H_5	O	NC_2H_5	0.97	6.01
12	H	OC_2H_5	NH	NC_2H_5	11.72	4.93
13	OCH_3	OC_2H_5	NH	NC_2H_5	9.55	5.02
14	F	OC_2H_5	NH	NC_2H_5	16.92	4.77
15	CF_3	OC_2H_5	NH	NC_2H_5	8.82	5.05
16	H	$NHNH_2$	O	O	0.97	6.01
17	OCH_3	$NHNH_2$	O	O	10.58	4.98
18	F	$NHNH_2$	O	O	20.88	4.68

Table 3.2 The chemical structures and their *Msm*Gyr B assay (IC_{50} in µM) values of 4-aminoquinoline derivatives (Continued)

Cpd.	R	R_1	X	Y	*Msm*Gyr B assay (IC_{50} in µM)	$\log(1/IC_{50})$
19	CF_3	$NHNH_2$	O	O	38.66	4.41
20	OCH_3	$NHNH_2$	NH	O	44.93	4.35
21	F	$NHNH_2$	NH	O	18.67	4.73
22	CF_3	$NHNH_2$	NH	O	47.25	4.33
23	H	$NHNH_2$	O	NC_2H_5	28.44	4.55
24	OCH_3	$NHNH_2$	O	NC_2H_5	12.63	4.90
25	F	$NHNH_2$	O	NC_2H_5	2.92	5.53
26	CF_3	$NHNH_2$	O	NC_2H_5	11.88	4.93
27	H	$NHNH_2$	NH	NC_2H_5	10.83	4.97
28	OCH_3	$NHNH_2$	NH	NC_2H_5	3.26	5.49
29	F	$NHNH_2$	NH	NC_2H_5	1.15	5.94
30	CF_3	$NHNH_2$	NH	NC_2H_5	26.34	4.58
31	OCH_3	OH	O	O	20.56	4.69
32	F	OH	O	O	31.56	4.50
33	CF_3	OH	O	O	27.83	4.56
34	H	OH	NH	O	11.33	4.95
35	OCH_3	OH	NH	O	38.92	4.41
36	F	OH	NH	O	14.98	4.82
37	CF_3	OH	NH	O	7.89	5.10
38	H	OH	O	NC_2H_5	21.66	4.66
39	OCH_3	OH	O	NC_2H_5	0.86	6.07
40	F	OH	O	NC_2H_5	6.82	5.17
41	CF_3	OH	O	NC_2H_5	7.91	5.10
42	H	OH	NH	NC_2H_5	11.32	4.95
43	OCH_3	OH	NH	NC_2H_5	1.32	5.88

Source: Medapi et al. (2015)

3.2 Molecular structures and optimization

All chemical structures of heteroaryl benzamides derivatives and 4-aminoquinoline derivatives were constructed using the standard tools available in Gauss View 3.07 program and then fully optimized using the M062X/6-31G* method implemented in Gaussian 09 program. The complex structure of heteroaryl benzamides derivatives and 4-aminoquinoline derivatives with *M. tuberculosis* InhA and GyrB was downloaded from protein data bank database PDB code: 4QXM (Guardia et al., 2016) and 4B6C (Pravin et al., 2013), respectively.

3.3 Molecular Docking calculations

In the field of molecular modeling, molecular docking is a method which predicts the preferred orientation of one molecule to a second when bound to each other to form a stable complex molecular docking is frequently used to predict the binding orientation of small molecule drug candidates to their protein targets in order to in turn predict the affinity and activity of the small molecule. Therefore molecular docking plays an important role in the rational design of drugs (Kitchen et al., 2004). Given the biological and pharmaceutical significance of molecular docking, considerable efforts have been directed towards improving the methods used to predict docking. Molecular docking can be thought of as a problem of “lock-and-key”. The protein is the “lock” and the small molecules are a “key”. Molecular docking research focuses on computationally simulating the molecular recognition process. It aims to achieve an optimized conformation for both the protein and ligand and relative orientation between protein and ligand such that the free energy of the overall system is minimized. To perform a molecular docking, the first requirement is a structure of the interested protein. Usually the structure has been determined in the lab using a biophysical technique such as X-ray crystallography, or less often, NMR spectroscopy. This protein structure and a database of potential ligands serve as inputs to a docking program. The success of a docking program depends on two components: the search algorithm and the scoring function.

3.3.1 Search algorithm

The search space in theory consists of all possible orientations and conformations of the protein paired with the ligand. Most docking programs in use account for a flexible ligand, and several attempt to model a flexible protein receptor.

Ligand flexibility

Conformations of the ligand may be generated in the absence of the receptor and subsequently docked or conformations may be generated on-the-fly in the presence of the receptor binding cavity, or with full rotational flexibility of every dihedral angle using fragment based docking (Zsoldos et al., 2007).

Receptor flexibility

Computational capacity has increased dramatically over the last decade making possible the use of more sophisticated and computationally intensive methods in computer-assisted drug design. Multiple static structures experimentally determined for the same protein in different conformations are often used to emulate receptor flexibility (Totrow and Abagyan, 2008). Alternatively rotamer libraries of amino acid side chains that surround the binding cavity may be searched to generate alternate but energetically reasonable protein conformations A variety of conformational search strategies have been applied to the ligand and to the receptor. These include systematic or stochastic torsional searches about rotatable bonds and genetic algorithms to evolve new low energy conformations.

3.3.2 Scoring function

The scoring function takes a pose as input and returns a number indicating the likelihood that the pose represents a favorable binding interaction. Most scoring functions are physics-based molecular mechanics force fields that estimate the energy of the pose. A low energy indicates a stable system and thus a likely binding interaction.

Scoring function in Autodock

$$\Delta G_{binding} = \Delta G_{vdW} + \Delta G_{H-bond} + \Delta G_{elec} + \Delta G_{desolv} + \Delta G_{tor} \qquad (3.1)$$

Molecular Mechanics Terms

Van der Waals

$$\Delta G_{vdW} = W_{vdW} \sum_{i,j} \left(A_{ij}/r_{ij}^{12} - B_{ij}/r_{ij}^{6} \right) \quad (3.2)$$

Hydrogen bonding

$$\Delta G_{H-bond} = W_{H-bond} \sum_{i,j} E(t) \left((C_{ij}/r_{ij}^{12} - D_{ij}/r_{ij}^{10}) + E_{H-bond} \right) \quad (3.3)$$

Electrostatics

$$\Delta G_{elec} = W_{elec} \sum_{i,j} \left(q_i q_j \right) / \left(\varepsilon(r_{ij}) r_{ij} \right) \quad (3.4)$$

Desolvation

$$\Delta G_{desolv} = W_{desolv} \sum_{i(C),j} \left(S_i V_j exp\left(-r_{ij}^2 / 2\sigma^2 \right) \right) \quad (3.5)$$

$\Delta G_{vdW} = \Delta G_{vdW}$; Lennard-Jones potential (with 0.5 Å smoothing), ΔG_{elec} with Solmajer & Mehler distance-dependent dielectric, ΔG_{hbond}; H-bonding Potential with Goodford Directionality, ΔG_{desolv}; Charge-dependent variant of Stouten Pairwise Atomic Solvation Parameters, ΔG_{tors}; Number of rotatable bonds

Change in torsional free energy when the ligand goes from unbound to bound

Torsional $\Delta G_{tor} = W_{tor} N_{tor}$

3.3.3 Autodock program

The program Autodock was developed to provide an automated procedure for predicting the interaction of ligands with biomacromolecular targets. The motivation for this work arises from problems in the design of bioactive compounds, and in particular the field of computer-aided drug design. Progress in biomolecular x-ray crystallography continues to provide a number of important protein and nucleic acid structures. These structures could be targets for bioactive agents in the control of animal and plant diseases, or simply key to understanding of a fundamental aspect of biology. The precise interaction of such agents or candidate

molecules is important in the development process. Indeed, Autodock can be a valuable tool in the x-ray structure determination process itself: given the electron density for a ligand, Autodock can help to narrow the conformational possibilities and help identify a good structure. The goal of Autodock has been to provide a computational tool to assist researchers in the determination of biomolecular complexes. In any docking scheme, two conflicting requirements must be balanced: the desire for a robust and accurate procedure, and the desire to keep the computational demands at a reasonable level. The ideal procedure would find the global minimum in the interaction energy between the substrate and the target protein, exploring all available degrees of freedom (DOF) for the system.

The original procedure developed for Autodock used a Monte Carlo (MC) simulated annealing (SA) technique for configurational exploration with a rapid energy evaluation using grid-based molecular affinity potentials. It thus combined the advantages of exploring a large search space and a robust energy evaluation. This has proven to be a powerful approach to the problem of docking a flexible substrate into the binding site of a static protein. Input to the procedure is minimal. The researcher specifies a rectangular volume around the protein, the rotatable bonds for the substrate, and an arbitrary or random starting configuration, and the procedure produces a relatively unbiased docking (Morris et al., 2018). The current version of Autodock (Autodock4.2), using the Lamarckian Genetic Algorithm and empirical free energy scoring function, typically will provide reproducible docking results for ligands with approximately 10 flexible bonds.

3.3.4 Overview of the Method

Rapid energy evaluation is achieved by precalculating atomic affinity potentials for each atom type in the substrate molecule in the manner described by Goodford. In the AutoGrid procedure the protein is embedded in a three-dimensional grid and a probe atom is placed at each grid point. The energy of interaction of this single atom with the protein is assigned to the grid point. An affinity grid is calculated for each type of atom in the substrate, typically carbon, oxygen, nitrogen and hydrogen, as well as a grid of electrostatic potential, either using a point charge of +1 as the probe, or using a Poisson-Boltzmann finite difference method, such as DELPHI. The energetics of a particular substrate configuration is then found by tri-linear

interpolation of affinity values of the eight grid points surrounding each of the atoms in the substrate. The electrostatic interaction is evaluated similarly, by interpolating the values of the electrostatic potential and multiplying by the charge on the atom (the electrostatic term is evaluated separately to allow finer control of the substrate atomic charges). The time to perform an energy calculation using the grids is proportional only to the number of atoms in the substrate, and is independent of the number of atoms in the protein.

Steps in Autodock4.2 calculations

Step 1 Coordinate File Preparation. Autodock4.2 is parameterized to use a model of the protein and ligand that includes polar hydrogen atoms, but not hydrogen atoms bonded to carbon atoms. An extended PDB format, termed PDBQT, is used for coordinate files, which includes atomic partial charges and atom types. The current Autodock force field uses several atom types for the most common atoms, including separate types for aliphatic and aromatic carbon atoms, and separate types for polar atoms that form hydrogen bonds and those that do not. PDBQT files also include information on the torsional degrees of freedom. In cases where specific sidechains in the protein are treated as flexible, a separate PDBQT file is also created for the sidechain coordinates. AutodockTools, the Graphical User Interface for Autodock, may be used for creating PDBQT files from traditional PDB files.

Step 2 Autogrid Calculation. Rapid energy evaluation is achieved by precalculating atomic affinity potentials for each atom type in the ligand molecule being docked. In the Autogrid procedure the protein is embedded in a three-dimensional grid and a probe atom is placed at each grid point. The energy of interaction of this single atom with the protein is assigned to the grid point. Autogrid affinity grids are calculated for each type of atom in the ligand, typically carbon, oxygen, nitrogen and hydrogen, as well as grids of electrostatic and desolvation potentials. Then, during the Autodock calculation, the energetics of a particular ligand configuration is evaluated using the values from the grids.

Step 3 Docking using Autodock. Docking is carried out using one of several search methods. The most efficient method is a Lamarckian genetic algorithm (LGA), but traditional genetic algorithms and simulated annealing are also available. For typical systems, Autodock is run several times to give several docked

conformations, and analysis of the predicted energy and the consistency of results is combined to identify the best solution.

Step 4 Analysis using Autodock Tools. Autodock Tools includes a number of methods for analyzing the results of docking simulations, including tools for clustering results by conformational similarity, visualizing conformations, visualizing interactions between ligands and proteins, and visualizing the affinity potentials created by AutoGrid (Morris et al., 2018).

3.3.5 Molecular docking calculations of heteroaryl benzamides derivatives and 4-aminoquinoline derivatives

All structures of heteroaryl benzamides derivatives and 4-aminoquinoline derivatives were fully optimized by *ab initio* quantum chemical calculations at M062X/6-31G* method. All quantum chemical calculations were calculated by Gaussian09 program. The X-ray structure of heteroaryl benzamides complexed with *M. tuberculosis* InhA and 4-aminoquinoline complexed with *M. tuberculosis* GyrB was taken from Protein data bank PDB code 4QXM (Guardia et al., 2016) and 4B6C (Pravin et al., 2013). Due to the binding pocket of heteroaryl benzamides inhibitor complexed with *M. tuberculosis* InhA residues and 4-aminoquinoline inhibitor complexed with *M. tuberculosis* GyrB residues. The molecular docking calculations of inhibitors in this study were performed by Autodock 4.2 program. Grid box on the binding site of ligand of heteroaryl benzamides derivatives was set as 40x40x40 $Å^3$ with grid spacing 2.00 Å. For 4-aminoquinoline derivatives set grid box on the binding site of ligand as 40x40x32 $Å^3$ with grid spacing 2.00 Å. The Lamarckian Genetic Algorithm (LGA) and 200 runs were used. All atoms of the protein and NAD^+ cofactor were kept rigid, whereas the ligand was flexible during the molecular docking calculations. To validate the parameters for molecular docking calculation using Autodock 4.2 program, root mean square deviation (RMSD) value between the X-ray structure and docking conformation of heteroaryl benzamides derivatives and 4-aminoquinoline derivatives in *M. tuberculosis* InhA and GyrB were used, respectively. The value of RMSD will be less than 1 Å. The binding mode with the lowest binding free energy of heteroaryl benzamides derivatives and 4-aminoquinoline derivatives compound obtained from molecular docking method was used for structural alignment of 3D-QSAR analyses.

3.3.6 The criteria determining interaction between protein and ligand

3.3.6.1 Hydrogen bonding interactions

Considering bond distance between hydrogen atom (H) with atom high electronegativity such as oxygen (O) and nitrogen (N) atoms should be less than 2.50 Å.

3.3.6.2 Pi-Pi interactions

Considering bond distance between aromatic ring with aromatic ring of amino acid with aromatic ring of inhibitor should be less than 4.00 Å.

3.3.6.3 Hydrogen-Pi interactions

Considering bond distance between hydrogen atom (H) and aromatic ring should be less than 4.00 Å.

3.3.6.4 Van der waals interactions

Considering from sum of Van der waals radii between both atoms were interested. Consider these interactions will be discussed in the section of results and discussion.

3.4 Molecular dynamics (MD) simulation

Molecular dynamics (MD) is a computer simulation of physical movements of atoms and molecules in the context of N-body simulation. The atoms and molecules are allowed to interact for a period of time, giving a view of the motion of the atoms. In the most common version, the trajectories of atoms and molecules are determined by numerically solving the Newton's equations of motion for a system of interacting particles, where forces between the particles and potential energy are defined by interatomic potentials or molecular mechanics force fields. All classical simulation methods rely on more or less empirical approximations called force fields to calculate interactions and evaluate the potential energy of the system as a function of point-like atomic coordinates. A force field consists of both the set of equations used to calculate the potential energy and forces from particle coordinates, as well as a collection of parameters used in the equations. For most purposes these approximations work great, but they cannot reproduce quantum effects like bond formation or breaking. All common force fields subdivide potential functions in two classes, bonded interactions and non-bonded interactions. Bonded interactions cover covalent bond-

stretching, angle-bending, torsion potentials when rotating around bonds, and out-of-plane improper torsion potentials, all which are normally fixed throughout a simulation as shown in Figure 3.1. The remaining non-bonded interactions consist of Lennard-Jones repulsion and dispersion as well as electrostatics.

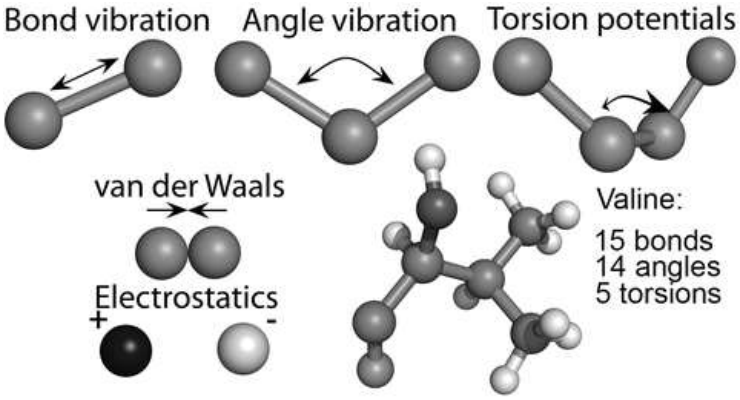

Figure 3.1 Typical molecular mechanics interactions.
Source: Nadine and Holger (2012)

The step of standard MD simulation is shown in Figure 3.2. Given the potential and force (negative gradient of potential) for all atoms, the coordinates are updated for the next step. The updated coordinates are then used to evaluate the potential energy again. For energy minimization, the steepest descent algorithm simply moves each atom a short distance in direction of decreasing energy.

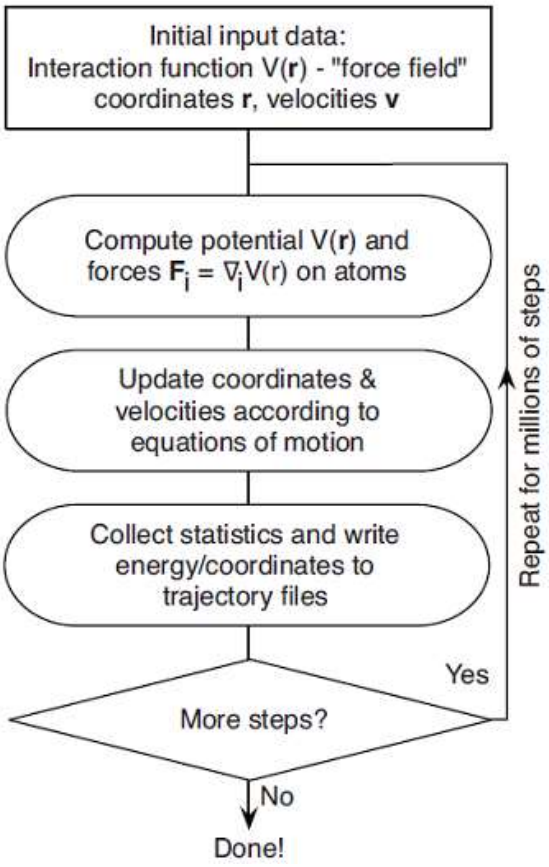

Figure 3.2 Simplified flowchart of a standard molecular dynamics simulation.

Source: Nadine and Holger (2012)

3.4.1 MD simulations of InhA and GyrB inhibitors

In this study, MD simulations were carried out using Amber12. Amber is the collective name for a suite of programs that allow users to carry out molecular dynamics simulations, particularly on biomolecules. The Amber software suite is divided into two parts: AmberTools12, a collection of freely available programs mostly under the GPL license, and Amber12, which is centered around the sander and pmemd simulation programs, and which continues to be licensed as before, under a more restrictive license. Amber is a suite of programs for use in molecular modeling and molecular simulations. It consists of a substructure database, a force field parameter file, and a variety of useful programs.

3.4.2 Starting structures for MD simulations

The X-ray crystal structures of heteroaryl benzamides complexed and 4-aminoquinoline complexed with *M. tuberculosis* InhA and GyrB taken from the Protein Data Bank with pdb codes of 4QXM and 4B6C, were served as the initial coordinates for MD simulations. In the case of heteroaryl benzamides complexed and 4-aminoquinoline bound complexes, their starting structures were taken from molecular docking calculations using Autodock 4.2 program.

3.4.3 Molecular dynamics simulations of InhA and GyrB inhibitors

Seven InhA inhibitors and eight GyrB inhibitors were selected to model the binding mode and key binding interactions in this work shown in Table 3.1 and Table 3.2, respectively. The chemical structures and their experimental biological activities of heteraryl benzamide derivatives and 4-aminoquinoline derivatives were selected from the literature. The biological activities of these compounds were expressed in terms of 50 % inhibitory concentration (IC_{50} in μM) values. The chemical structures of these inhibitors were constructed using the standard tools available in GaussView 3.07 program and were then fully optimized using the M062X/6-31G* method implemented in Gaussian 09 program. The initial coordinates for molecular dynamics simulations of the complexes was obtained from molecular docking calculations using Autodock 4.02 program. Molecular dynamics simulations were performed to predict the inhibitors in the InhA binding pocket. TIP3P water model and Na^+ were chosen to represent water for salvation and ions for neutralize system. To reduce the bad steric interactions of solvate water molecules and Na^+ ions of each system, the inhibitor-InhA complex and inhibitor-GyrB complex was first minimized by 1,000 steps with atomic positions of solute species restraint with using force constant of 500 kcal/mol $Å^2$. Non-bonded cut-off was set to 8 Å. The threshold value of the energy- gradient foe the convergence was set as 0.001 kcal/mol/ Å. Then, the whole system was minimized by 1,500 steps as the same conditions of water and ions minimization without restraining condition. Next, the systems were gradually warmed up from 0 to 300 K in the first 20 ps followed by maintaining the temperature at 300 K in the last 10 ps with 2 fs time simulation steps in a constant volume boundary. The solute species were restrained to their initial coordinate structures with a weak force constant of 10 kcal/mol $Å^2$ during the temperature warming. This was followed

by 70 ps of the position-restrained dynamics simulation with a restrain weight of 2 kcal/mol $Å^2$ at 300 K under an isobaric condition. Finally, 30 ns molecular dynamics simulations of InhA inhibitors and 60 ns molecular dynamics simulations of GyrB inhibitors without any restraints were performed using the same conditions. The root mean square deviations (RMSDs) of the protein enzyme, inhibitors and cofactor, binding interactions were analysed based on the equilibrium state obtained. The binding free energies were calculated to evaluate the binding affinities of inhibitors in InhA binding pocket using the Molecular Mechanics Poisson- Boltzmann Surface Area (MM-PBSA) (Wang et al., 2001; Wang et al., 2006; Hou et al., 2011; Erik, 2015) and Normal-mode (Kaledin et al., 2004) methods. 250 snapshots were used to calculate the binding free energy in this work. The single snapshot that showed the calculated binding free energy closed to experimental binding free energy was selected to analyze the binding mode and binding interactions.

3.4.4 Calculations of binding free energies

The binding free energy calculations between InhA and heyeroaryl benzamide inhibitors were calculated using the Molecular Mechanics Poisson Boltzmann Surface Area (MM-PBSA) and normal-mode methods. 100 snapshots were extracted to calculate. The binding free energies (ΔG_{bind}) were obtained as shown in Equations (3.8) and (3.9).

$$\Delta G_{bind} = G_{com} - (G_{rec} + G_{ligand}) \quad (3.6)$$

$$\Delta G_{bind} = \Delta H - T\Delta S \quad (3.7)$$

$$\Delta H = \Delta G_{MM} + \Delta G_{solv} \quad (3.8)$$

where G_{com}, G_{rec} and G_{ligand} are the free energies of the complex, receptor and inhibitor ligand, respectively. In general, the binding free energy composes of an enthalpy (ΔH) and an entropy contribution ($-T\Delta S$). The enthalpy contribution (ΔH) contains the gasphase molecular mechanics energy (ΔG_{MM}) calculated with a sander module and the salvation free energy (ΔG_{solv}) calculated with the PBSA program of the AMBER suite as shown in Equation (3.11).

$$\Delta G_{\text{bind}} = \Delta G_{MM} + \Delta G_{solv} - T\Delta S \quad (3.9)$$

ΔG_{MM} is divided into non-covalent van der Waals component (ΔG_{vdw}), electrostatic energies component (ΔG_{ele}) and bond, angle, dihedral energies (ΔG_{INT}) in Equation (3.12).

$$\Delta G_{MM} = \Delta G_{vdw} + \Delta G_{ele} + \Delta G_{INT} \quad (3.10)$$

The entropy contribution ($-T\Delta S$) to the binding free energy was estimated using normal-mode analysis with the AMBER Nmode module. Due to the high computational cost in the entropy calculation, the residues around the ligand (less than 12 Å) were only considered for normal-mode calculations and 100 snapshots were used. The contributions of entropy ($T\Delta S$) to binding free energy from changes of the translational, rotational and vibrational degrees of freedom were calculated as follows:

$$\Delta S = \Delta S_{translational} + \Delta S_{rotational} + \Delta S_{vibrational} \quad (3.11)$$

The best snapshots of complex InhA/NAD^+/heteroaral benzamide derivatives minimized obtain from binding free energies 100 snapshots. And then calculate the binding free energies (ΔG_{bind}) were shown in Equations (3.6) and (3.7).

3.5 Quantitative Structure Activity Relationship Analysis (QSAR)

Quantitative Structure Activity Relationship (QSAR) is an analytical application that can be applied to interpretation of quantitative relationship between the biological activities of a particular molecule and its structure. Biological activity can be expressed quantitatively as in the concentration of a substance required to give a certain biological response. When physicochemical properties are expressed by numbers, they can form a mathematical relationship with biological activity. The main assumption is the factors governing the events in a biological system are represented by the descriptors characterizing the compounds. Therefore, QSAR attempt to find structural features of a molecule affect its activity and could be modified to enhance their properties.

3.5.1 QSAR models

The QSAR models are mathematical relationship which relates a structure-related property to the presence or absence, or potency of another property or activity of interest. QSAR models most basic mathematical form is:

Activity = f (physiochemical or structural properties) or

$$y = a_1x_1 + a_2x_2 + a_3x_3 + \ldots$$

Where y is dependent variables of x_i (i = 1, 2, 3,…) or activity

a is coefficient

x is independent variables (physicochemical properties or descriptors)

3.5.2 Comparative Molecular Similarity Indices Analysis (CoMSIA)

CoMSIA is an extension of the CoMFA methodology. Both are based on the assumption that changes in binding affinities of ligands are related to changes in molecular properties, represented by fields. They differ only in the implementation of the fields. In both CoMFA and CoMSIA, a group of structurally aligned molecules are represented in terms of fields around the molecule. CoMFA calculates steric fields using a Lennard-Jones potential, and electrostatic fields using a coulombic potential. While this approach has been widely accepted and exceptionally valuable, it is not without problems. In particular, both potential functions are very steep near the van der Waals surface of the molecule, causing rapid changes in surface descriptions, and requiring the use of cut-off values so calculations are not done inside the molecular surface. Due to the cut-off settings and the steepness of the potentials close to the molecular surfaces, CoMFA contour maps are not contiguously connected and accordingly difficult to interpret. To overcome the outlined problem, CoMSIA approach has been developed. Similarity indices are calculated to derive molecular descriptors for a comparative analysis. They do not exhibit a direct measure of similarity determined between all mutual pairs of molecules. Instead, they are indirectly evaluated via the similarity of each molecule in the dataset with a common probe atom that is placed at the intersections of a surrounding lattice. In determining this similarity, the mutual distance between the probe atom and the atoms of

the molecules of the dataset is considered. As functional form Gaussian-type functions with no singularities have been selected to describe this distance dependence, no arbitrary definition of cutoff limits is any longer required. Indices can be calculated at all grid-points. In principle, any relevant physico-chemical property can be considered in this approach to calculate a field of similarity indices. The applied Gaussian-type functional form defines a significantly smoother distance dependence compared to the Lennard-Jones potential. The obtained indices are evaluated in a PLS analysis according to the usual CoMFA protocol. Applying CoMFA and CoMSIA to the same datasets, results in similar statistical significance being obtained. However, the major improvement is achieved with respect to the contour maps derived from the results. CoMSIA, contour maps can easily be interpreted and used as a visualization tool in designing novel compounds.

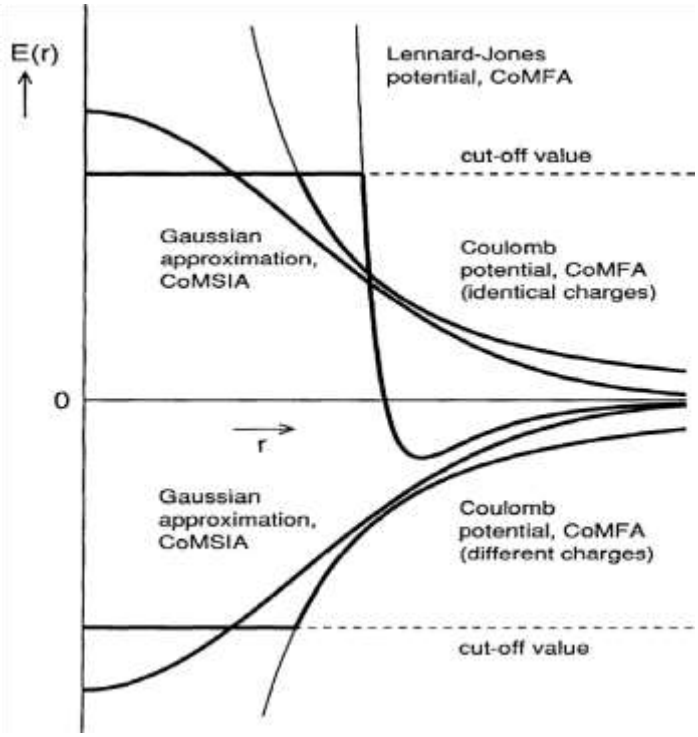

Figure 3.3 Shapes of various functions.

Source: Kubinyi (1993)

Five different similarity fields of CoMSIA include steric, electrostatic, hydrophobic, hydrogen bond donor and hydrogen bond acceptor fields. The equation used to calculate the similarity indices is as follows in equation 3.14.

$$A_{F,k}^{q}(j) = \sum_{i} w_{probe,k} w_{ik} e^{-\alpha r_{iq}^{2}} \qquad (3.12)$$

Where: A = Similarity index at grid point q, summed over all atoms of the molecule j under investigation.

$w_{probe,\ k}$ = Probe atom with radius 1 Å, charge +1, hydrophobicity +1, hydrogen bond donating +1, hydrogen bond accepting +1.

w_{ik} = Actual value of the physicochemical property k of atom i.

r_{iq} = Mutual distance between the probe atom at grid point q and atom i of the test molecule.

α = Attenuation factor, with a default value of 0.3, and an optimal value normally between 0.2 and 0.4.

3.5.3 Quantitative Structure Activity Relationship Analysis (QSAR) of InhA inhibitors and GyrB inhibitors

The molecular modeling software of SYBLY-X2.0 with CoMSIA approach was used to determine the relationship between structure and biological activity of heteroaryl benzamide derivatives and 4-aminoquinoline derivatives. Five physico-chemical properties including steric field, electrostatic field, hydrophobic field, hydrogen bond acceptor field and hydrogen bond donor field are considered to develop CoMSIA models to set up CoMSIA models, CoMSIA descriptors were used as indepentdent variable and log ($1/IC_{50}$) value were used as depentdent variable. To investigate the linear relationship between molecular descriptors and activity, the partial least square (PLS) method with leave-one-out-method (LOO) cross-validations method were carried out to determine the optimal number of components. The final non cross-validated analysis with the optimal number of components was performed and employed to analyze the result. Non cross-validation correlation coefficient (r^2)

and the leave-one-out-cross-validated correlation coefficient (q^2) were applied to evaluate the predictive ability of CoMSIA models.

CHAPTER 4
RESULT AND DISCUSSION

The results derived from molecular modeling and computer-aided molecular design approaches were applied into two targets for anti-tuberculosis. The first target is enoyl-ACP reductase (InhA) inhibitors. The second target is DNA gyras subunit B (GyrB) inhibitors. The details of results that observed in this study were discussed in this chapter.

4.1 Enoyl-ACP reductase (InhA) inhibitors

4.1.1 Molecular docking calculations of heteraryl benzamide derivatives

4.1.1.1 Validation of the docking method

The binding modes of heteraryl benzamide derivatives in the *Mycobacterium Tuberculosis* (*M. tuberculosis*) InhA binding pocket were investigated using Autodock 4.2 program. Heteraryl benzamide derivatives atomic charges were assigned as Restrained Electrostatic Potential (RESP) and the inhibitors were docked into binding pocket. Firstly, to ensure that the ligand orientation and the position obtained from the docking studies are similar to the binding modes of the crystal structure, the Autodock docking parameters has to be validated for X-ray crystallographic data of heteraryl benzamide derivatives (PDB: 4QXM) for *M. tuberculosis* InhA binding pocket was used as an initial structure for molecular docking calculations. The numbers of grid points in the x, y, and z dimensions with 40x40x40 $Å^3$ were used to define the 3D grid box size. The results showed that Autodock determine the docked orientation of the original orientation found in X-ray crystal structure shown in Figure 4.1. The root mean square deviations (RMSD) between the calculation and x-ray crystal ligand coordinates are 0.50 Å. This indicates the good alignment of the experimental and calculated positions.

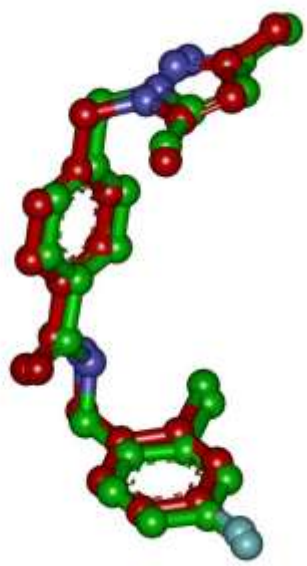

Figure 4.1 Superimposition of the docked ligand (green) and the X-ray structure (red) of heteraryl benzamide derivatives in the binding pocket of InhA.

Figure 4.1 illustrates superimposition of the docked ligand (green) and the X-ray structure (red) of heteraryl benzamide derivatives in the binding pocket of InhA as shown in the Figure 4.2. The results obtained docking binding mode of the heteraryl benzamide derivatives close to the original binding mode found in X-ray crystal structure. For the results of the original X-ray crystal structure, the hydrogen bond interactions were found as the crucial interactions for binding in InhA binding site. At amide (-NH-) interacted with Met98 at 2.07 Å distance and nitrogen atom of 3,5-dimethyl-1*H*-pyrazol-1-yl ring with NAD^+ cofactor at 2.71 Å distance as shown in the Figure 4.2 (a). Moreover, hydrophobic interactions with Phe97, Tyr158, Met161 and Met199 were found. The crucial interactions of heteraryl benzamide derivatives from docked ligand in InhA binding pocket formed the hydrogen bond interactions were found as the crucial interactions between hydrogen atom of amide (-NH-) with Met98 at 1.97 Å distance, the hydroxyl (-OH) group of NAD^+ cofactor at 2.67 Å distance and between the nitrogen atom of 3,5-dimethyl-1*H*-pyrazol-1-yl ring as shown in the Figure 4.2 (b). Moreover, hydrophobic interactions

with Phe97, Tyr158, Met161 and Met199 were found. The crucial interactions of heteraryl benzamide derivatives from X-ray crystal structure and docked in the InhA binding pocket as shown in the Table 4.1.

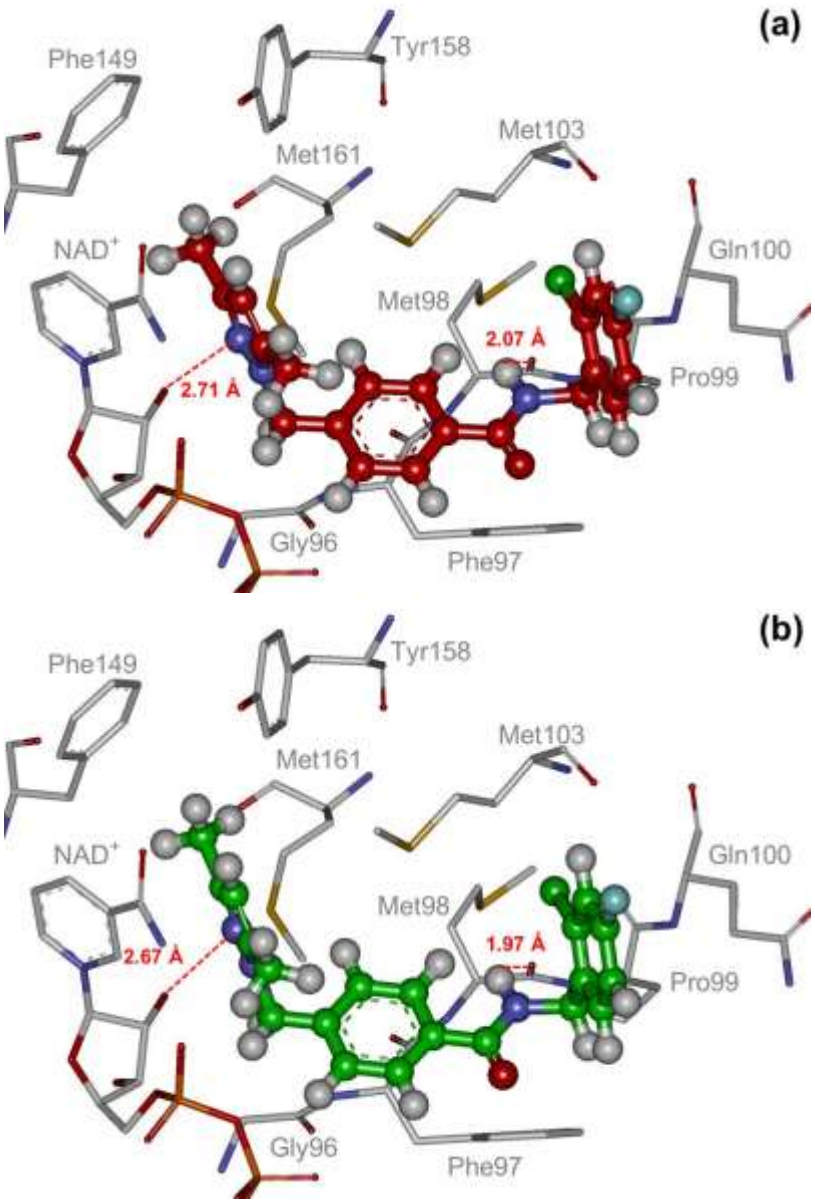

Figure 4.2 X-ray structure of heteraryl benzamide derivatives (red) (a) and docked heteraryl benzamide derivatives (green) (b) in the InhA binding pocket.

Table 4.1 The crucial interactions of heteraryl benzamide derivatives from X-ray crystal structure and docked in the InhA binding pocket

Interactions	Distances (in angstrom (Å)) of heteraryl benzamide derivatives and amino acid residues	
	X-ray crystal structure	**Docking calculation**
Hydrogen bond	Met98: 2.07	Met98: 1.97
	NAD^+: 2.71	NAD^+: 2.67
Hydrophobic interactions	Phe97: 1.85	Phe97: 1.95
	Tyr158: 2.06	Tyr158: 2.04
	Met161: 2.22	Met161: 2.14
	Met199: 2.19	Met199: 1.99

4.1.1.2 Molecular docking analysis of high active compounds

The fourteen compounds including compound **19**, **22**, **17**, **01**, **18**, **15**, **12**, **16**, **11**, **09**, **08**, **21**, **32** and **28** showed high active compounds against InhA inhibitors. Heteraryl benzamide derivatives with biological activities (log ($1/IC_{50}$)) range of 6.60-7.70 were considered as high active compounds as shown in Table 4.2.

Compounds **19** and **22** were considered as high active compounds against InhA inhibitors with biological activities (log ($1/IC_{50}$)) range of 7.70 and 7.40, respectively. Figure 4.3 shows binding orientation of compound **19** and **22** as highest active compounds obtained from molecular docking calculations. In addition, the interaction distances of other highest active compounds are summary in Table 4.2. The docked conformation of compound **19** in InhA binding pocket formed the hydrogen bond interactions were found as the crucial interactions for binding in InhA binding site. At amide (-NH-) interacted with Met98, nitrogen atom of pyridine ring with NAD^+ cofactor and hydrogen bond interactions with Leu207. Moreover, hydrophobic interactions with Phe97, Phe149, Tyr158 and Met161 were observed as shown in Figure 4.3. Compound **22** formed hydrogen bond interactions between amide (-NH-) interacted with Met98, nitrogen atom of pyridine ring with NAD^+ cofactor and hydrogen bond interactions could be formed with Leu207 residue. Moreover, hydrophobic interactions with Phe97, Phe149, Tyr158, Met161 and Met199 were

found. Therefore, the crucial interaction obtained from molecular docking calculations is in agreement with the experimental results that showed the high potency for against InhA inhibitors.

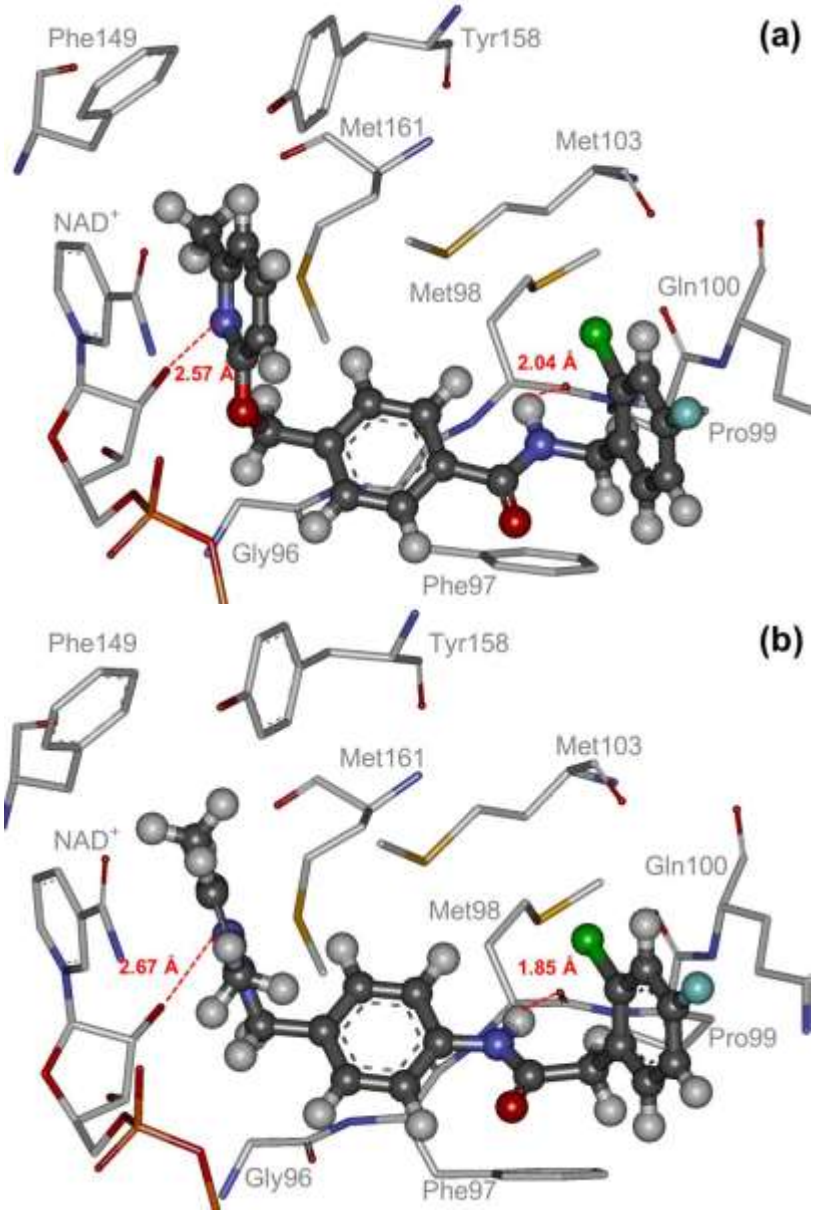

Figure 4.3 Compound 19 (a) and compound 22 (b) as high active compounds in InhA binding pocket.

Table 4.2 Crucial interactions of high active compounds in InhA binding pocket

Cpd.	Distances (in angstrom (Å)) of high active compounds and amino acid residues		
	Hydrogen bond interactions	**Hydrophobic interactions**	**σ-π, π-π interactions**
19	Met98: 2.04 NAD^+: 2.57	Phe97: 2.38 Phe149: 1.97 Tyr158: 1.63 Tys165: 2.05	Phe97 (σ-π) : 4.26 NAD^+ (π-π) : 4.33
22	Met98: 1.86 NAD^+: 2.67	Phe97: 2.06 Phe149: 2.19 Tyr158: 2.26 Met161: 2.29 Met199: 2.31 Leu207: 2.32	NAD^+ (π-π) : 4.52
C 17	Met98: 2.05	Phe97: 1.90 Phe149: 2.01 Tyr158: 1.77 Lys165: 2.29	NAD^+ (π-π) : 4.17
01	Met98: 2.04 Leu207: 2.09 NAD^+: 2.36	Phe97: 1.95 Tyr158: 2.04 Met161: 2.14 Met199: 1.99	NAD^+ (π-π) : 4.56
18	Met98: 2.03	Phe149: 2.34 Tyr158: 1.69 Met199: 1.95	Phe97 (σ-π) : 4.15 Gln100 (σ-π) : 4.13 NAD^+ (π-π) : 4.22

Table 4.2 Crucial interactions of high active compounds in InhA binding pocket (Continued)

Cpd.	Distances (in angstrom (Å)) of high active compounds and amino acid residues		
	Hydrogen bond interactions	**Hydrophobic interactions**	**σ-π, π-π interactions**
15	Met98: 2.423	Tyr158: 2.073 Met161: 2.188 Leu207: 1.523	NAD^+ (π-π) : 4.17
12	Met98: 2.09 NAD^+: 2.35	Phe97: 2.22 Phe149: 2.34 Tyr158: 2.13 Met199: 2.22 Leu207: 2.09	Gln100 (σ-π) : 4.16 NAD^+ (π-π) : 4.87
16	Met98: 1.97	Phe97: 2.24 Met161: 2.05	NAD^+ (π-π) : 4.36
11	Met98: 2.03 Gln100: 2.42 Ala198: 2.38 NAD^+: 2.27	Phe97: 1.30 Tyr149: 1.95 Met161: 2.23 Leu197: 1.92 Leu207: 2.05	Gln100 (σ-π) : 4.23 NAD^+ (π-π) : 4.15
09	Met98: 2.17 NAD^+: 2.33	Phe97: 2.01 Tyr158: 1.97 Met199: 1.92	NAD^+ (π-π) : 4.31
08	Met98: 2.08 Gln100: 2.02 NAD^+: 2.33	Phe97: 2.05 Pro99: 2.38 Tyr158: 2.03 Met199: 1.99 Leu207: 1.53	NAD^+ (π-π) : 4.36

Table 4.2 Crucial interactions of high active compounds in InhA binding pocket (Continued)

Cpd.	Distances (in angstrom (Å)) of high active compounds and amino acid residues		
	Hydrogen bond interactions	**Hydrophobic interactions**	**σ-π, π-π interactions**
21	Met98: 2.02 NAD^+: 2.12	Phe97: 2.39 Tyr158: 2.17 Met161: 1.91 Leu207: 2.35	Phe97 (σ-π) : 4.32 NAD^+ (π-π) : 4.32
32	Met98: 2.03	Phe97: 2.09 Tyr158: 1.86 Met161: 2.13 Leu207: 2.37	NAD^+ (π-π) : 4.16
28	Met98: 2.08 NAD^+: 2.33	Phe149: 2.26 Tyr158: 2.16 Met161: 1.67	NAD^+ (π-π) : 4.01

4.1.1.3 Molecular docking analysis of moderate active compounds

The heteraryl benzamide derivatives of moderate active compounds are compound **03**, **05**, **06**, **34**, **31**, **02**, **23**, **24**, **25**, **36**, **20**, **07**, **13**, **10**, **14** and **35** with the biological activities (log ($1/IC_{50}$)) range 5.80-6.59. The crucial interactions of moderate active compounds were summarized in Table 4.3.

Compounds **25** and **24** were considered as moderate active compounds against InhA inhibitors with biological activities (log ($1/IC_{50}$)) range of 6.00 and 5.92, respectively. The crucial interactions of moderate active compounds were summarized in Table 4.3 and Figure 4.4. The crucial interactions of compound **25** showed that the hydrogen bond interactions of amide (-NH-), hydrogen bond interactions of this substituent with Met98 in the InhA binding pocket were reported and hydrogen bond interactions could be formed between nitrogen atom of 3,5-dimethyl-1*H*-pyrazol-1-yl ring with NAD^+ cofactor. Moreover, hydrophobic

interactions with Phe97, Phe149, Tyr158 and Met199 were observed as shown in Table 4.3. Compound **24** formed three hydrogen bond interactions including oxygen atom of carbonyl (C=O) with Met98 and hydrogen atom of methyl (-CH_3) with NAD^+ cofactor and hydrogen bond interactions could be formed with Met98 and Thr196. Therefore, the crucial interaction obtained from molecular docking calculations is in agreement with the experimental results that shown the moderate potency for against InhA inhibitors.

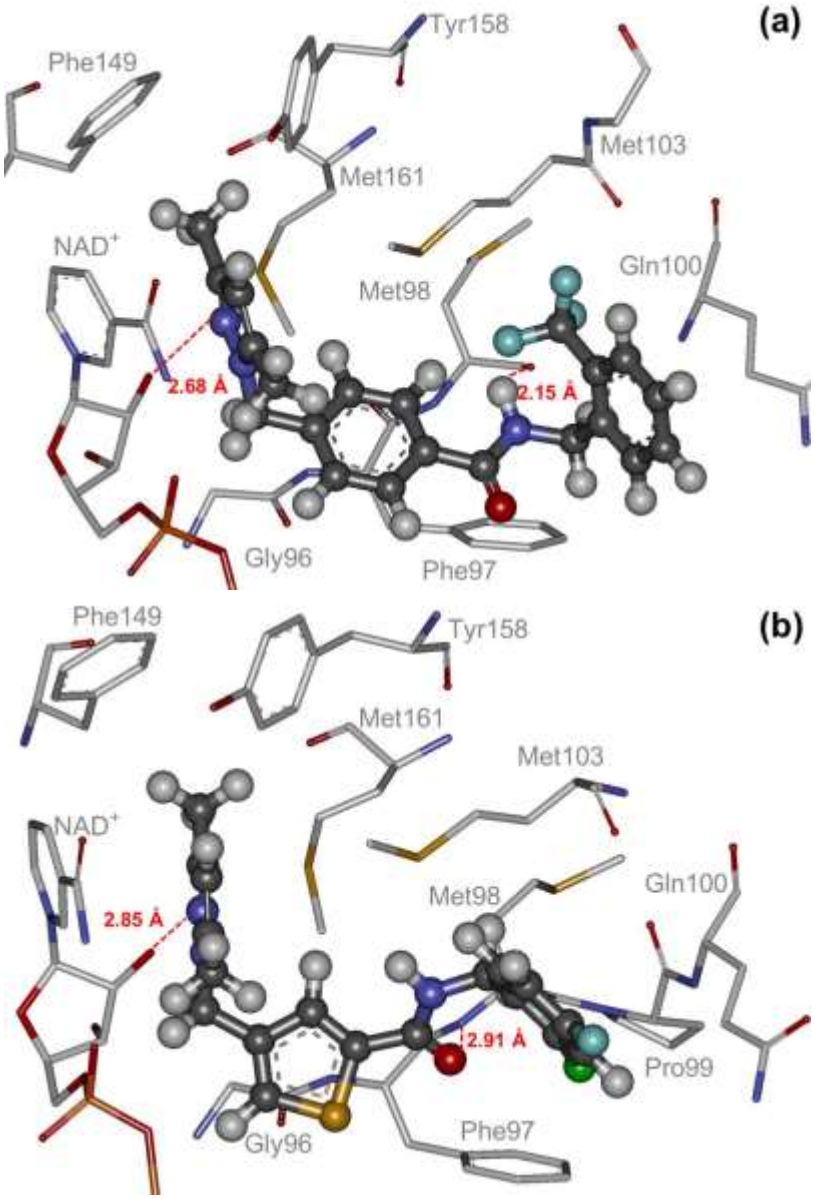

Figure 4.4 Compound 25 (a) and compound 24 (b) as moderate active compounds in InhA binding pocket.

Table 4.3 Crucial interactions of moderate active compounds in InhA binding pocket

Cpd.	Distances (in angstrom (Å)) of moderate active compounds and amino acid residues		
	Hydrogen bond interactions	**Hydrophobic interactions**	**σ-π, π-π interactions**
03	Met98: 1.95 Met103: 2.12 NAD^+: 2.38	Phe97: 2.35 Phe149: 2.33 Tyr158: 2.20 Met161: 2.08 Ala198: 1.98 Met199: 2.03 Ala201: 1.77 Ile202: 2.00 Ala206: 2.25 Leu207: 1.60	NAD^+ (π-π) : 4.15
05	Met97: 2.03 NAD^+: 2.27	Gln100: 2.10 Phe149: 2.33 Tyr158: 2.13 Met161: 2.29 Met199: 2.31 Leu207: 1.70	Gln100 (σ-π) : 4.02 NAD^+ (π-π) : 4.16
06	Met97: 2.09 Met103: 2.16 NAD^+: 2.35	Phe97: 2.26 Tyr158: 198 Met161: 1.95 Met199: 1.99 Leu207: 1.61	NAD^+ (π-π) : 4.17
34	Met98: 2.03 NAD^+: 2.48	Phe97: 2.34 Phe149: 1.95 Tyr158: 1.77 Met161: 2.08	NAD^+ (π-π) : 4.36

Table 4.3 Crucial interactions of moderate active compounds in InhA binding pocket (Continued)

Cpd.	Distances (in angstrom (Å)) of moderate active compounds and amino acid residues		
	Hydrogen bond interactions	**Hydrophobic interactions**	**σ-π, π-π interactions**
31	Met98: 1.92 NAD^+: 2.42	Phe97: 2.29 Tyr158: 0.91 Met161: 1.88 Lys165: 2.40	Phe97 (σ-π) : 4.53 NAD^+ (π-π) : 4.13
02	Met98: 2.08 NAD^+: 2.33	Phe97: 2.38 Tyr158: 2.06 Met161: 2.22 Met199: 2.18 Leu207: 1.83	Gln100 (σ-π) : 4.03 NAD^+ (π-π) : 4.23
23	Met98: 1.94	Phe97: 2.21 Phe149: 1.97 Met199: 2.24 Leu207: 2.33	NAD^+ (π-π) : 4.17
24	Met98: 1.84 NAD^+: 2.38	Tyr158: 2.08 Met199: 1.48 Ile202: 1.74	NAD^+ (π-π) : 4.16
25	Met98: 2.16 NAD^+: 2.37	Phe97: 2.31 Phe149: 2.37 Tyr158: 2.10 Met199: 2.06 Leu207: 2.09	Gln100 (σ-π) : 4.16 NAD^+ (π-π) : 4.51
36	Met98: 1.95	Phe97: 2.16 Tyr158: 2.25 Met199: 2.27 Leu207: 2.33	Phe97 (σ-π) : 4.51 NAD^+ (π-π) : 4.16

Table 4.3 Crucial interactions of moderate active compounds in InhA binding pocket (Continued)

Cpd.	Distances (in angstrom (Å)) of moderate active compounds and amino acid residues		
	Hydrogen bond interactions	**Hydrophobic interactions**	**σ-π, π-π interactions**
20	Met98: 2.01	Phe97: 1.93 Tyr158: 2.13 Leu207: 2.29	NAD^+ (π-π) : 4.16
07	Met98: 2.05 NAD^+: 2.27	Phe97: 2.25 Tyr158: 1.99 Met161: 1.93 Leu207: 1.79	Phe97 (σ-π) : 4.17 Gln100 (σ-π) : 4.17 NAD^+ (π-π) : 4.10
13	Met98: 2.10	Phe97: 1.95 Phe149: 2.40 Tyr158: 2.19	NAD^+ (π-π) : 4.18
10	Met98: 2.04 Met103: 2.02 NAD^+: 2.41	Phe97: 2.13 Tyr158: 2.08 Met199: 2.00 Leu207: 1.77	NAD^+ (π-π) : 4.32
14	Met98: 1.93 NAD^+: 2.37	Tyr158: 2.22 Met161: 1.63 Ala198: 2.36 Met199: 1.50 Ile202: 2.14	Phe97 (σ-π) : 4.51 NAD^+ (π-π) : 4.17
35	Met98: 1.95	Phe97: 2.16 Tyr158: 2.25 Met199: 2.27 Leu207: 2.33	Phe97 (σ-π) : 4.16 NAD^+ (π-π) : 4.26

4.1.1.4 Molecular docking analysis of low active compounds

Nine compounds of heteraryl benzamide derivatives are low active compounds including compound **38**, **26**, **37**, **33**, **30**, **29**, **04**, **27** and **39** with the biological activities (log ($1/IC_{50}$)) range 5.21-5.77. The crucial interactions of low active compounds were summarized in Table 4.4.

Compound **26** and **38** were selected for explaining the binding mode and binding interaction of less active compound with the log ($1/IC_{50}$) was 5.23 and 5.21, respectively. The crucial interactions of less active compounds were summarized in Table 4.4. The crucial interactions of these compounds were shown in Figure 4.5. The results indicate that compound **26** hydrogen bond interactions of amide (-NH-) with Met98 in the InhA binding pocket were reported. Moreover, hydrophobic interactions with Phe97, Tyr158, Met161 and Met199 were found. For compound **38** the result shows that hydrogen bond interactions between nitrogen atom of 3,5-dimethyl-1*H*-pyrazol-1-yl ring with NAD^+ cofactor in the InhA binding pocket. Moreover, hydrophobic interactions with Tyr158, Met161, Ala198, Met199 and Ile202 were found. Therefore, the crucial interaction obtained from molecular docking calculations is in agreement with the experimental results that showed the low potency for against InhA inhibitors.

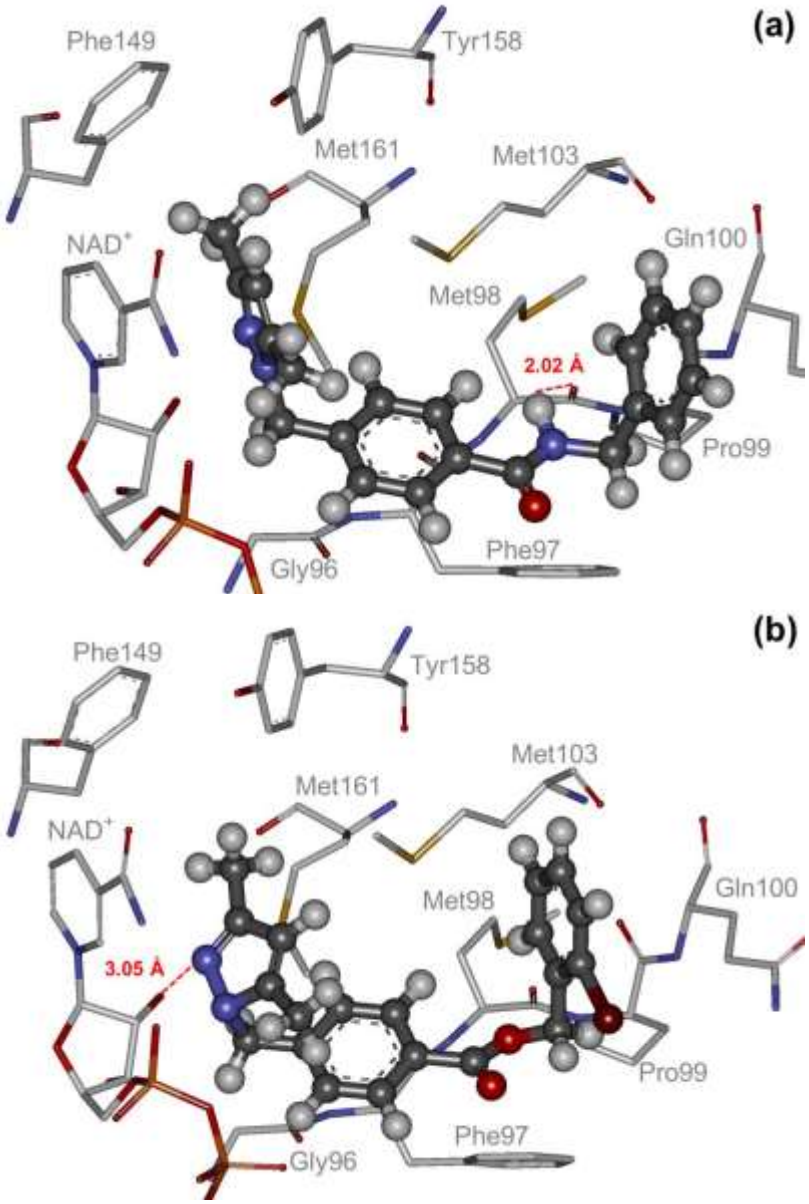

Figure 4.5 Compound 26 (a) and compound 38 (b) as less active compounds in InhA binding pocket.

Table 4.4 Crucial interactions of low active compounds in InhA binding pocket

Cpd.	Distances (in angstrom (Å)) of low active compounds and amino acid residues		
	Hydrogen bond interactions	**Hydrophobic interactions**	**σ-π, π-π interactions**
38	Met98: 2.10 Met103: 2.49 Thr196: 2.15	Tyr158: 1.93 Met161: 2.26 Ala198: 1.49 Met199: 1.35 Ile202: 1.66	Phe97 (σ-π) : 4.66
26	Met98: 2.02 Met103: 2.10 NAD^+: 2.36	Phe97: 2.33 Tyr158: 2.11 Met199: 2.03 Leu207: 1.54	NAD^+ (π-π) : 4.13
37	Met98: 2.10 NAD^+: 2.25	Phe97: 1.95 Tyr158: 1.59 Met161: 1.88 Met199: 1.87	NAD^+ (π-π) : 4.16
33	Met98: 2.10	Phe97: 2.04 Phe149: 1.96 Tyr158: 1.77	NAD^+ (π-π) : 4.17
30	Met98: 2.10	Phe97: 2.02 Tyr158: 2.06 Met161: 2.25 Leu207: 2.22	NAD^+ (π-π) : 4.17
29	Met98: 2.09 NAD^+: 2.25	Tyr158: 2.01 Met161: 2.13 Leu207: 1.86	Phe97 (σ-π) : 4.56 NAD^+ (π-π) : 4.17

Table 4.4 Crucial interactions of low active compounds in InhA binding pocket (Continued)

Cpd.	Distances (in angstrom (Å)) of low active compounds and amino acid residues		
	Hydrogen bond interactions	**Hydrophobic interactions**	**σ-π, π-π interactions**
04	Met98: 2.04 Gln100: 2.21 NAD^+: 2.26	Phe97: 2.38 Phe149: 2.37 Tyr158: 2.11 Met161: 2.08 Ile202: 1.94 Leu207: 1.96	Gln100 (σ-π) : 4.16 NAD^+ (π-π) : 4.16
27	Met98: 2.04 Met103: 2.17 NAD^+: 2.20	Phe149: 2.37 Tyr158: 2.02 Leu207: 1.74	Gln100 (σ-π) : 4.29 NAD^+ (π-π) : 4.27
39	Met98: 1.94 Gln100: 3.12 NAD^+: 2.33	Phe97: 1.99 Phe149: 2.22 Tyr158: 2.28 Met199: 2.26	NAD^+ (π-π) : 4.26

4.1.1.5 Summaries of the crucial interactions of InhA inhibitor from molecular docking calculations

Based on the molecular docking calculations results, the structural concept of heteroaryl benzamide derivatives is of key importance for binding in InhA binding pocket as summarized in Figure 4.6. Therefore, this fragment is crucial for favorable IC_{50} values. Among all nitrogen atom of pyridine ring and 3,5-dimethyl-1*H*-pyrazol-1-yl ring has hydrogen bond interaction with hydroxyl group of NAD^+ cofactor because this ring is near NAD^+ cofactor in InhA binding pocket. The hydrogen atom of amide (-NH-) group of all structures has hydrogen bond interaction with backbone of Met98. Moreover, benzene ring in the central part has

hydrophobic interactions with Gly96 and Phe97, and pyridine ring and 3,5-dimethyl-1*H*-pyrazol-1-yl ring have hydrophobic interactions with Phe149, Tyr158, Met161 and Met199 in InhA binding pocket.

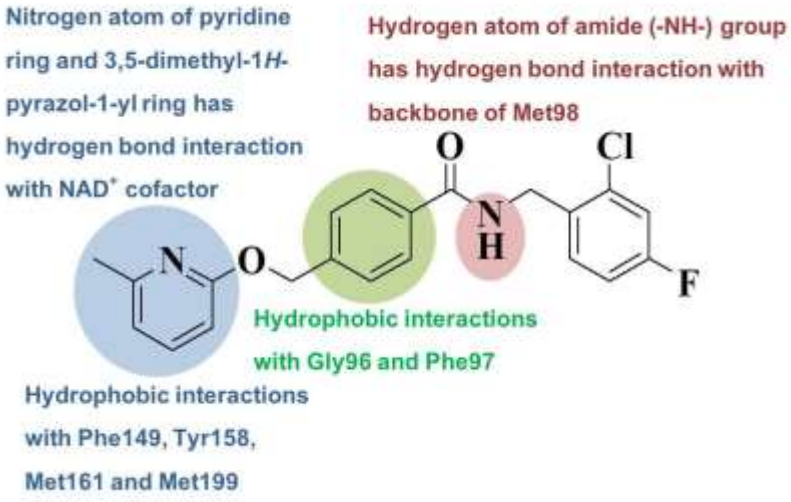

Figure 4.6 Structural concept for good IC_{50} correlation of heteroaryl benzamide derivatives summarized from molecular docking calculations.

4.1.2 Molecular dynamics simulations of heteraryl benzamide derivatives

4.1.2.1 Structural stability during molecular dynamics (MD) simulations

To evaluate the reliable stability of the MD trajectories, the RMSDs for all atoms of InhA, NAD^+ cofactor and heteraryl benzamide derivatives relative to the initial minimized structure over the 30 ns of simulation times were calculated and plotted in Figure 4.7. There are three solute species in each MD system including InhA, NAD^+ cofactor and inhibitor. The plateau characteristic of the RMSD plot over the simulation time is the criteria to indicate the equilibrium state of each solute species. For the equilibrium state of each MD system, the RMSD plots of all solute species have to reach the plateau characteristic. InhA, NAD^+ cofactor and inhibitor in each system reach the equilibrium state at a different time. For the system of heteraryl benzamide derivatives and NAD^+ cofactor reach equilibrium at an early time point, whereas InhA reaches the equilibrium state after 5 ns. Therefore, after 5 ns the RMSD plots of all solute species reach the plateau characteristic, indicating the equilibrium state of this MD system. The RMSD plots of these compounds over 30 ns

showed large fluctuations in the range of about 0.5-3.0 Å. Therefore, the data in terms of binding free energy, interaction energy and structure of each system after an equilibrium state were analyzed.

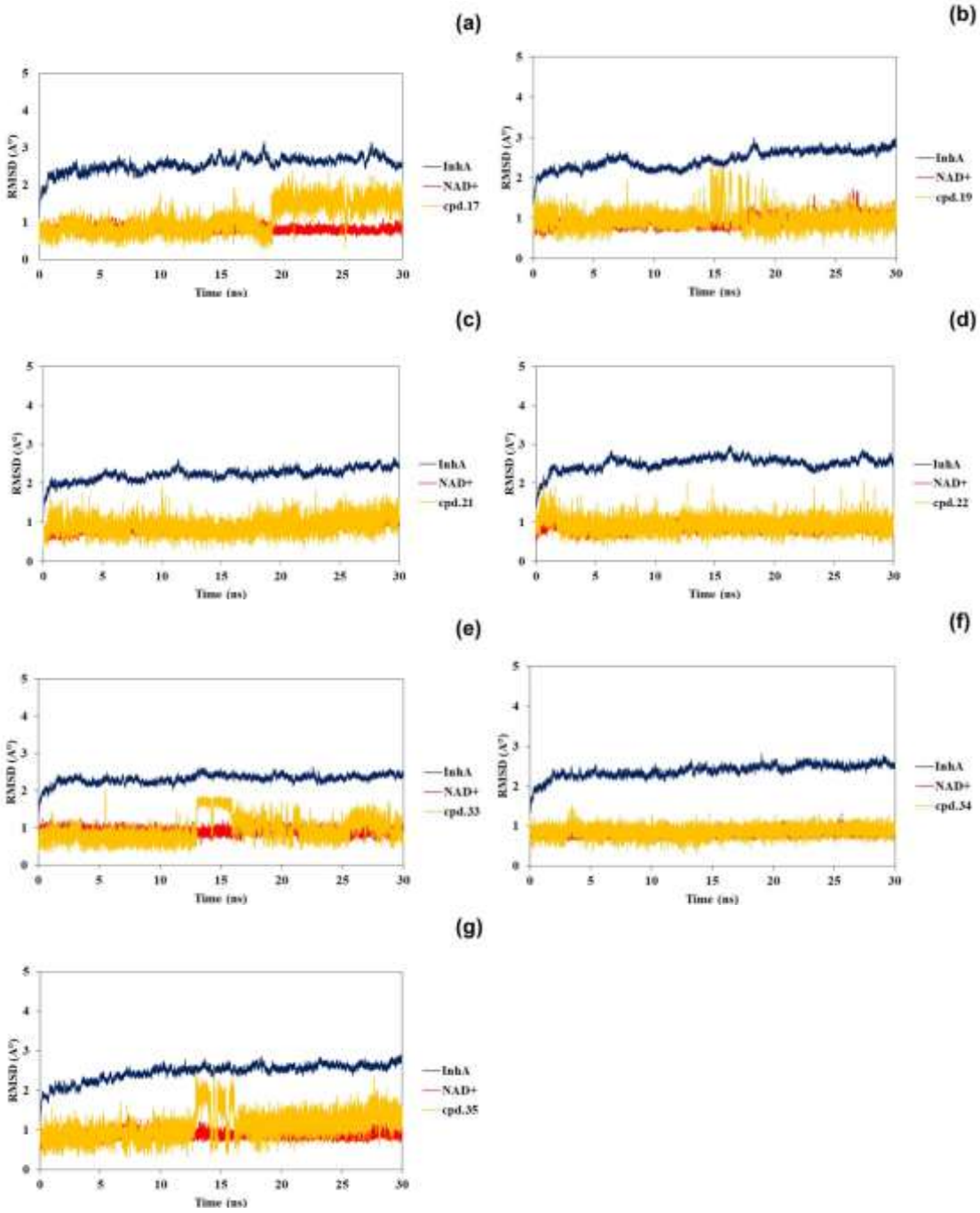

Figure 4.7 RMSDs of heteraryl benzamide derivatives, compounds 17 (a), 19 (b), 21 (c), 22 (d), 33 (e), 34 (f) and 35 (g) complexed with the InhA.

4.1.2.2 Binding free energy calculations

To confirm that the result obtained from MD simulations was reliable to predict the binding mode and binding interactions of inhibitor complexed with InhA, binding free energy calculations were performed. The binding free energies of the selected compounds were calculated by the Molecular Mechanics Poisson Boltzmann Surface Area (MM-PBSA) method. The comparison between the experimental binding free energies (ΔG_{exp}) and the calculated binding free energies (ΔG_{cal}) of selected compounds are shown in Table 4.5 and Figure 4.8. The calculated binding free energy derived from MM-PBSA method was closed to experimental binding free energy. The correlations coefficient (r^2) between the experimental binding free energy and calculated binding free energy shown good linear correlation with $r^2 = 0.8642$. These results could be confirmed that the obtained structures from MD simulations were reliable. Therefore, the binding mode and crucial binding interactions of inhibitors in InhA binding pocket were further analyzed.

Table 4.5 Binding free energies in kcal/mol computed by the MM-PBSA method (n=100 snapshot)

Compound	IC_{50} (μM)	ΔH	TΔS	ΔG_{cal}	ΔG_{exp} [a]
17	0.05	-31.26±3.61	-21.82±5.47	-9.45±3.85	-10.03
19	0.02	-30.34±3.03	-20.05±4.43	-10.29±3.62	-10.57
21	0.19	-29.61±3.48	-21.00±4.85	-8.61±3.67	-9.23
22	0.04	-38.93±3.22	-28.41±4.58	-10.52±3.51	-10.16
33	3.40	-34.07±3.33	-26.35±6.33	-7.72±5.22	-7.51
34	1.55	-39.88±4.00	-31.60±5.22	-8.28±4.01	-7.98
35	0.26	-34.75±3.36	-25.52±4.69	-9.23±3.56	-9.04

[a] derived from ΔG_{exp}=RT ln[activity], where activity is the activity against InhA expressed in IC_{50}. R represents the gas constant (1.988 cal/mol K), T represents the temperature (300 K)

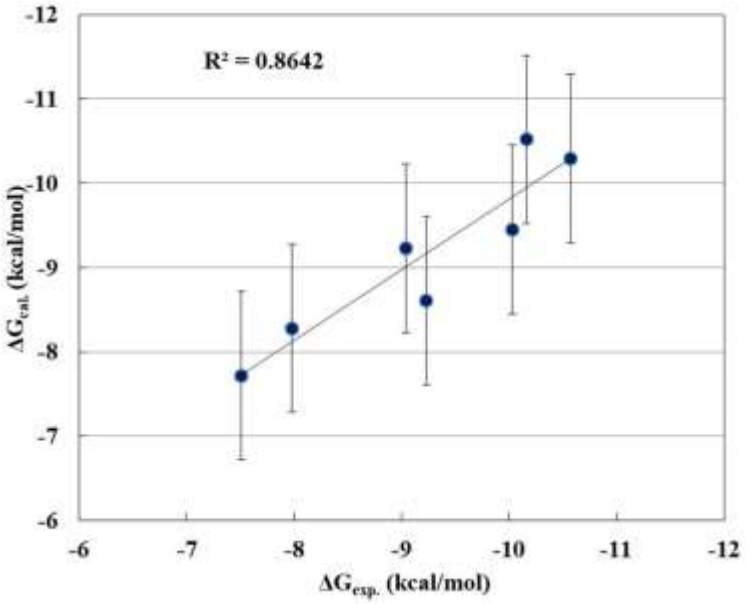

Figure 4.8 Correlation of binding free energy obtained from experimental and binding free energy obtained from calculation using MM-PBSA method.

4.1.2.3 Binding mode and binding interaction analysis of InhA inhibitor

1) Binding mode and binding interaction of picolinamide and *N*-phenylformamide

The picolinamide in compound **21** with IC_{50} 0.19 µM lead to approximately of InhA inhibition compared to *N*-phenylformamide in compound **22** with IC_{50} 0.04 µM. The results indicate that compound **21** hydrogen bond interactions of amide (-NH-) with Met98 at 2.13 Å distance. The nitrogen atom of 3,5-dimethyl-1*H*-pyrazol-1-yl ring with NAD^+ cofactor at 2.82 Å distance in the InhA binding pocket were reported. Moreover, hydrophobic interactions were found with Met161 residue. For compound **22** the result shows that hydrogen bond interactions between hydrogen atom of amide (-NH-) with Met98 at 1.85 Å distance in the InhA binding pocket. Moreover, hydrophobic interactions with Met161, Ala198 and Ala201 were found. The orientation of picolinamide of compound **21** in the pocket was different from that observed for *N*-phenylformamide in compound **22** was shown in Figure 4.9. Therefore, the crucial interaction obtained from based on MD simulations is in

agreement with the experimental results that shown the high potency for against InhA inhibitors.

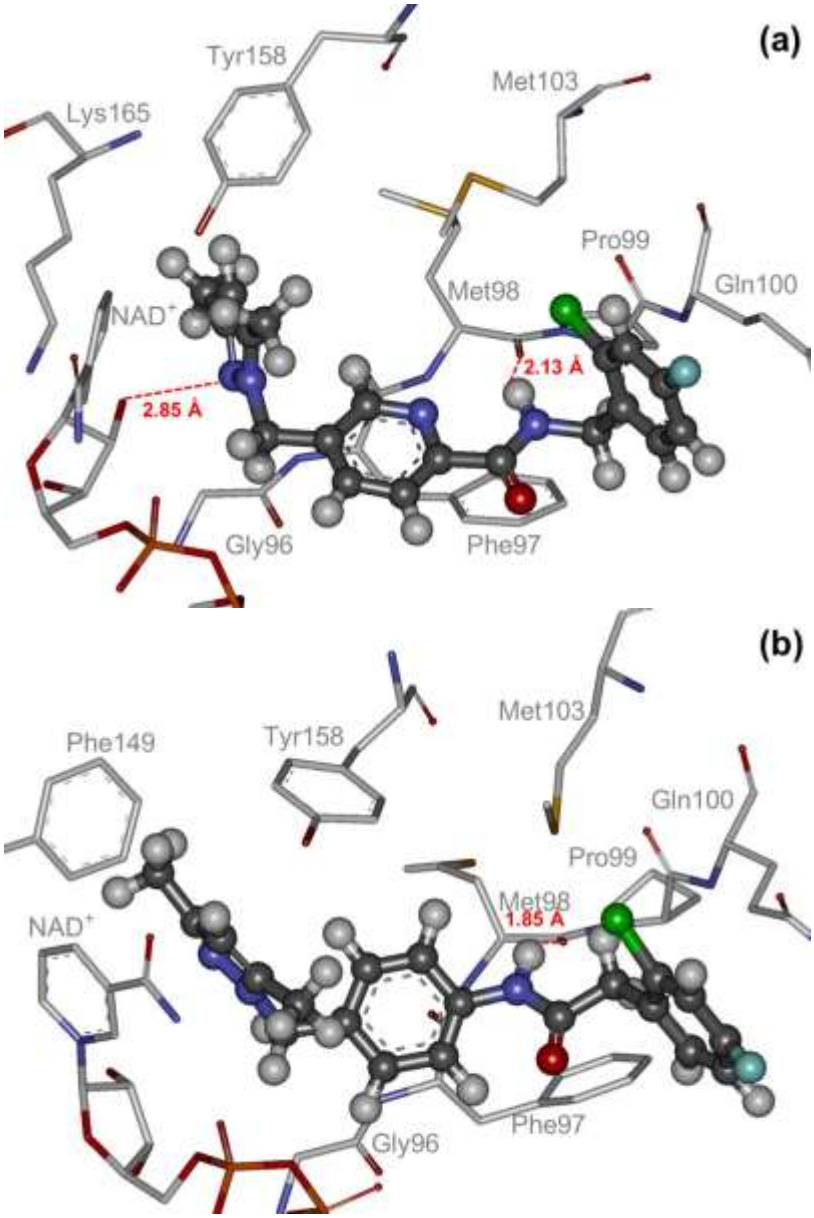

Figure 4.9 Binding modes and binding interactions of compound 21 (a) and compound 22 (b) in the InhA binding pocket derived from MD simulations.

The effect of picolinamide and *N*-phenylformamide to clearly revealed the reason for this significant difference in IC_{50} values of compound **21** and compound **22** by investigating of the total interaction energies between InhA residues and the compounds. Figure 4.10 shows the total interaction energies for all InhA residues. The values of total interaction energies of compound **21**, compound **22** are -45.13 and -48.03 kcal/mol, respectively. It can explain the trend of the IC_{50} values of the two compounds. The Figure 4.10 (a) demonstrates that the compound **21** interacts most strongly with Phe97, Met98, Gln100, Met161 and NAD^+ cofactor, compound are more attractive with energies of -4.60, -3.82, -3.61, -4.08 and -12.89 kcal/mol, respectively. In addition, it is elucidated from Figures 4.10 (b) that the compound **22** have interacts most strongly with Phe97, Met98, Gln100, Met161, Ala198 and NAD^+ cofactor are -4.53, -4.48, -3.84, -4.24, -3.13 and -11.62 kcal/mol, respectively. The NAD^+ cofactor interact strongly with both the compounds. Therefore, we concluded that NAD^+ cofactor, Met98 and Phe97 are important for the binding between InhA and the heteroaryl benzamide derivatives.

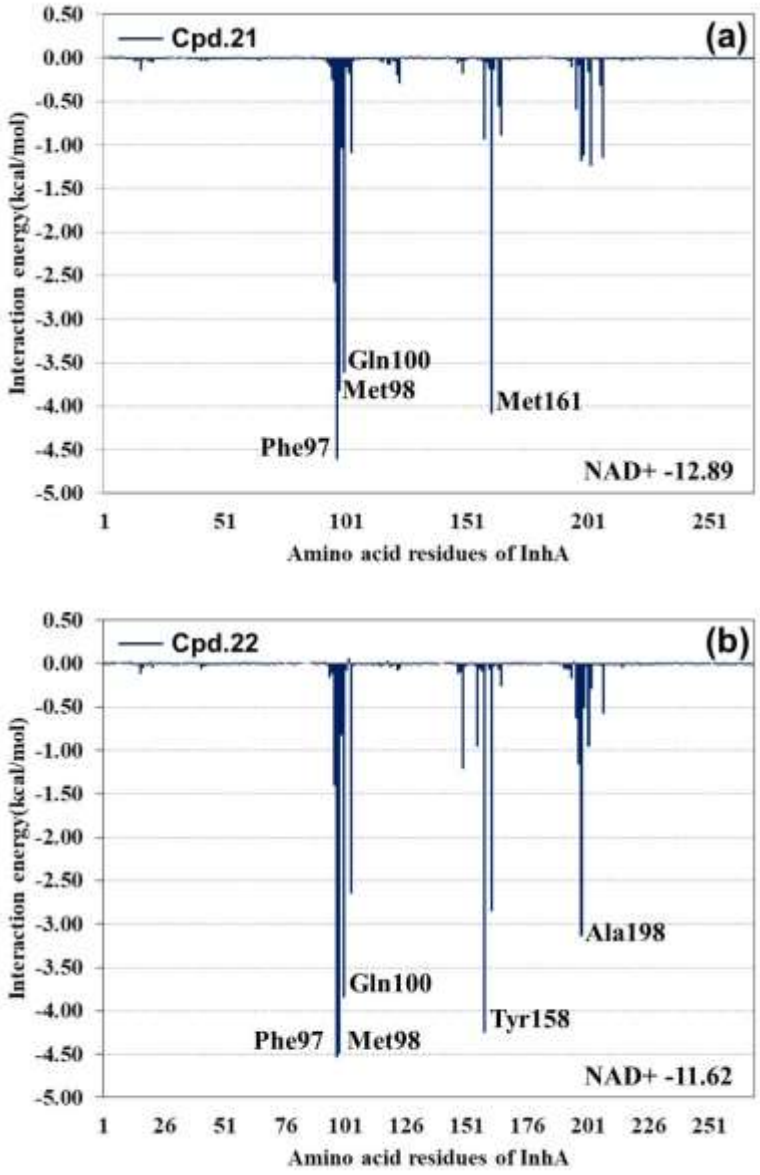

Figure 4.10 Interaction energies per-residues of InhA with compound 21 (a) and compound 22 (b).

2) Binding mode and binding interaction of monoatomic linker between benzene ring and pyridine ring

Among these derivatives selected two types of the heteroayl benzamide derivatives. Only the monoatomic linker between benzene ring and pyridine rings is different in the two compounds. However, their IC_{50} values are significantly different to each other; 0.05 μM for the compound **17** and 3.40 μM for

the compound **33**. The chain between benzene ring and pyridine ring compared in compound **17** is methane (-CH_2-) and oxygen atom (-O-) in compound **33**. The difference of binding mode and binding interaction of linker between benzene ring and pyridine ring produced different position of inhibitors from MD simulations are shown in Figure 4.11. Interactions of compound **17** in InhA binding pocket formed the hydrogen bond interactions were found as the crucial interactions for binding in InhA binding site. At hydrogen atom of pyridine ring with NAD^+ cofactor at 2.88 Å distance. Moreover, hydrophobic interactions with Leu197 and Ala201 were found. For compound **33** the result shows that hydrogen bond interactions between nitrogen atom of amide (-NH-) with Met98 at 2.09 Å distance in the InhA binding pocket, hydrophobic interaction with Tyr158 and Leu207. From this result, to enhance the biological activity of heteraryl benzamide derivatives can be concluded that all, the linker between benzene ring and pyridine ring is short linker and have hydrophilic group. Therefore, the crucial interaction obtained from MD simulations is in agreement with the experimental results that showed the high potency for against InhA inhibitors.

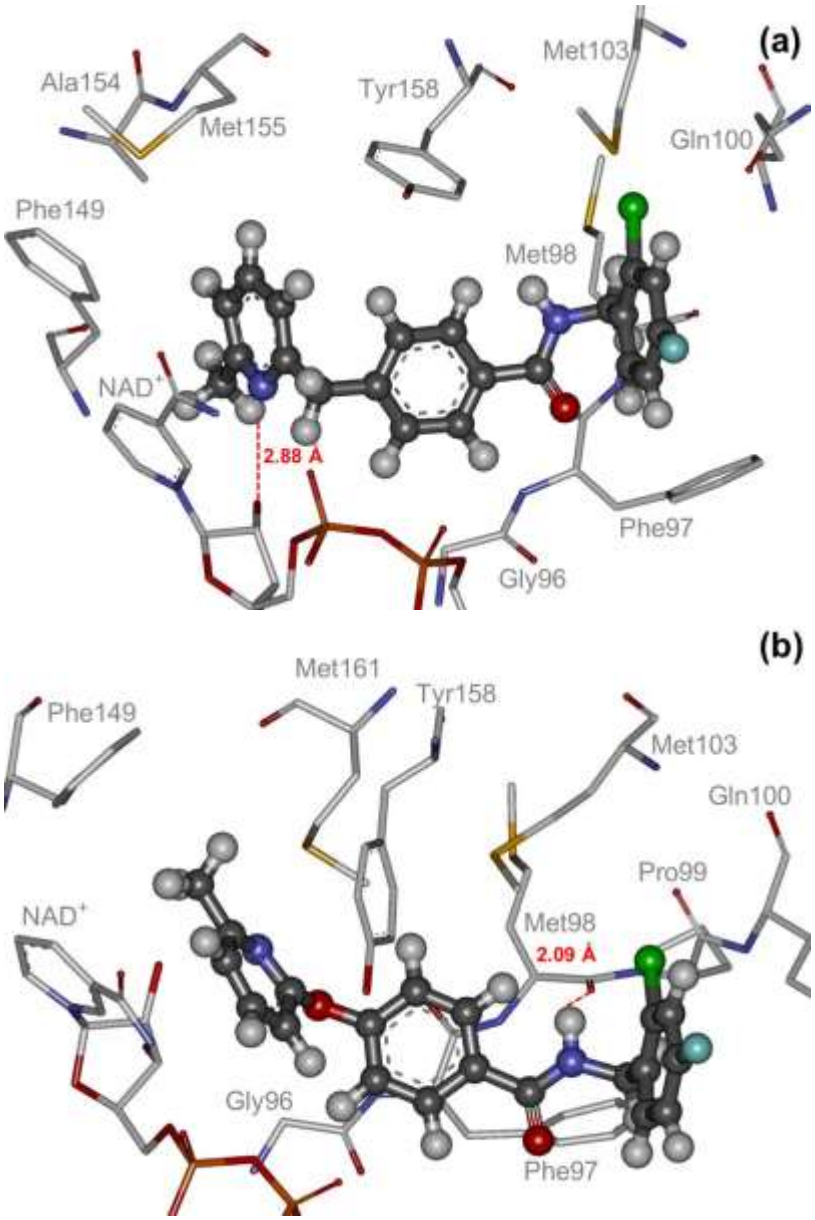

Figure 4.11 Binding modes and binding interactions of compound 17 (a) and compound 33 (b) in the InhA binding pocket derived from MD simulations.

3) Binding mode and binding interaction of diatomic linker between benzene ring and pyridine ring

The diatomic linker between benzene ring and pyridine ring compared in compound **19** is methanone (-OCH_2-) with IC_{50} 0.02 µM, methylthio (-SCH_2-) in compound **35** with IC_{50} 0.26 µM and ethane (-CH_2CH_2-) in compound **34** with IC_{50} 1.55 µM. The difference of binding mode and binding interaction of linker between benzene ring and pyridine ring produced different position of inhibitors from MD simulations are shown in Figure 4.12. Compound **19** formed hydrogen bond interactions between hydrogen atom of ethanone (-OCH_2-) chain interacted with Gly96 and hydrogen bond interaction with NAD^+ cofactor at 2.53 and 2.48 Å distance, respectively. Moreover, hydrophobic interactions with Tyr158, Met161 and Ala198 were found. The compound **35** has hydrogen bond interaction between hydrogen atom of amide (-NH-) group with Met98 residue at 2.37 Å distance. Moreover, hydrophobic interactions with Met161 and Ile202 residues were found. The last interactions of compound **34** in InhA binding pocket formed the hydrogen bond interactions were found as the crucial interactions for binding in InhA binding site. At hydrogen atom of amide (-NH-) group with Met98 residue at 2.21 Å distance. Moreover, hydrophobic interactions with Phe149 and Met199 were found. From this result, to enhance the biological activity of heteraryl benzamide derivatives it can be concluded that the diatomic linker between benzene ring and pyridine ring is short linker and have hydrophilic group. Therefore, the crucial interaction obtained from MD simulations is in agreement with the experimental results that shown the high potency for against InhA inhibitors.

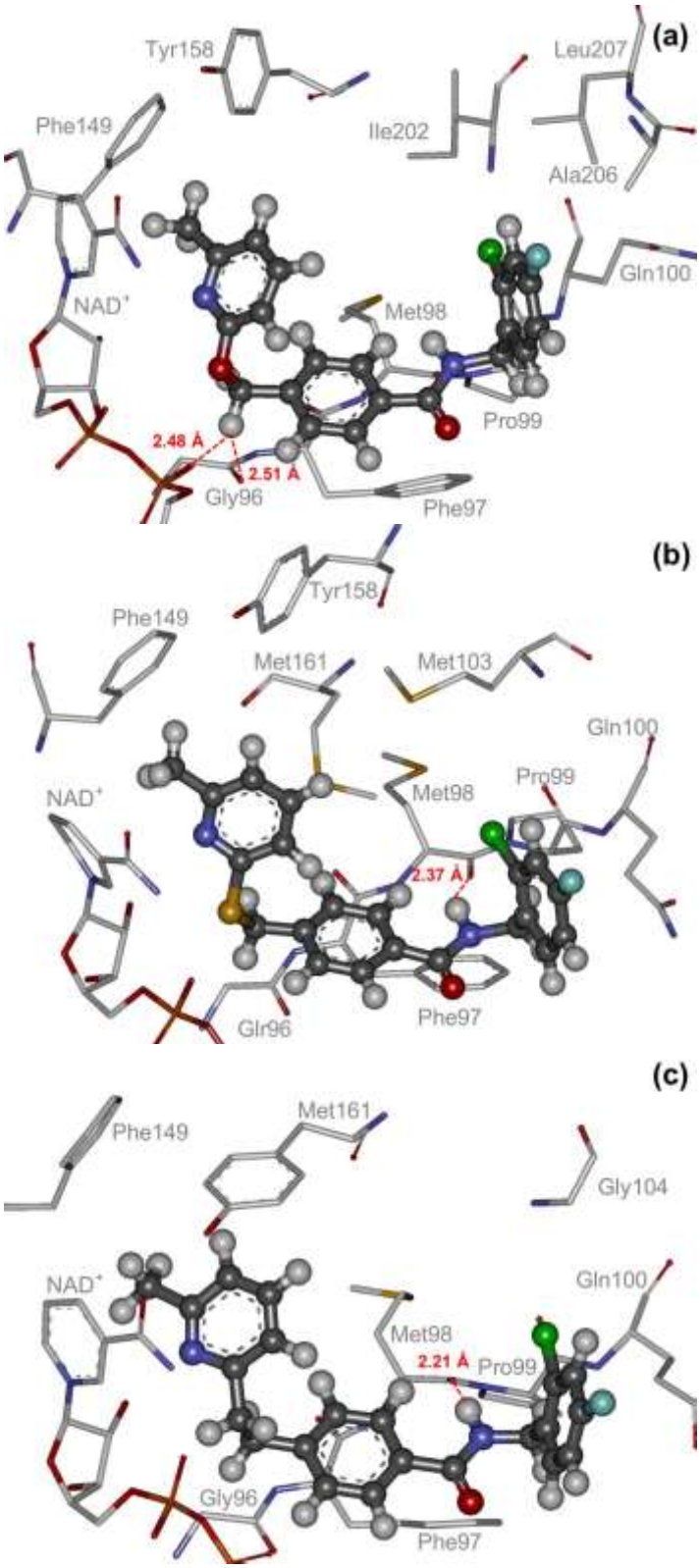

Figure 4.12 Binding modes and binding interactions of compound 19 (a), compound 35 (b) and compound 34 (c) in the InhA binding pocket derived from MD simulations

The effect of diatomic linker between benzene ring and pyridine ring compared in compound **19** is methanone (-OCH_2-), methylthio (-SCH_2-) in compound **35** and ethane (-CH_2CH_2-) in compound **34** to clarify the reason for this significant difference in IC_{50} values of compounds, investigated the total interaction energies between InhA residues and the compounds. Figure 4.13 (a) shows the total interaction energies for all InhA residues. The compound **19** interacts most strongly with Phe97, Met98, Gln100, Met103 and NAD^+ cofactor, compound are more attractive with energies of -4.11, -3.29, -3.37, -3.18 and -10.67 kcal/mol, respectively. In addition, it is elucidated from Figures 4.13 (b) that the compound **35** have interacts most strongly with Phe97, Met98, Gln100, Met161, Ala198 and NAD^+ cofactor are -3.64, -3.56, -3.60, -3.68, -3.14 and -9.30 kcal/mol, respectively. The NAD^+ cofactor interact strongly with both the compounds. Therefore, we concluded that NAD^+ cofactor, Met98 and Phe97 are important for the binding between InhA and the derivatives. The lase interactions of compound **34** in InhA residues have interacts energies with Phe97, Met98, Gln100, Met103, Met161, Ala198 and NAD^+ cofactor as shown in Figures 4.13 (c). The compound is more attractive with energies of -4.30, -3.80, -3.46, -3.79, -4.24, -3.62 and -10.17 kcal/mol, respectively. In addition, the distance between the benzene ring and the pyridine ring is shortened by the replacement, resulting in the separation of the pyridine ring from NAD^+ cofactor. In addition, as shown in Figure 4.12, the distance between the compound **34** and Met98 is significantly longer than that between the compound **35** and compound **19** have two hydrogen bond interactions with Gly96 and NAD^+ cofactor. Therefore, it is concluded that the -OCH_2- group of the compound **19** is important for the strong binding between InhA and the compound **19**.

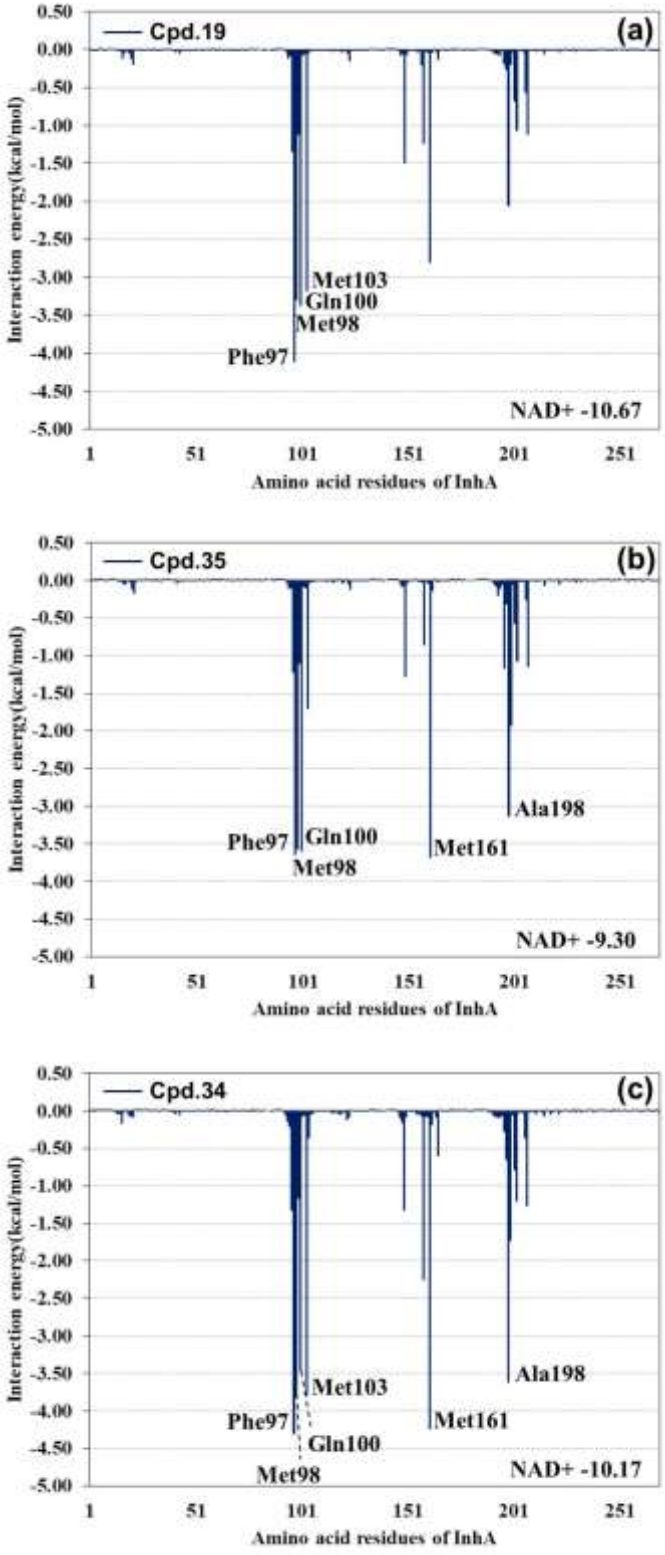

Figure 4.13 Interaction energies per-residues of InhA with compound 19 (a), compound 35 (b) and compound 34 (b).

4.1.2.4 Summaries of the crucial interactions of InhA inhibitor from molecular dynamics simulations

Based on the molecular dynamics simulations results, it can be concluded that the structural concept of heteroaryl benzamide derivatives that favor for binding interactions in InhA binding pocket summarized in Figure 4.14. Therefore, this fragment is crucial for favorable IC_{50} values. In the central part of heteroaryl benzamide derivatives, the picolinamide have hydrogen bond interactions between hydrogen atom of amide (-NH-) with backbone of Met98 and nitrogen atom of pyridine ring and 3,5-dimethyl-1*H*-pyrazol-1-yl ring has hydrogen bond interaction with NAD^+ cofactor, the *N*-phenylformamide has hydrogen bond between hydrogen atom of amide (-NH-) with backbone of Met98. Moreover, the central part of heteroaryl benzamide derivatives at picolinamide and *N*-phenylformamide have hydrophobic interactions with Met161, Ala198 and Ala201. At the atomic linker between benzene ring and pyridine ring should have diatomic linker, high electronegativity and hydrophilic group such as compound **19**, the diatomic linker between benzene ring and pyridine ring is methanone (-OCH_2-) have hydrogen bond interactions between hydrogen atom of diatomic linker with Gly96 and NAD^+ cofactor. Moreover, benzene ring in the central part have hydrophobic interactions with Gly96 and Phe97, and pyridine ring have hydrophobic interactions with Phe149, Tyr158, Met161 and Met199 in InhA binding pocket.

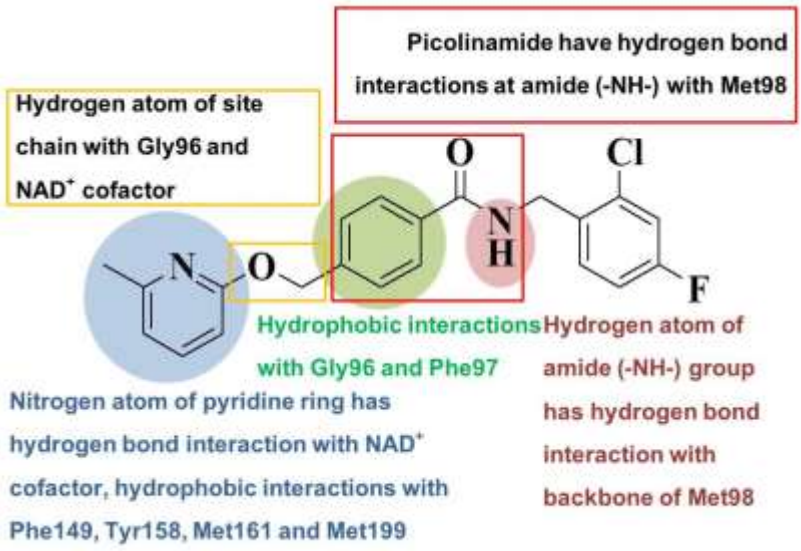

Figure 4.14 Structural concept for good IC_{50} correlation of heteroaryl benzamide derivatives summarized from molecular dynamics simulations.

4.1.3 Quantitative Structure Activity Relationship Analysis of heteraryl benzamide derivatives

4.1.3.1 CoMSIA model

The statistical parameters of CoMSIA model generated based on docking alignment illustrated in Table 4.6. The CoMSIA analyses using different combinations of steric, electrostatic, hydrophobic, hydrogen donor and hydrogen acceptor fields were added to give more specific properties of interactions between inhibitors and the enzyme target. CoMSIA model with the different combined fields were built up. Based on better statistical values and more descriptor variables, the model containing steric, electrostatic, hydrophobic and hydrogen acceptor fields was selected as the best CoMSIA model for prediction. This CoMSIA model exhibits highly predictive with r_{cv}^2 and r^2 of 0.50 and 0.96, respectively. CoMSIA model, the contribution of steric, electrostatic, hydrophobic and hydrogen acceptor fields is 10.00%, 39.50%, 31.60% and 18.90%, respectively, indicating that the electrostatic fields show greater influence on inhibitory activity than others.

Table 4.6 The statistical parameters of CoMSIA model of heteraryl benzamide derivatives

Model	Statistical parameters						
	r_{cv}^2	r^2	N	S_{press}	SEE	F	Fraction
S/E	0.45	0.94	6	0.60	0.20	54.74	19.00/81.00
S/H	0.18	0.95	3	0.68	0.18	72.48	19.30/80.70
S/A	0.18	0.92	3	0.68	0.22	43.46	50.50/49.50
S/D	-0.05	0.77	3	0.77	0.38	12.33	63.00/37.00
S/E/H	0.49	0.96	6	0.57	0.16	90.11	11.00/51.00/37.80
S/E/A	0.50	0.95	6	0.57	0.18	66.97	16.40/57.50/26.10
S/E/D	0.34	0.91	6	0.65	0.24	38.95	13.40/70.10/16.60
S/E/H/A	**0.50**	**0.96**	**5**	**0.56**	**0.15**	**100.61**	**10.00/39.50/31.60/18.90**
S/E/H/D	0.47	0.97	6	0.59	0.14	117.38	7.90/43.80/33.70/14.70
S/E/H/A/D	0.47	0.97	6	0.59	0.14	117.68	7.10/34.30/26.80/17.20/14.60

Bold values indicate the best CoMSIA model. r_{cv}^2, leave-one-out (LOO) cross-validated correlation coefficient; r^2, non-cross-validated correlation coefficient; N, optimum number of components; S_{press}, Standard error of prediction, SEE, standard error of estimate; F, F-test value; S, steric field; E, electrostatic field; H, hydrophobic field; A, hydrogen acceptor field and D, hydrogen donor field

4.1.3.2 Validation of the CoMSIA model

The experimental and calculated activities for the training set derived from the best CoMSIA model are given in Table 4.6 and the correlations between experimental and calculated activities are shown in Figure 4.15. In the order to verify the predictive ability of the obtained model, the biological activities of the test set were predicted by CoMSIA model. All test set compounds shown predicted values with in one logarithmic unit difference from the experimental values as presented in Table 4.7. These results show that CoMSIA model are low accuracy for predicting the inhibitory activity.

Table 4.7 The experimental and calculated activities of the training set from CoMSIA model

Compound	log(1/IC_{50})		
	Experimental	CoMSIA model	
		Calculated	Residues
01[b]	7.30	-	-
02	5.90	5.84	0.06
03	5.80	5.77	0.03
04	5.60	5.52	0.08
05	5.80	5.56	0.24
06	5.80	5.54	0.26
07	6.27	6.11	0.16
08	6.92	6.92	0.00
09[a]	7.05	7.09	-0.04
10[b]	6.46	-	-
11	7.05	6.14	0.91
12	7.10	6.77	0.33
13	6.30	6.77	-0.47
14	6.49	6.78	-0.29
15	7.22	6.52	0.70
16[a]	7.05	6.21	0.84
17	7.30	6.83	0.48
18	7.22	6.86	0.36
19	7.70	7.11	0.59
20	6.26	6.69	-0.43
21	6.72	6.21	0.52
22	7.40	6.31	1.09
23	5.92	6.29	-0.37
24	5.92	5.74	0.18

[a]test set, [b]outlier of CoMSIA model

Table 4.7 The experimental and calculated activities of the training set from CoMSIA model (Continued)

Compound	log(1/IC_{50})		
	Experimental	CoMSIA model	
		Calculated	Residues
25	6.00	6.37	-0.37
26	5.23	5.72	-0.49
27[a]	5.60	6.89	-1.29
28	6.60	6.37	0.23
29	5.51	6.03	-0.52
30	5.49	6.11	-0.62
31[a]	5.85	6.58	-0.73
32	6.60	6.88	-0.28
33[b]	5.47	-	-
34[b]	5.81	-	-
35[a]	6.59	5.20	1.39
36	6.24	6.84	-0.60
37	5.30	6.37	-1.07
38	5.21	4.84	0.37
39[a]	5.77	6.15	-0.38

[a]test set, [b]outlier of CoMSIA model

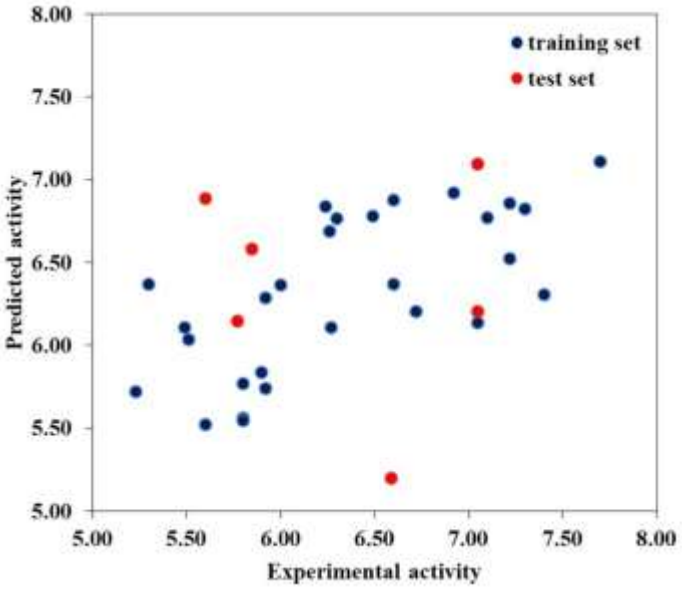

Figure 4.15 Plots between the experimental and predicted activities of training and test sets from CoMSIA model.

4.1.3.3 CoMSIA contour maps

To easily visualize the importance of steric, electrostatic, hydrophobic and hydrogen acceptor fields, CoMSIA contour maps were demonstrated as shown in Figures 4.16. CoMSIA steric contours, green and yellow contours indicate favorable and unfavorable areas, respectively. CoMSIA electrostatic contours, blue and red contours indicate favorable electropositive and electronegative regions, respectively. For CoMSIA hydrophobic contour, yellow and white contours represent the favorable and unfavorable hydrophobic regions, respectively. For CoMSIA hydrogen acceptor contour, magenta and red contours represent the favorable hydrogen acceptor group and unfavorable hydrogen acceptor group, respectively.

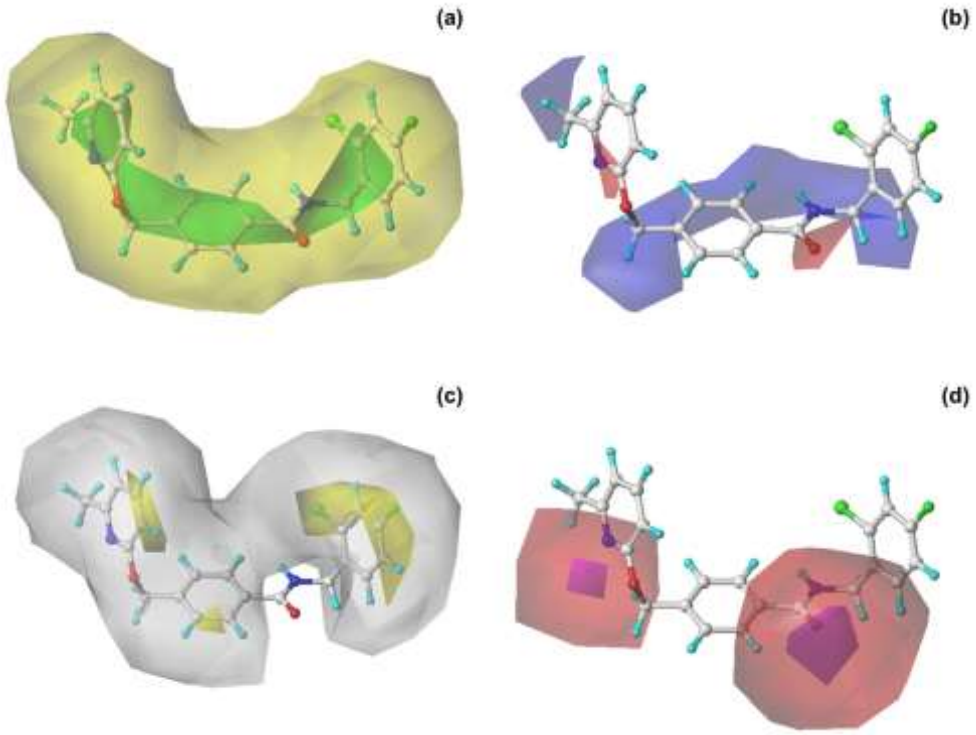

Figure 4.16 Steric (a), Electrostatic (b), Hydrophobic (c) and Hydrogen bond acceptor (d) CoMSIA contours in combination with compound 19.

From Figure 4.16, in this case the CoMSIA model shown big contours maps of steric hydrophobic and hydrogen bond acceptor fields because they are lower than 0.60 of leave-one-out (LOO) cross-validated correlation coefficient (r_{cv}^2). Therefore CoMSIA contour maps in this case can not explain the structural requirement obtained from CoMSIA model to improve the biological activity against InhA.

Electrostatic contour map, red contour, appeared at the oxygen atom of carbonyl (C=O) group and nitrogen atom of pyridine ring indicated that electron withdrawing group of this fragment was required. Moreover, blue contour appeared at methyl ($-CH_3$) group of pyridine ring indicated that electron donating group of this fragment was required. For example compound **32** ($\log(1/IC_{50}) = 6.60$) shown the biological activity lower than compound **17** ($\log(1/IC_{50}) = 7.30$) due to compound **17** has 2-methylpyridine group shown more electron donating group than 2-trifluoropyridine group of compound **32**, respectively. It indicates that negative

charge properties referred to electron withdrawing substituent was required to design new and more potent activity of InhA inhibitor as anti-tuberculosis agents.

4.1.3.4 The structural requirement obtained from CoMSIA model to improve the biological activity against InhA should be as following;

(1) At the oxygen atom of carbonyl (C=O) group and nitrogen atom of pyridine ring, electron withdrawing group of this fragment was required.

(2) At methyl (-CH_3) group of pyridine ring, the electron donating group of this fragment was required.

The results can be concluded that the structural requirements of heteroaryl benzamide derivatives that favor for binding interactions in the InhA binding pocket and aid to design new and more potent heteroaryl benzamide derivatives as anti-tuberculosis agents.

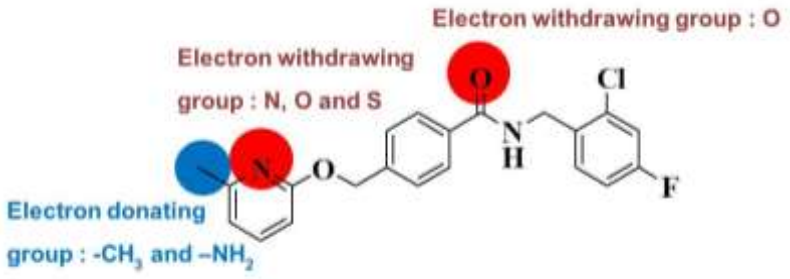

Figure 4.17 The structural requirement of heteroaryl benzamide derivatives in binding pocket obtained from 3D-QSAR study.

4.1.4 The structural concept for good IC_{50} correlation based on the integrated results from molecular dynamics simulations and 3D-QSAR CoMSIA model

Based on the molecular dynamics simulations and 3D-QSAR CoMSIA model results, structural concept of heteroaryl benzamide derivatives is summarized in Figure 4.18. At amide (-NH-) has hydrogen bond interaction between hydrogen atom with backbone of Met98. The oxygen atom of carbonyl (C=O) group indicated that electron withdrawing group. Nitrogen atom of pyridine ring has hydrogen bond interaction with hydroxyl group of NAD^+ cofactor in InhA binding pocket and indicated that electron withdrawing group. At methyl ($-CH_3$) group of pyridine ring indicated that electron donating group of this fragment was required. Moreover, the pyridine ring has hydrophobic interactions with Phe149, Tyr158, Met161 and Met19.

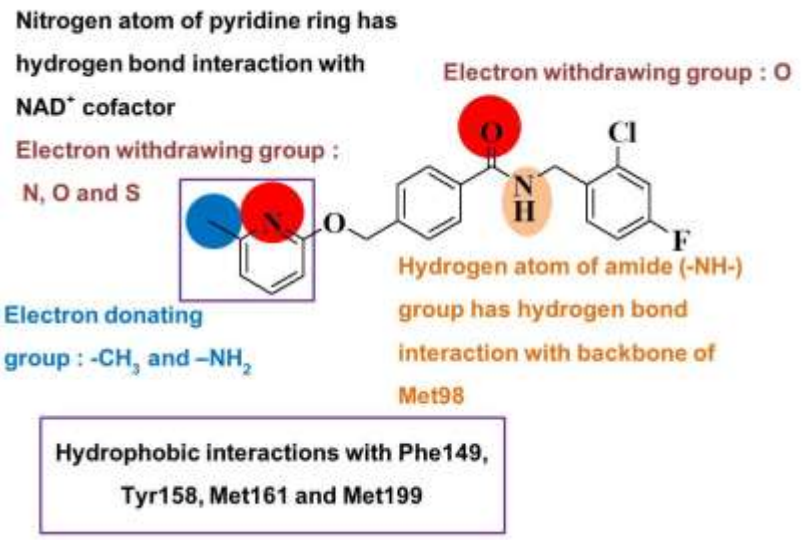

Figure 4.18 Structural concept for good IC_{50} correlation of heteroaryl benzamide derivatives summarized from molecular dynamics simulations and 3D-QSAR CoMSIA model.

4.2 DNA gyras subunit B (GyrB) inhibitors

4.2.1 Molecular docking calculations of 4-aminoquinoline derivatives

4.2.1.1 Validation of the docking method

Molecular docking calculations using the Autodock 4.2 program were employed in this study with the aims to generate the initial structure for molecular docking calculations. The available X-ray crystal structure of GyrB in a complex (PDB code 4B6C) was used as an initial structure for molecular docking calculations. The numbers of grid points in the x, y, and z dimensions with 40x40x32 $Å^3$ were used to define the 3D grid box size. The center of this box was placed in the crystal structure. The Lamarckian Genetic Algorithm was employed to generate the conformation of the GyrB binding pocket. The numbers of GA runs were set to 200 with the default search algorithm parameters. The docking calculations were verified by the RMSD value between the docked and observed X-ray conformations in its pocket. The root mean square deviations (RMSD) value close to 1 Å was acceptable. The obtained results show that the molecular docking calculation was reliable to predict the binding mode and binding interactions with RMSD of 0.92 angstrom as shown in Figure 4.19.

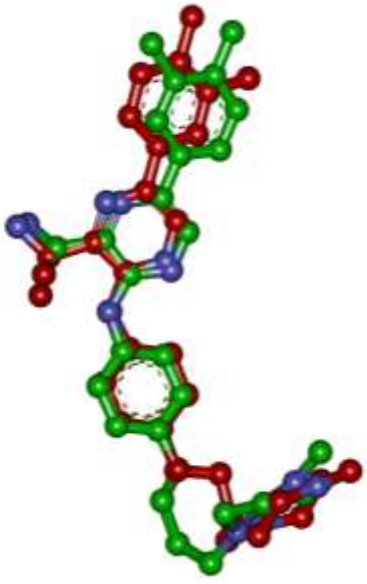

Figure 4.19 Superimposition of the docked ligand (green) and the X-ray structure of GyrB inhibitor (red).

The superimposition of the docked ligand (green) and the X-ray structure (red) in the binding pocket of InhA as shown in the Figure 4.19. The results obtained docking binding mode of the original binding mode found in X-ray crystal structure. The results of the original X-ray crystal structure are shown in Figure 4.20 (a) and the crucial interactions summary in Table 4.8. The binding mode of original X-ray crystal structure could form three hydrogen bond interactions between hydrogen atom of methyl (-CH_3) group with the oxygen atom of the Asp97A backbone at 2.32 Å distance, the hydrogen atom of amide (-NH_2) group and the oxygen atom of backbone of Ala53A and Asp79A at 2.29 and 2.06 Å distance, respectively. Moreover, hydrophobic interactions with Ala53A, Pro85A and Val99A were found. The crucial interactions of docked ligand in GyrB binding pocket formed the hydrogen bond interactions were found as the crucial interactions between methyl (-CH_3) group with the oxygen atom of the Asp97A and Val123A backbone at 2.14 and 2.40 Å distance, respectively. The hydrogen atom of amide (-NH_2) group and the oxygen atom of the Asp79A backbone at 2.22 distance are shown in the Figure 4.20 (b). Moreover, hydrophobic interactions with Ala53A, Pro85A and Val99A were found. The crucial interactions of X-ray crystal structure and docked in the GyrB binding pocket are shown in the Table 4.8.

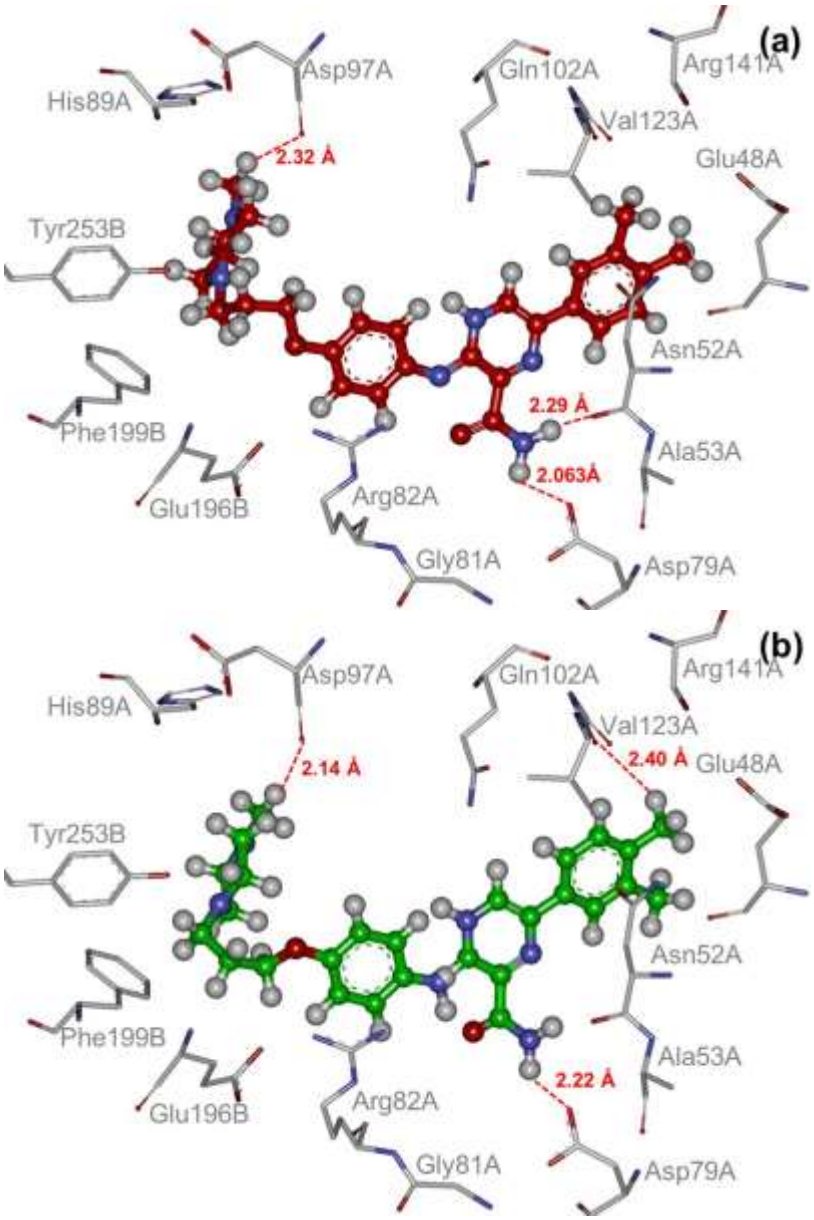

Figure 4.20 Original X-ray crystal structure (red) (a) and docked ligand (green) (b) of X-ray crystal structure in the GyrB binding pocket.

Table 4.8 The crucial interactions of X-ray crystal structure and docked in the GyrB binding pocket

Interaction	Distances (in angstrom (Å)) of aminopyrazinamides derivatives and amino acid residues	
	X-ray crystal structure	**Docking calculation**
Hydrogen bond	Ala53A: 2.32	Asp79A: 2.22
	Asp79A: 2.06	Asp97A: 2.14
	Asp97A: 2.32	Val123A: 2.40
Hydrophobic interactions	Ala53A: 1.60	Ala53A: 1.69
	Pro85A: 1.96	Pro85A: 1.75
	Val99A: 2.27	Val99A: 2.20

4.2.1.2 Molecular docking analysis of high active compounds

The 4-aminoquinoline derivatives of high active compounds including compound **39**, **16**, **11**, **29**, **43**, **25**, **28**, **08**, **40**, **41**, **37**, **15**, **13**, **17** and **27** with the biological activities (log ($1/IC_{50}$)) range 4.97-6.07. The crucial interactions of moderate active compounds were summarized in Table 4.9.

Compounds **39** and **16** were considered as high active compounds against GyrB inhibitors with biological activities (log ($1/IC_{50}$)) range of 6.07 and 6.01, respectively. Figure 4.21 shows binding orientation of compound **39** and **16** as highest active compound obtained from molecular docking calculations. In addition, the interaction distances of other highest active compounds are summary in Table 4.9. The dock conformation of compound **39** in GyrB binding pocket formed the hydrogen bond interactions were found as the crucial interactions for binding in GyrB binding site. At methoxy ($-OCH_3$) interacted with Gln102A and Tyr114A. The hydrogen atom of hydroxyl (-OH) group interacted with Thr169A. Moreover, hydrogen bond interactions with Gly122A and Glu196B. Moreover, hydrophobic interactions with Val99A, Val123A and Phe199A were observed as shown in Figure 4.21. For compound **16** form hydrogen bond interactions between $NHNH_2$ with Asp79A residue. Moreover, hydrogen bond interactions could be formed with Gly83A, Gln102A, Gly122A and Glu196B. Moreover, hydrophobic interactions with Val99A,

Tyr114A and Val123A were found. Therefore, the crucial interaction obtained from molecular docking calculations is in agreement with the experimental results that shown the high potency for against GyrB inhibitors.

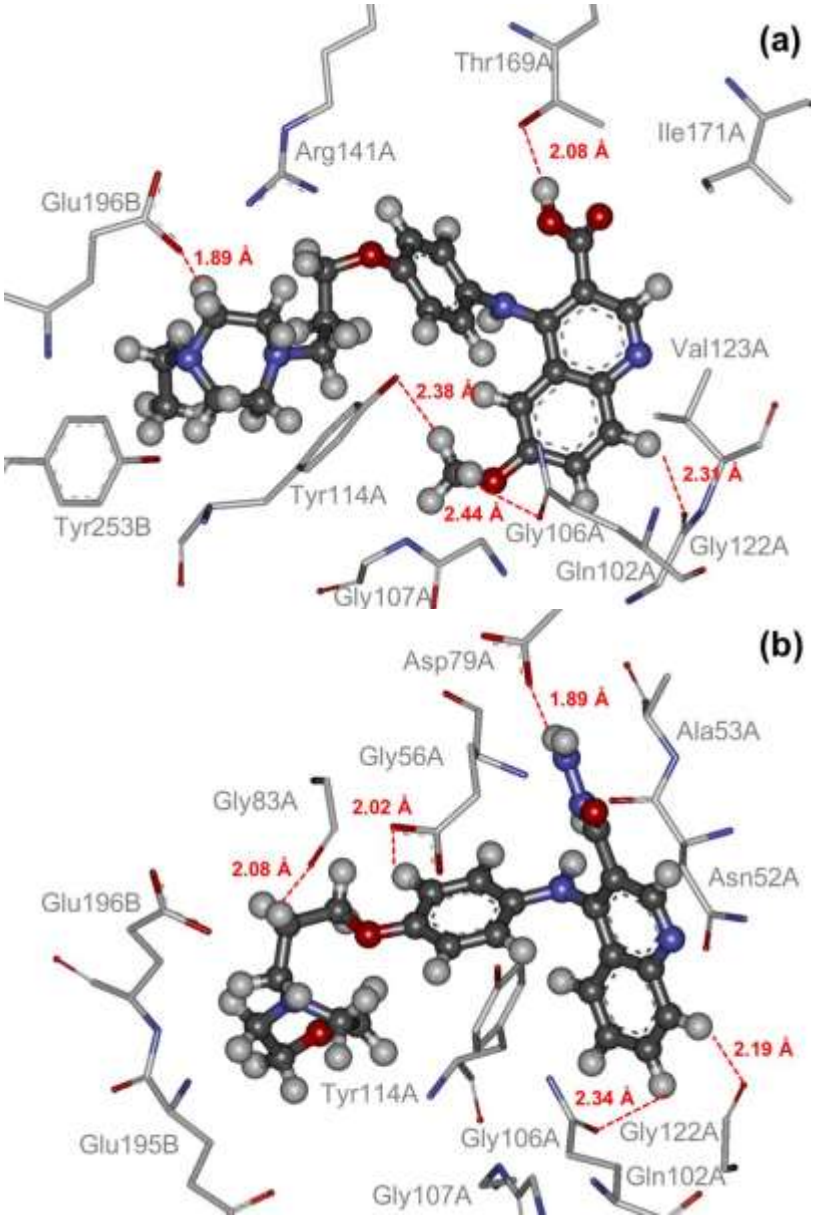

Figure 4.21 Compound 39 (a) and compound 16 (b) as high active compounds in GyrB binding pocket.

Table 4.9 Crucial interactions of high active compounds in GyrB binding pocket

Cpd.	Distances (in angstrom (Å)) of high active compounds and amino acid residues		
	Hydrogen bond interactions	**Hydrophobic interactions**	**σ-π, π-π interactions**
39	Gly122A: 2.31 Thr169A: 2.08 Glu196B: 1.89	Pro85A: 1.62 Val99A: 1.88 Val123A: 1.63	Arg82A (σ-π) : 3.52 Lys108A (σ-π) : 3.15
16	Asn52A: 2.26 Glu56A: 2.02 Asp79A: 1.89 Arg82A: 1.88 Gly83A: 2.08 Gln102A: 2.34 Gly122A: 2.10 Glu196B: 2.08	Pro85A: 174 Val99A: 1.68 Thr113A: 1.35 Val123A: 1.99 Thr169A: 1.60	Lys108A (σ-π) : 3.42
11	Glu56A: 2.42 Asp79A: 2.40 Gln102A: 2.25 Gly107A: 1.94 Gly122A: 2.05	Ala53A: 2.38 Ile84A: 2.38 Pro85A: 1.16 Val99A: 1.79 Thr113A: 1.85 Val123A: 2.33	Lys108A (σ-π) : 3.50
29	Asn52A: 2.24 Glu56A: 2.13 Asp79A:1.98 Gly122A: 2.07 Thr169A: 2.37	Pro85A: 1.10 Val99A: 1.42 Tyr114A: 1.74 Val123A: 1.88	Lys108A (σ-π) : 3.46

Table 4.9 Crucial interactions of high active compounds in GyrB binding pocket (Continued)

Cpd.	Distances (in angstrom (Å)) of high active compounds and amino acid residues		
	Hydrogen bond interactions	**Hydrophobic interactions**	**σ-π, π-π interactions**
43	Glu56A: 2.28 Gly83A: 2.01 Tyr114A: 2.06 Glu112A: 2.26 Gln195B: 2.35 Tyr253B: 2.09	Pro85A: 1.06 Val99A: 1.88 Val123A: 1.72 Phe199B: 1.79	Arg82A (σ-π) : 3.16 Lys108A (σ-π) : 3.13
25	Asn52A: 2.22 Glu56A: 2.43 Asp97A: 1.95 Thr169A: 2.43	Pro85A: 2.19 Val99A: 1.54 Val123A: 2.02 Phe199B: 2.19	Arg82A (σ-π) : 3.17 Lys108A (σ-π) : 3.20
28	Asn52A: 2.17 Asp79A: 1.96 Gly83A: 1.47 Thr169A: 2.07	Pro85A: 1.81 Val99A: 2.01 Tyr114A: 1.88 Val123A: 1.59	Arg82A (σ-π) : 3.19 Lys108A (σ-π) : 3.20
08	Asn52A: 2.18 Glu56A: 2.16 Asp79A: 2.12 Gly83A: 1.95 Gln102A: 2.24 Gly107A: 2.05 Tyr114A: 2.43 Gly122A: 2.26	Ala53A: 2.36 Pro85A: 1.49 Val99A: 1.66 Thr113A: 2.39 Ile171A: 1.93 Phe199B: 2.00	Lys108A (σ-π) : 3.50

Table 4.9 Crucial interactions of high active compounds in GyrB binding pocket (Continued)

Cpd.	Distances (in angstrom (Å)) of high active compounds and amino acid residues		
	Hydrogen bond interactions	**Hydrophobic interactions**	**σ-π, π-π interactions**
40	Glu56A: 2.467 Tyr114A: 2.26 Thr169A: 2.16 Arg192B: 2.12 Glu196B: 2.16 Tyr253B: 2.15	Pro85A: 1.62 Val99A: 1.42 Val123A: 2.08	Lys108A (σ-π) : 3.50
41	Gln102A: 2.38 Gly107A: 1.86 Lys108A: 2.34 Tyr114A: 2.27 Gly122A: 2.40 Thr169A: 2.25	Pro85A: 1.36 Val99A: 1.88	Arg82A (σ-π) : 3.16 Lys108A (σ-π) : 3.49
37	Glu56A: 2.40 Gly83A: 1.85 Gln102A: 2.29 Gly107A: 2.05 Tyr114A: 2.28 Gly122A: 2.46 Thr169A: 2.27 Tyr253B: 2.04	Pro85A: 1.43 Val99A: 1.91 Val123A: 1.73	Arg82A (σ-π) : 3.16 Lys108A (σ-π) : 3.18

Table 4.9 Crucial interactions of high active compounds in GyrB binding pocket (Continued)

Cpd.	Distances (in angstrom (Å)) of high active compounds and amino acid residues		
	Hydrogen bond interactions	**Hydrophobic interactions**	**σ-π, π-π interactions**
15	Glu56A: 2.06 Asp79A: 2.41 Gly83A: 1.75 Asp97A: 2.47 Gln102A: 2.27 Gly107A: 1.97 Gly122A: 2.16 Glu196B: 2.32	Ala53A: 2.27 Pro85A: 2.36 Val99A: 1.30 Thr169A: 1.97	Lys108A (σ-π) : 3.17
13	Glu56A: 2.49 Gly83A: 1.91 Gln102A: 2.03 Gly122A: 2.19	Pro85A: 1.60 Val99A: 1.70 Thr113A: 2.22 Val123A: 1.69 Thr169A: 1.63	Arg82A (σ-π) : 3.19 Lys108A (σ-π) : 3.16
17	Asn52A: 2.22 Glu56A: 2.37 Asp79A: 1.91 Gly122A: 2.15 Thr169A: 2.32	Pro85A: 1.57 Val99A: 1.44 Lys108A: 2.11 Thr113A: 1.90 Tyr114A: 1.69 Val123A: 1.82	Arg82A (σ-π) : 3.18 Lys108A (σ-π) : 3.16
27	Asn52A: 2.20 Asp79A: 2.01 Gly83A: 1.55 Gly122A: 2.06 Thr169A: 2.17 Glu196B: 2.23	Pro85A: 1.68 Val99A: 1.89 Val123A: 1.83	Lys108A (σ-π) : 3.16

4.2.1.3 Molecular docking analysis of moderate active compounds

The fourteen compounds including compound **31**, **21**, **05**, **03**, **14**, **09**, **36**, **02**, **24**, **12**, **26**, **07**, **34** and **42** were showed as moderate active compounds against GyrB inhibitors. 4-aminoquinoline derivatives with biological activities (log ($1/IC_{50}$)) range of 4.69-4.95 were considered as high active compounds as shown in Table 4.10.

Compounds **02** and **36** were considered as moderate active compounds against GyrB inhibitors with biological activities (log ($1/IC_{50}$)) range of 4.83 and 4.82, respectively. The crucial interactions of moderate active compounds were summarized in Table 4.10 and Figure 4.22. The crucial interactions of compound **02** shown that the hydrogen bond interactions of methoxy (-OCH_3), hydrogen bond interactions of this substituent with Tyr114A in the GyrB binding pocket were reported. Moreover, hydrogen bond interactions could be formed Glu56A, Gly122A and Glu196B. Moreover, hydrophobic interactions with Ala53A, Val99A and Val123A were observed as shown in Table 4.10. For compound **36** form three hydrogen bond interactions including hydrogen atom of hydroxyl group (-OH) with Thr169A residue. Moreover, hydrogen bond interactions could be formed Gln102A and Glu196B, and amine (-NH) with Gly83A residue, hydrophobic interactions with Pro85A, Val99A and Tyr114A. Therefore, the crucial interaction obtained from molecular docking calculations is in agreement with the experimental results that shown the moderate potency for against GyrB inhibitors.

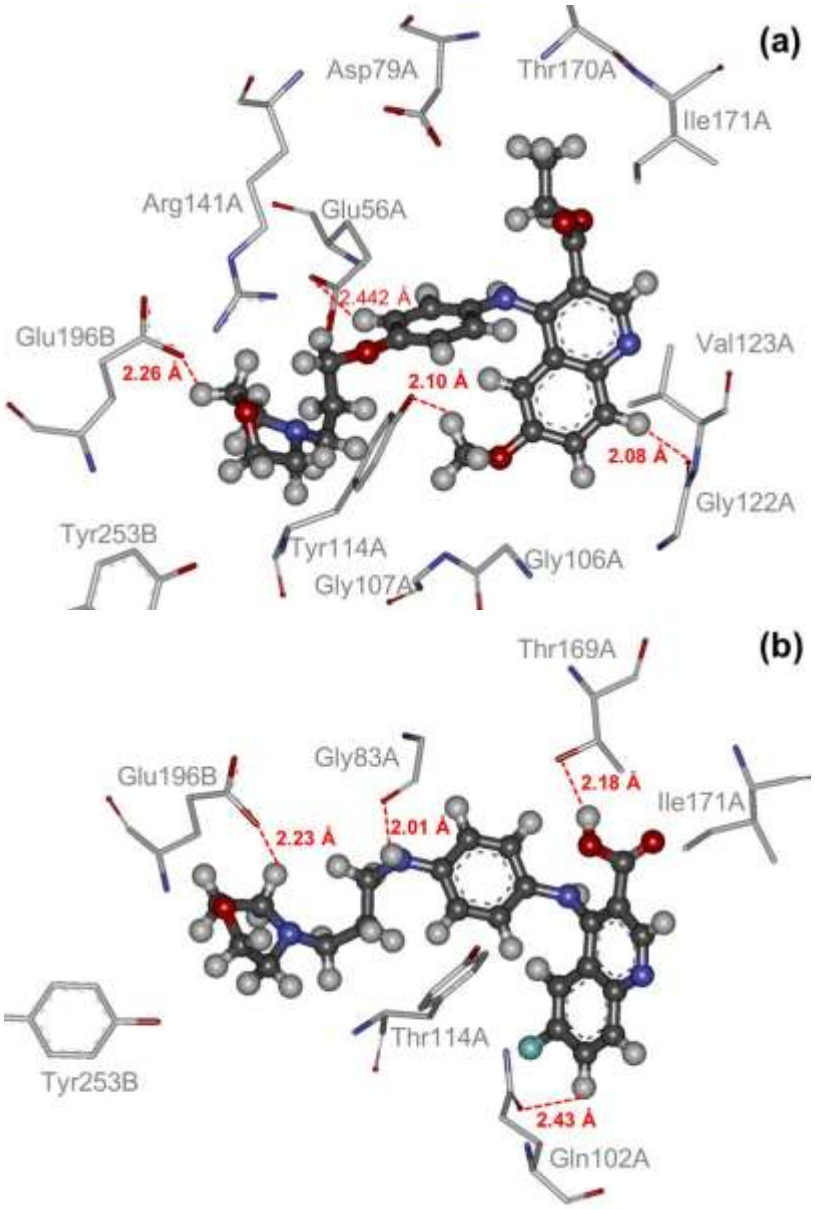

Figure 4.22 Compound 02 (a) and compound 36 (b) as moderate active compounds in GyrB binding pocket.

Table 4.10 Crucial interactions of moderate active compounds in GyrB binding pocket

Cpd.	Distances (in angstrom (Å)) of moderate active compounds and amino acid residues		
	Hydrogen bond interactions	**Hydrophobic interactions**	**σ-π, π-π interactions**
31	Glu56A: 2.10 Tyr114A: 2.17 Gly122A: 2.24 Arg141A: 1.87 Thr169A: 2.24 Glu196B: 2.35	Pro85A: 1.87 Val99A: 1.43 Val123A: 1.76	Lys108A (σ-π) : 3.20
21	Asn52A: 2.27 Glu56A: 2.09 Asp79A: 2.07 Gly83A: 1.29 Gly122A: 2.29 Arg141A: 2.20 Thr169A: 1.922 Glu196B: 2.40	Pro85A: 1.85 Val99A: 2.05 Val123A: 1.92	Arg82A (σ-π) : 3.50 Lys108A (σ-π) : 3.20
05	Gly83A: 2.12 Tyr114A: 2.24 Arg141A: 1.93 Glu196B: 2.10	Ala53A: 1.92 Pro85A: 2.15 Val99A: 2.04 Lys108A: 2.00 The169A: 2.34 Ile171A: 2.32	Arg82A (σ-π) : 3.20 Lys108A (σ-π) : 3.50

Table 4.10 Crucial interactions of moderate active compounds in GyrB binding pocket (Continued)

Cpd.	Distances (in angstrom (Å)) of moderate active compounds and amino acid residues		
	Hydrogen bond interactions	**Hydrophobic interactions**	**σ-π, π-π interactions**
03	Glu56A: 2.08 Gln102A: 2.42 Tyr114A: 2.29 Gly122A: 2.23 Ayg141A: 1.86 Glu196B: 2.19	Ala53A: 1.96 Pro85A: 1.66 Val99A: 1.47	Lys108A (σ-π) : 3.49
14	Glu56A: 2.32 Gly83A: 2.36 Gln102A: 2.43 Tyr114A: 2.28 Gly122A: 2.32 Glu196B: 2.21	Ala53A: 1.51 Pro85A: 2.16 Val99A: 2.05 Val123A: 1.84	Arg82A (σ-π) : 3.16 Lys108A (σ-π) : 3.20
09	Asn52A: 2.15 Glu56A: 2.24 Asp79A: 2.48 Gly122A: 1.92 Glu196B: 2.20	Ala53A: 2.07 Pro85A: 1.76 Val99A: 1.69 Gly107A: 1.81 Thr113A: 2.09 Val123A: 1.90 Thr169A: 2.24	Lys108A (σ-π) : 3.11

Table 4.10 Crucial interactions of moderate active compounds in GyrB binding pocket (Continued)

Cpd.	Distances (in angstrom (Å)) of moderate active compounds and amino acid residues		
	Hydrogen bond interactions	**Hydrophobic interactions**	**σ-π, π-π interactions**
36	Gly83A: 2.01 Gln102A: 2.43 Tyr114A: 2.37 Gly122A: 2.35 Arg141A: 2.07 Thr169A: 2.18 Glu196A: 2.23	Pro85A: 1.15 Val99A: 1.99 Val123A: 1.77	Arg82A (σ-π) : 3.20 Lys108A (σ-π) : 3.18
02	Glu56A: 2.44 Gln102A: 2.33 Tyr114A: 2.10 Gly122A: 2.08 Arg141A: 2.12 Glu196B: 2.26	Ala53A: 2.31 Pro85A: 1.82 Val99A: 2.17 Thr169A: 2.23	Lys108A (σ-π) : 3.15
24	Asn52A: 2.21 Glu56A: 2.23 Asp79A: 1.98 Gly83A: 2.32 Gln102A: 2.12 Thr169A: 2.22 Arg192B: 2.14 Glu196B: 2.24	Pro85A: 1.50 Val99A: 1.44 Tyr114A: 1.81 Val123A: 1.79 Phe199B: 2.19	Lys108A (σ-π) : 3.19

Table 4.10 Crucial interactions of moderate active compounds in GyrB binding pocket (Continued)

Cpd.	Distances (in angstrom (Å)) of moderate active compounds and amino acid residues		
	Hydrogen bond interactions	**Hydrophobic interactions**	**σ-π, π-π interactions**
12	Glu56A: 2.49 Gln102A: 2.46 Tyr114A: 2.35 Gly122A: 2.17 Glu196B: 2.08	Ala53A: 1.99 Pro85A: 1.52 Val99A: 1.33 Lys108A: 1.85 Val123A: 2.20 Ile171A: 2.02	Arg82A (σ-π) : 3.50 Lys108A (σ-π) : 3.47
26	Asn52A: 2.14 Gln102A: 2.22 Gly107A: 2.05 Lys108A: 2.38 Tyr114A: 2.22	Pro85A: 1.59 Val99A: 2.27 Val123A: 2.12	Arg82A (σ-π) : 3.42 Lys108A (σ-π) : 3.19
07	Glu56A: 2.27 Asp79A: 2.49 Gly83A: 1.88 Tyr114A: 2.43 Gly122A: 2.04 Gln195B: 2.40 Glu196B: 2.14	Ala53A: 1.62 Pro85A: 185 Val99A: 1.31 Ile171A: 2.09 Tyr253B: 2.39	Lys108A (σ-π) : 3.50
34	Glu56A: 2.42 Gly83A: 1.90 Gln102A: 2.41 Tyr114A: 2.26 Arg141A: 2.22 Thr169A: 2.20 Glu196A: 2.04	Pro85: 1.15 Vall99A: 2.01	Arg82A (σ-π) : 3.19 Lys108A (σ-π) : 3.60

Table 4.10 Crucial interactions of moderate active compounds in GyrB binding pocket (Continued)

Cpd.	Distances (in angstrom (Å)) of moderate active compounds and amino acid residues		
	Hydrogen bond interactions	**Hydrophobic interactions**	**σ-π, π-π interactions**
42	Glu56A: 2.13 Gly83A: 2.03 Tyr114A: 2.29 Gly122A: 2.24 Thr169A: 2.18 Glu196B: 2.06	Pro85A: 1.05	Arg82A (σ-π) : 3.20 Lys108A (σ-π) : 3.49

4.2.1.4 Molecular docking analysis of low active compounds

The fourteen compounds of 4-aminoquinoline derivatives as low active compounds including compound **22**, **20**, **04**, **19**, **35**, **32**, **23**, **33**, **30**, **10**, **01**, **06**, **38** and **18** with the biological activities (log ($1/IC_{50}$)) range 4.33-4.68. The crucial interactions of low active compounds were summarized in Table 4.11.

Compound **20** and **22** were selected for explained the binding mode and binding interaction of less active compound with the log($1/IC_{50}$) was 4.35 and 4.33, respectively. The crucial interactions of low active compounds were summarized in Table 4.11. The crucial interactions of these compounds were showed in Figure 4.23. The results indicate that compound **20** hydrogen bond interactions of $NHNH_2$ with Asp79A in the GyrB binding pocket were reported. Moreover, hydrogen bond interactions could be formed with Glu56A and Gly122A. Moreover, hydrophobic interactions with Pro85A and Val108A were found. For compound **22** the result shows that hydrogen bond interactions of $NHNH_2$ with Asp79A in the GyrB binding pocket and hydrogen bond interactions could be formed with Gly83A and Thr169A. Moreover, hydrophobic interactions with Asn52A were found. Therefore, the crucial interaction obtained from molecular docking calculations is in agreement with the experimental results that shown the low potency for against GyrB inhibitors.

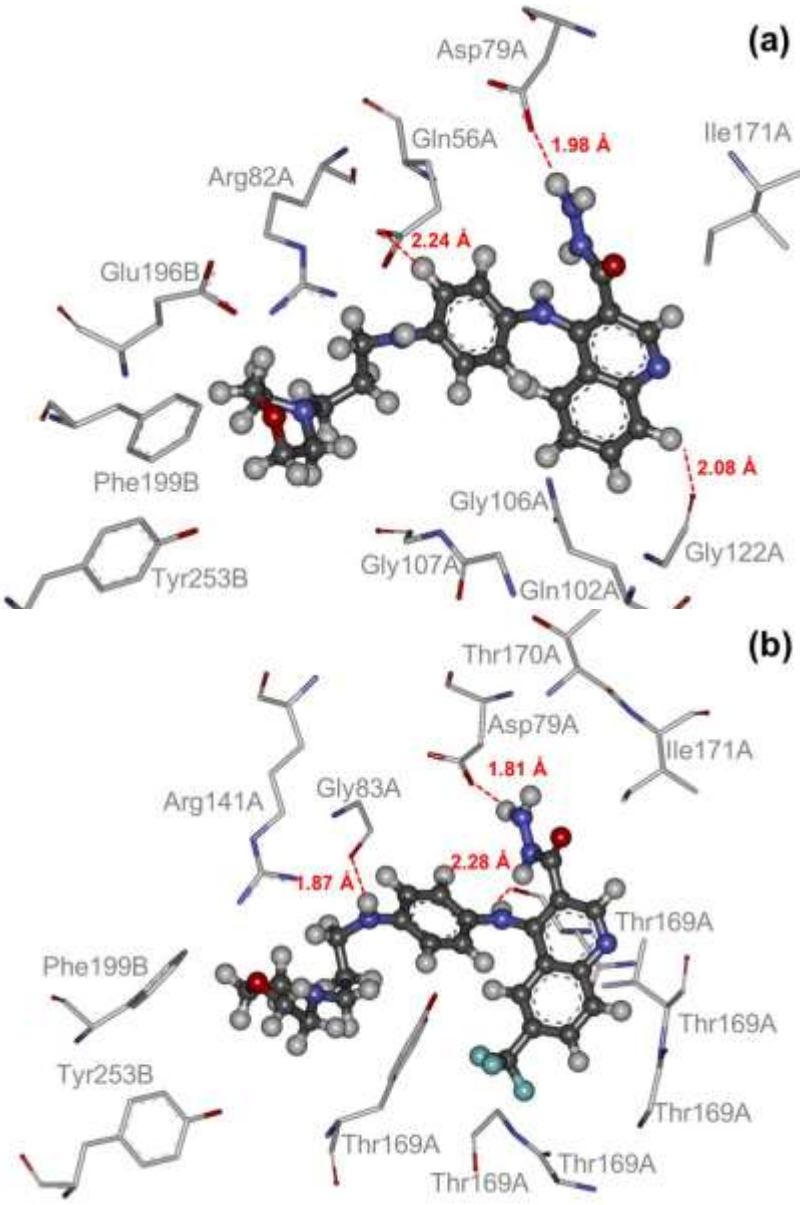

Figure 4.23 Compound 20 (a) and compound 22 (b) as low active compounds in GyrB binding pocket.

Table 4.11 Crucial interactions of low active compounds in GyrB binding pocket

Cpd.	Distances (in angstrom (Å)) of low active compounds and amino acid residues		
	Hydrogen bond interactions	**Hydrophobic interactions**	**σ-π, π-π interactions**
22	Asn52A: 2.08 Glu56A: 2.35 Asp79A: 1.81 Gly83A: 1.87 Gln102A: 2.23 Gly107A: 1.91 Lys108A: 2.28 Tyr114A: 2.47 Glt122A: 2.36 Arg141A: 2.03 Glu196B: 2.45	Ile84A: 2.26 Pro85A: 1.05 Val99A: 1.84 Val123A: 2.10	Arg82A (σ-π) : 3.19 Lys108A (σ-π) : 3.50
20	Asn52A: 2.26 Glu56A: 2.24 Asp79A: 1.98 Gly83A: 2.25 Gly122A: 2.08 Arg141A: 1.95 Thr169A: 2.27 Glu196B: 2.09	Pro85A: 0.98 Val99A: 1.45 Val123A: 1.74	Lys108A (σ-π) : 3.49

Table 4.11 Crucial interactions of low active compounds in GyrB binding pocket (Continued)

Cpd.	Distances (in angstrom (Å)) of low active compounds and amino acid residues		
	Hydrogen bond interactions	**Hydrophobic interactions**	**σ-π, π-π interactions**
04	Asn52A: 2.14 Glu56A: 2.22 Asp79A: 2.10 Gly83A: 2.10 Pro85A: 1.70 Gln102A: 2.26 Gly122A: 2.37	Ala53A: 2.33 Val99A: 1.54 Thr113A: 1.45 Val123A: 1.12 Thr169A: 1.42	Lys108A (σ-π) : 3.19
19	Asn52A: 2.03 Glu56A: 2.09 Asp79A: 1.92 Gln102A: 2.22 Gly107A: 1.86 Gly122A: 2.43 Arg141A: 1.96 Glu196B: 2.27	Pro85A: 2.33 Val99A: 1.81 Val123A: 2.24 Thr169A: 1.63	Arg82A (σ-π) : 3.50 Lys108A (σ-π) : 3.75
35	Glu56A: 2.37 Gly83A: 1.84 Tyr114A: 2.29 Arg141A: 2.34 Thr169A: 2.13 Glu196A: 2.13	Pro85A: 1.01	Arg82A (σ-π) : 3.49 Lys108A (σ-π) : 3.47

Table 4.11 Crucial interactions of low active compounds in GyrB binding pocket (Continued)

Cpd.	Distances (in angstrom (Å)) of low active compounds and amino acid residues		
	Hydrogen bond interactions	**Hydrophobic interactions**	**σ-π, π-π interactions**
32	Glu56A: 2.38 Gly122A: 2.27 Arg141A: 1.85 Thr169A: 2.06 Glu196B: 2.00	Pro85A: 1.52 Val99A: 1.53 Val123A: 1.67	Arg82A (σ-π) : 3.50 Lys108A (σ-π) : 3.20
23	Asn52A: 2.21 Glu56A: 2.42 Asp79A: 1.97 Gly122A: 2.10 Thr169A: 2.30	Pro85A: 1.54 Val99A: 1.82 Tyr114A: 1.71 Val123A: 1.83 Phe199B: 1.98	Arg82A (σ-π) : 3.20 Lys108A (σ-π) : 3.20
33	Glu56A: 2.43 Gln102A: 2.24 Gly107A: 1.96 Lys108A: 2.19 Tyr114A: 2.26 Gly122A: 2.05	Pro85A: 1.65 Val99A: 1.07	Lys108A (σ-π) : 3.20
30	Asn52A: 2.14 Gly83A: 1.53 Gln102A: 2.19 Gly107A: 2.01 Lys108A: 2.40 Tyr114A: 2.33	Pro85A: 1.76 Val123A: 1.87	Arg82A (σ-π) : 3.20 Lys108A (σ-π) : 3.50 Phe199B (π- σ) : 3.50

Table 4.11 Crucial interactions of low active compounds in GyrB binding pocket (Continued)

Cpd.	Distances (in angstrom (Å)) of low active compounds and amino acid residues		
	Hydrogen bond interactions	**Hydrophobic interactions**	**σ-π, π-π interactions**
10	Glu56A: 2.31 Asp79A: 2.44 Gln102A: 2.44 Tyr114A: 2.39 Gly122A: 2.10 Glu196B: 2.33	Ala53A: 1.71 Pro85A: 2.07 Val99A: 2.00 Thr169A: 1.86	Lys108A (σ-π) : 3.50
01	Glu56A: 2.30 Arg82A: 2.23 Tyr114A: 2.49 Arg141A: 1.98 Glu196B: 2.36	Ala53A: 2.18 Pro85A: 1.71 Val99A: 1.32 Lys108A: 2.04 Thr113A: 2.23 Thr169A: 2.11	Lys108A (σ-π) : 3.50
06	Asn52A: 2.27 Glu56A: 2.15 Asp79A: 2.41 Gly83A: 2.15 Gln102A: 2.11 Gly122A: 2.27 Arg141A: 1.98 Glu196B: 2.30	Ala53A: 1.90 Pro85A: 1.34 Val99A: 1.47 Gly106A: 2.00 Gly107A: 2.19 Lys108A: 1.89 Tyr114A: 1.83 Val123A: 1.80 Thr169A: 2.04 Phe199B: 2.09	Lys108A (σ-π) : 3.15

Table 4.11 Crucial interactions of low active compounds in GyrB binding pocket (Continued)

Cpd.	Distances (in angstrom (Å)) of low active compounds and amino acid residues		
	Hydrogen bond interactions	**Hydrophobic interactions**	**σ-π, π-π interactions**
38	Asn52A: 2.43 Glu56A: 2.29 Gln102A: 1.74 Tyr113A: 1.77 Glu196B: 2.08	Pro85A: 2.16 Val99A: 1.95	Lys108A (σ-π) : 3.50
18	Asn52A: 2.35 Glu56A: 2.13 Asp79A: 2.03 Gly122A: 2.09 Thr169A: 2.05 Glu196B: 2.28	Pro85A: 2.08 Val99A: 1.59 Lye108A: 2.22 Thr113A: 2.00 Tyr114A: 1.85 Val123A: 1.87	Lys108A (σ-π) : 3.50

4.2.1.5 Summaries of the crucial interactions of GyrB inhibitor from molecular docking calculations

Based on the molecular docking calculations results, the structural concept of 4-aminoquinoline derivatives is of key importance for binding in GyrB binding pocket is summarized in Figure 4.24. Therefore, this fragment is crucial for favorable IC_{50} values. The R substituent has hydrogen bond interactions between hydrogen atom of R substituent with backbone of Gly106A and oxygen atom of Tyr114A. For the R_1 substituent have hydrogen bond interactions between hydrogen atom of R_1 substituent with oxygen atom of Asp79A and Thr169A in the binding pocket. The X substituent has hydrogen bond interaction between hydrogen atom of amide (-NH-) at X substituent with backbone of Gly83A. Moreover, hydrogen atom of quinoline ring has hydrogen bond interactions with backbone of Gln120A and Gly122A, hydrophobic interactions at this position with Gln102A, Gly122A and

Val123A residues. At 4-animo position has hydrogen bond interaction with backbone of Thy169A. Hydrogen atom of benzene ring has hydrogen bond interaction with Gly56A and hydrophobic interactions with Pro85A, Val99A and Tyr114A. The hydrogen atom of cycle has hydrogen bond interaction with Glu196B and hydrophobic interaction with Val108A and Glu196B in GyrB binding pocket.

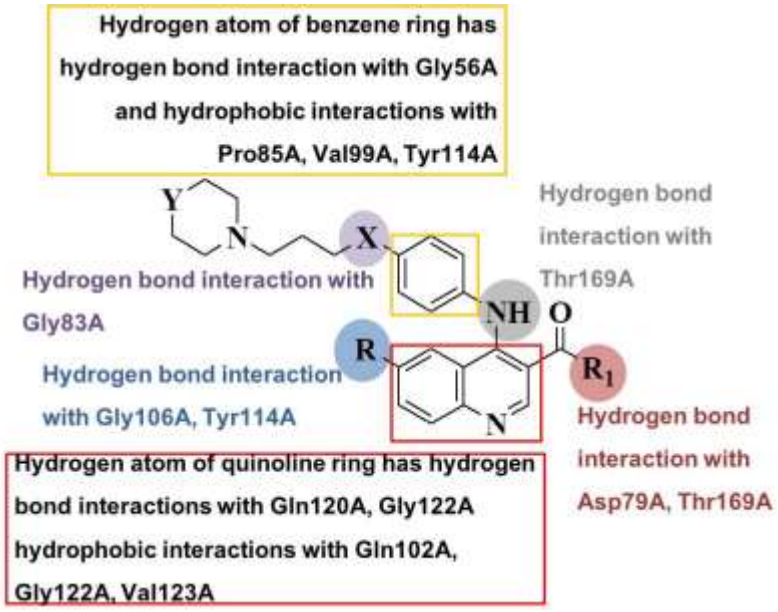

Figure 4.24 Structural concept for 4-aminoquinoline derivatives summarized from molecular docking calculations.

4.2.2 Molecular dynamics simulations of 4-aminoquinoline derivatives

4.2.2.1 Structural stability during molecular dynamics (MD) simulations

Molecular dynamics simulations of 4-aminoquinoline derivatives in GyrB were performed. In order to compare the binding behavior of GyrB and 4-aminoquinoline derivatives relative to the initial minimized structure over the 60 ns of simulation times were calculated and plotted in Figure 4.25. There are two solute species in each MD system including GyrB and inhibitor. The plateau characteristic of the RMSD plot over the simulation time is the criteria to indicate the equilibrium state of each solute species. For the equilibrium state of each MD system, the RMSD plots of all solute species have to reach the plateau characteristic. GyrB and inhibitor in each system reach the equilibrium state at a different time. For the system of

4-aminoquinoline derivatives reach equilibrium at an early time point, whereas GyrB reaches the equilibrium state after 5 ns. In the case of compound **09**, **24**, **31**, **38**, **39**, **40**, **41** and **43** there are MD system reaches equilibrium after 30, 45, 30, 40, 30, 30, 20 and 35 ns, respectively as shown in Figure 4.25 (a)-(h). The RMSD plots of these compounds over 60 ns shown large fluctuations in the range of about 5.00-20.00 Å. Therefore, the data in terms of binding free energy, interaction energy and structure of each system after an equilibrium state were analyzed.

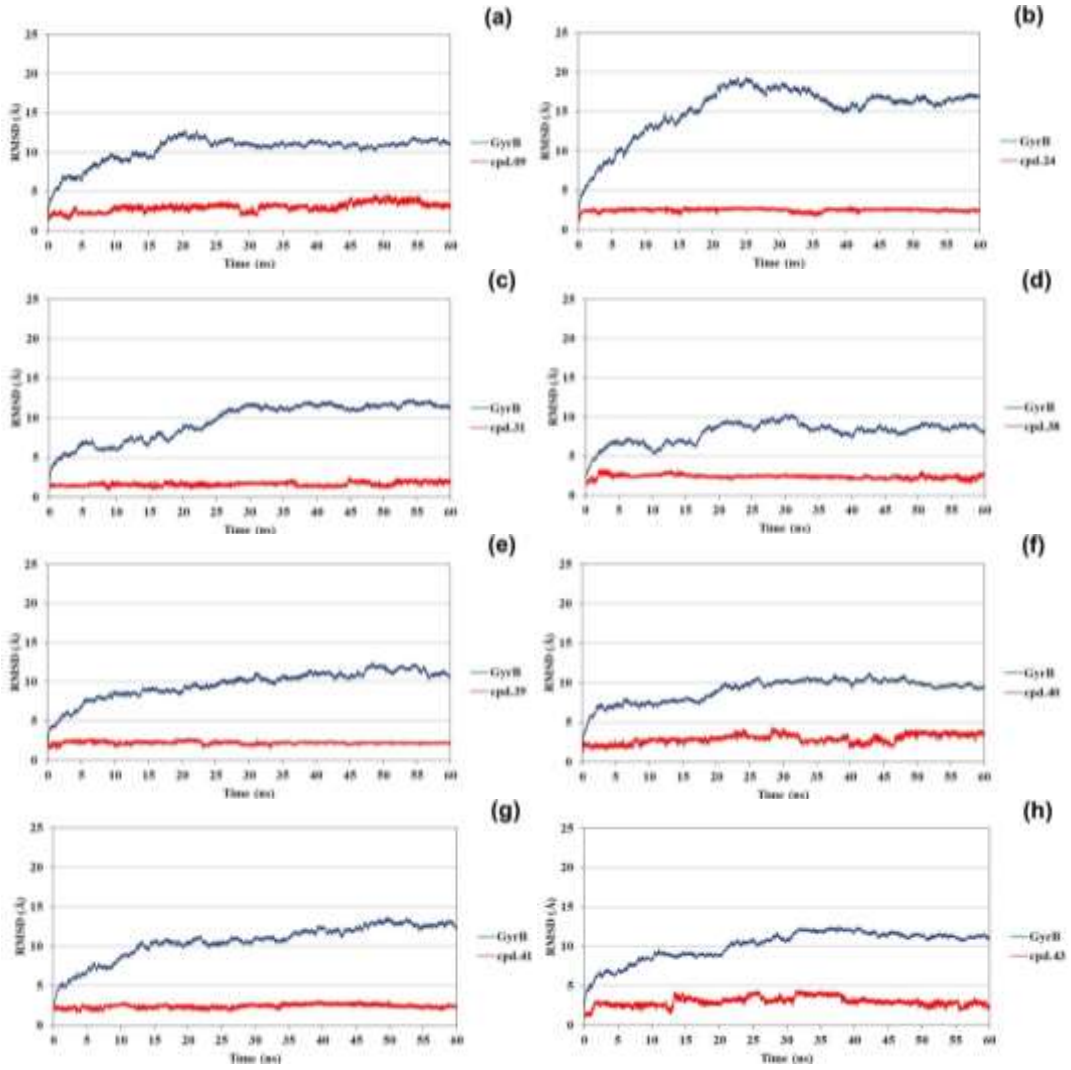

Figure 4.25 RMSDs of 4-aminoquinoline derivatives, compounds 09 (a), 24 (b), 31 (c), 38 (d), 39 (e), 40 (f), 41 (g) and 43 (h) complexed with the GyrB.

4.2.2.2 Binding mode and binding interaction analysis of GyrB inhibitor

Compounds **39** was considered as the highest active compounds against GyrB with biological activities (IC_{50}) range of 0.86 µM. Figure 4.26 shows binding orientation of compound highest active compound obtained from molecular dynamics (MD) simulations. The binding interactions of compound **39** in GyrB binding pocket formed the hydrogen bond interactions were found as the crucial interactions for binding in GyrB binding site. At amide (-NH-) interacted with Val49A at 2.501 Å distance. The hydrogen atom of compound **39** at site chain interacted with Glu56A and Gly83A at 2.49 Å and 2.47 Å, respectively. Moreover, hydrophobic interactions with Val49A, Glu56A and Gly83A were observed as shown in Figure 4.24.

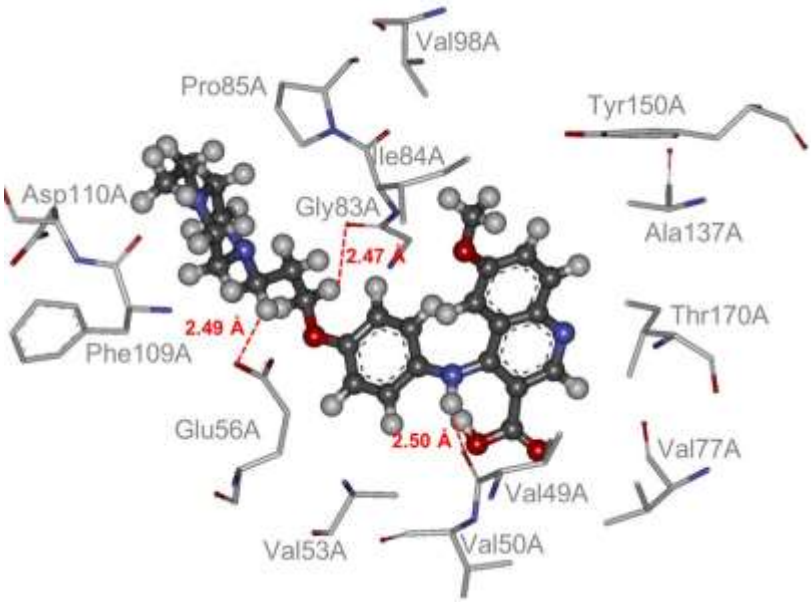

Figure 4.26 The binding mode of the highest activity compound 39 obtained from MD simulations.

1) Binding mode and binding interaction of R substituent

The R substituent compared in compound **39** is methoxy (-OCH_3) with IC_{50} 0.86 µM, fluoro (-F) in compound **40** with IC_{50} 6.82 µM, trifluoro (-CF_3) in compound **41** with IC_{50} 7.91 µM and hydrogen atom (-H) in compound **38** with IC_{50} 21.66 µM. The difference of binding mode and binding interaction of R substituent different of inhibitors from MD simulations are shown in Figure 4.27. Compound **40** form hydrogen bond interactions between hydrogen atom of compound **40** interacted with backbone of His507B at 2.45 Å distance. Moreover, hydrophobic interactions with Pro85A, Ala445B and Tyr508B were found. The compound **41** has hydrogen bond interaction between oxygen atom of hydroxyl (-OH) group with Ala53A residue at 3.07 Å distance. Moreover, hydrophobic interactions with Pro85A, Ala137A and Ile171A residues were found. The last interactions of compound **38** in GyrB binding pocket formed the hydrogen bond interactions were found as the crucial interactions for binding in GyrB binding site. At hydrogen atom of amide (-NH-) group with Asn52A residue at 2.41 Å distance. Moreover, hydrophobic interactions with Val49A, Pro85A and Ile171A were found. From this result, to enhance the biological activity of 4-aminoquinoline derivatives it can be concluded that all, the R substituent is large substituent and have high electronegativity group when compare with compound **39**. Therefore, the crucial interaction obtained from MD simulations is in agreement with the experimental results that shown the low potency for against GyrB inhibitors.

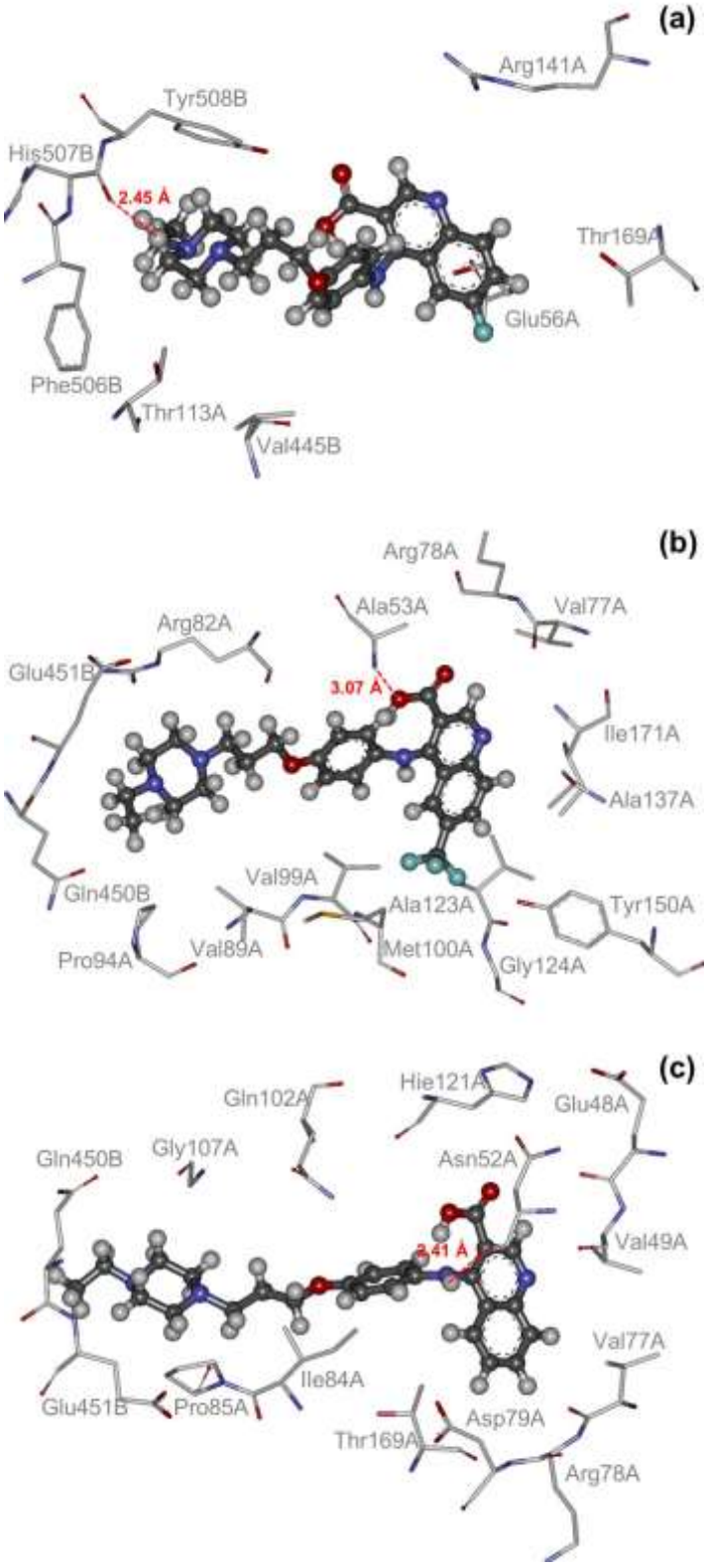

Figure 4.27 Binding modes and binding interactions of compound 40 (a), compound 41 (b) and compound 38 (c) in the GyrB binding pocket derived from MD simulations.

2) Binding mode and binding interaction of R_1 substituent

Among these derivatives, two types of the 4-aminoquinoline derivatives were selected. Only the R_1 substituent is different in the two compounds. However, their IC_{50} values are significantly different to each other; 12.63 μM for the compound **24** and 15.12 μM for the compound **09**. The R_1 substituent in compound **24** is $–NHNH_2$ and $–OC_2H_5$ in compound **09**. The difference of binding mode and binding interaction of R_1 substituent different position of inhibitors from MD simulations are shown in Figure 4.28. Interactions of compound **24** in GyrB binding pocket formed the hydrogen bond interactions were found as the crucial interactions for binding in GyrB binding site. At hydrogen atom of $-NHNH_2$ with Asp55A and Asp79A at 2.02 Å and 1.87 Å distance, respectively. Moreover, hydrophobic interactions with Tyr114A were found. For compound **09**, the result shows that hydrophobic interaction with Pro85A, Met100A and Pro509B. From this result, to enhance the biological activity of 4-aminoquinoline derivatives it can be concluded that all, the R_1 substituent is large chain and hydrophilic group. Therefore, the crucial interaction obtained from MD simulations is in agreement with the experimental results that shown the low potency for against GyrB.

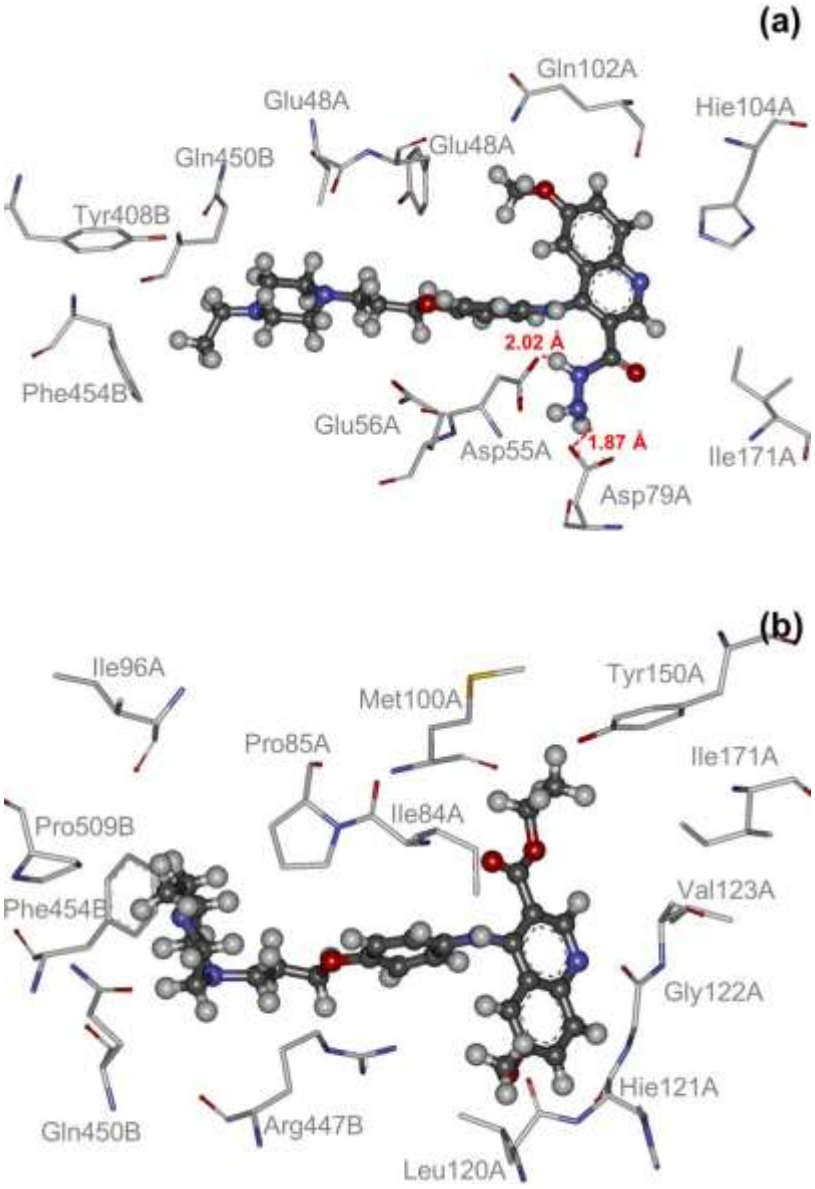

Figure 4.28 Binding modes and binding interactions of compound 24 (a), and compound 09 (b) in the GyrB binding pocket derived from MD simulations.

3) Binding mode and binding interaction of X substituent

Compounds **43** were considered as high active compounds against InhA inhibitors with biological activities IC_{50} of 1.32 µM. The X substituent in compound **43** is amide (-NH-) group. Figure 4.29 shows binding orientation of compound **43** obtained from MD simulations. The interactions of compound **43** in GyrB binding pocket formed the hydrogen bond interactions between hydrogen atom

of hydroxyl (-OH) group interacted with Glu56A at 1.94 Å distance. Moreover, hydrophobic interactions with Met93A and Met100A were observed as shown in Figure 4.27. The orientation of amide (-NH-) group of compound **43** in the pocket was different from that observed for oxygen atom (-O-) in compound **39** was shown in Figure 4.29. Therefore, the crucial interaction obtained from based on MD simulations in agreement with the experimental results that shown the high potency for against GyrB inhibitors.

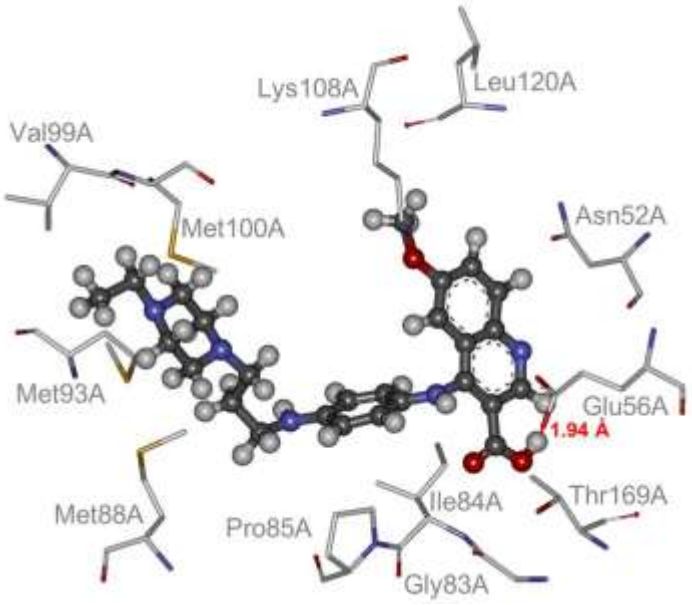

Figure 4.29 Binding modes and binding interactions of compound 43 in the GyrB binding pocket derived from MD simulations.

4) Binding mode and binding interaction of Y substituent

Compound **31** were considered as high active compounds against GyrB with biological activities IC_{50} of 20.56 µM. The X substituent in compound **24** is oxygen atom (-O-). The difference of binding mode and binding interaction of Y substituent different position of inhibitors from MD simulations are shown in Figure 4.30. Interactions of compound **31** in GyrB binding pocket formed the hydrogen bond interactions were found as the crucial interactions for binding in GyrB binding site. At hydrogen atom of compound **31** with Tyr114A at 2.48 Å distance. Moreover, hydrophobic interactions with Ala53A, Ile84A and Val99A were

observed as shown in Figure 4.28. From this result, to enhance the biological activity of 4-aminoquinoline derivatives can be concluded that all, the Y substituent is large chain. Therefore, the crucial interaction obtained from MD simulations is in agreement with the experimental results that shown the low potency for against GyrB inhibitors.

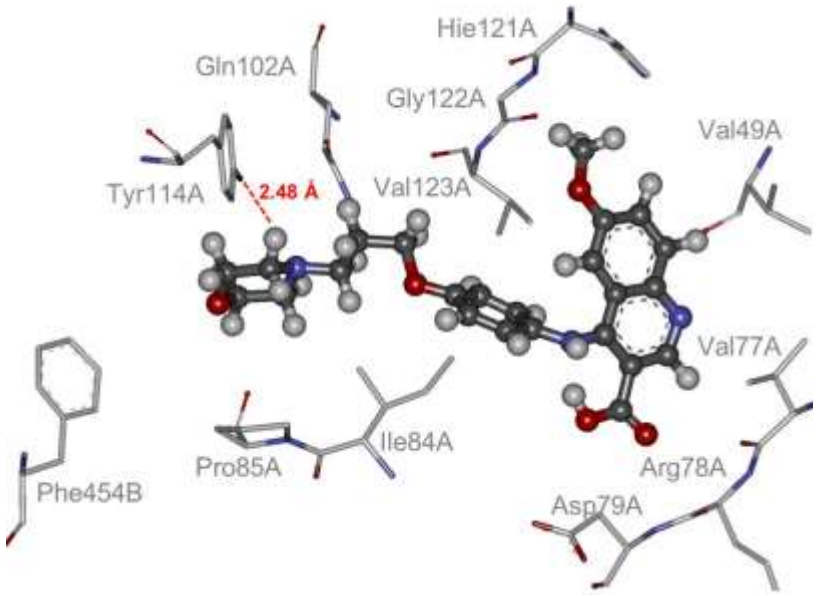

Figure 4.30 Binding modes and binding interactions of compound 31 in the GyrB binding pocket derived from MD simulations.

4.2.2.3 Summaries of the crucial interactions of GyrB inhibitor from molecular dynamics simulations

Based on the molecular dynamics simulations results, from results can be concluded that the structural concept of 4-anminoquinoline derivatives that favor for binding interactions in GyrB binding pocket summarized in Figure 4.31. Therefore, this fragment is crucial for favorable IC_{50} values. The R_1 substituent has hydrogen bond interactions between hydrogen atom of R_1 substituent with Ala53A, Asp5A, Glu56A and Asp79A, hydrophobic interaction with Met100A. At the 4-animo position have hydrogen bond interactions with Val49A and Asn52A. Moreover, at benzene ring have hydrophobic interaction with Glu56A and Gly83A, and hydrogen atom of the cycle shows hydrogen bond interactions with Tyr114A and His507B, hydrophobic interaction with Pro85A in GyrB binding pocket.

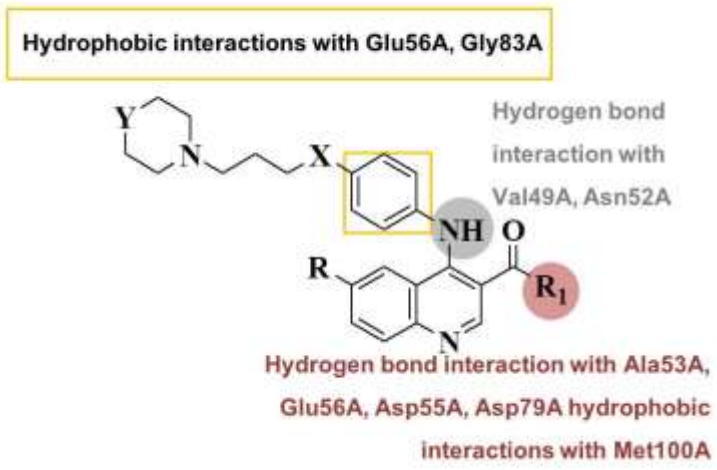

Figure 4.31 Structural concept for 4-aminoquinoline derivatives summarized from molecular dynamics simulations.

4.2.3 Quantitative Structure Activity Relationship Analysis of 4-aminoquinoline derivatives

4.2.3.1 CoMSIA model

The statistical parameters of CoMSIA model generated based on docking alignment illustrated in Table 4.12. The CoMSIA analyses using different combinations of steric, electrostatic, hydrophobic and hydrogen donor hydrogen acceptor fields were added to give more specific properties of interactions between inhibitors and the enzyme target. CoMSIA model with the different combined fields were built up. Based on the better statistical values and more descriptor variables, the model containing steric, electrostatic and hydrogen donor fields was selected as the best CoMSIA model for prediction. This CoMSIA model exhibits highly predictive with r_{cv}^2 and r^2 of 0.68 and 0.98, respectively. CoMSIA model, the contribution of steric, electrostatic and hydrogen donor fields is 20.70%, 45.80% and 33.50%, respectively, indicating that the electrostatic field shows greater influence on inhibitory activity than others.

Table 4.12 The statistical parameters of CoMSIA model of 4-aminoquinoline Derivatives

model	Statistical parameters						
	r_{cv}^2	r^2	N	S_{press}	SEE	F	Fraction
S/E	0.65	0.98	6	0.25	0.06	200.89	29.50/70.50
S/H	0.47	0.95	6	0.31	0.09	74.76	42.90/57.10
S/A	0.36	0.92	6	0.34	0.12	49.02	34.50/65.50
S/D	0.36	0.90	6	0.34	0.13	35.79	48.30/51.70
S/E/H	0.63	0.97	6	0.25	0.07	155.68	21.60/51.50/26.80
S/E/A	0.51	0.97	6	0.29	0.07	137.15	17.80/39.90/42.30
S/E/D	**0.68**	**0.98**	**6**	**0.24**	**0.06**	**162.78**	**20.70/45.80/33.50**
S/E/H/A	0.56	0.97	6	0.28	0.07	151.11	14.30/33.00/16.70/36.00
S/E/H/D	0.64	0.97	6	0.25	0.07	130.17	15.90/37.50/18.80/27.80
S/E/H/A/D	0.53	0.97	6	0.29	0.07	144.55	11.40/24.10/13.00/31.50/20.00

Bold values indicate the best CoMSIA model. r_{cv}^2, leave-one-out (LOO) cross-validated correlation coefficient; r^2, non-cross-validated correlation coefficient; N, optimum number of components; S_{press}, Standard error of prediction, SEE, standard error of estimate; F, F-test value; S, steric field; E, electrostatic field; H, hydrophobic field; A, hydrogen acceptor field and D, hydrogen donor field

4.2.3.2 Validation of the CoMSIA model

The experimental and calculated activities for the training set derived from the best CoMSIA model are given in Table 4.13 and the correlations between experimental and calculated activities are shown in Figure 4.32. In the order to verify the predictive ability of the obtained model, the biological activities of the test set were predicted by CoMSIA model. All test set compounds showed predicted values within one logarithmic unit difference from the experimental values as presented in Table 4.13. These results show that CoMSIA model are low accuracy for predicting the inhibitory activity.

Table 4.13 The experimental and calculated activities of the training set from CoMSIA model

Compound	log(1/IC_{50})		
	Experimental	CoMSIA model	
		Calculated	Residues
01	4.64	4.62	0.02
02	4.83	4.75	0.08
03	4.77	4.59	0.18
04[b]	4.41	-	-
05	4.75	4.76	-0.01
06	4.65	4.65	0.00
07[b]	4.95	-	-
08	5.18	5.24	-0.06
09	4.80	5.17	-0.37
10[b]	4.63	-	-
11[a]	6.01	5.84	0.17
12	4.93	4.67	0.26
13	5.02	5.21	-0.19
14	4.77	4.99	-0.22
15	5.05	4.85	0.20
16[b]	6.01	-	-
17	4.98	5.14	-0.16
18[a]	4.68	4.94	-0.26
19	4.41	4.56	-0.15
20	4.35	4.31	0.04
21	4.73	4.61	0.12
22	4.33	4.01	0.32
23[a]	4.55	4.39	0.16
24[b]	4.90	-	-
25	5.53	5.45	0.08

[a]test set, [b]outlier of CoMSIA model

Table 4.13 The experimental and calculated activities of the training set from CoMSIA model (Continued)

Compound	log(1/IC_{50})		
	Experimental	CoMSIA model	
		Calculated	Residues
26	4.93	4.91	0.02
27[b]	4.97	-	-
28	5.49	5.10	0.39
29	5.94	5.46	0.48
30	4.58	4.74	-0.16
31	4.69	4.85	-0.16
32	4.50	4.67	-0.17
33[a]	4.56	4.40	0.16
34	4.95	4.64	0.31
35	4.41	4.68	-0.27
36[a]	4.82	4.68	0.14
37	5.10	4.98	0.13
38[b]	4.66	-	-
39	6.07	5.44	0.64
40	5.17	5.26	-0.09
41[a]	5.10	4.79	0.31
42	4.95	5.01	-0.06
43[a]	5.88	5.63	0.25

[a]test set, [b]outlier of CoMSIA model

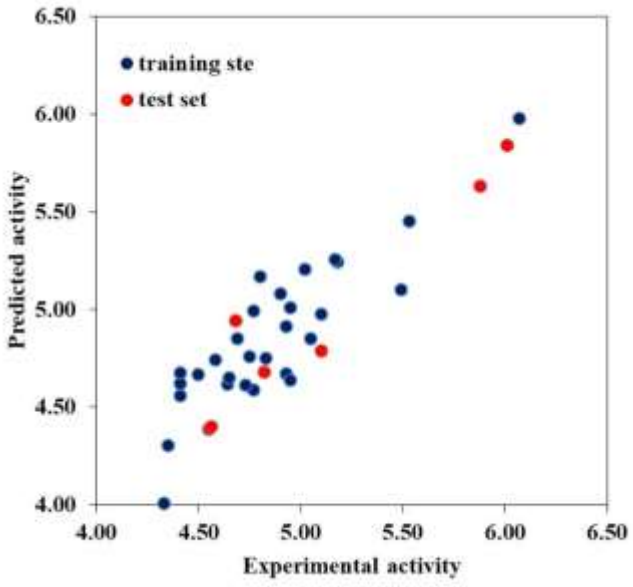

Figure 4.32 Plots between the experimental and predicted activities of training and test sets from CoMSIA model.

4.2.3.3 CoMSIA contour maps

To easily visualize the importance of steric, electrostatic, hydrophobic and hydrogen acceptor fields, CoMSIA contour maps were demonstrated as shown in Figures 4.33. CoMSIA steric contours, green and yellow contours indicate favorable and unfavorable areas, respectively. CoMSIA electrostatic contours, blue and red contours indicate favorable electropositive and electronegative regions, respectively. For CoMSIA hydrogen donor contour, cyan and purple contours represent the favorable hydrogen donor group and unfavorable hydrogen donor group, respectively.

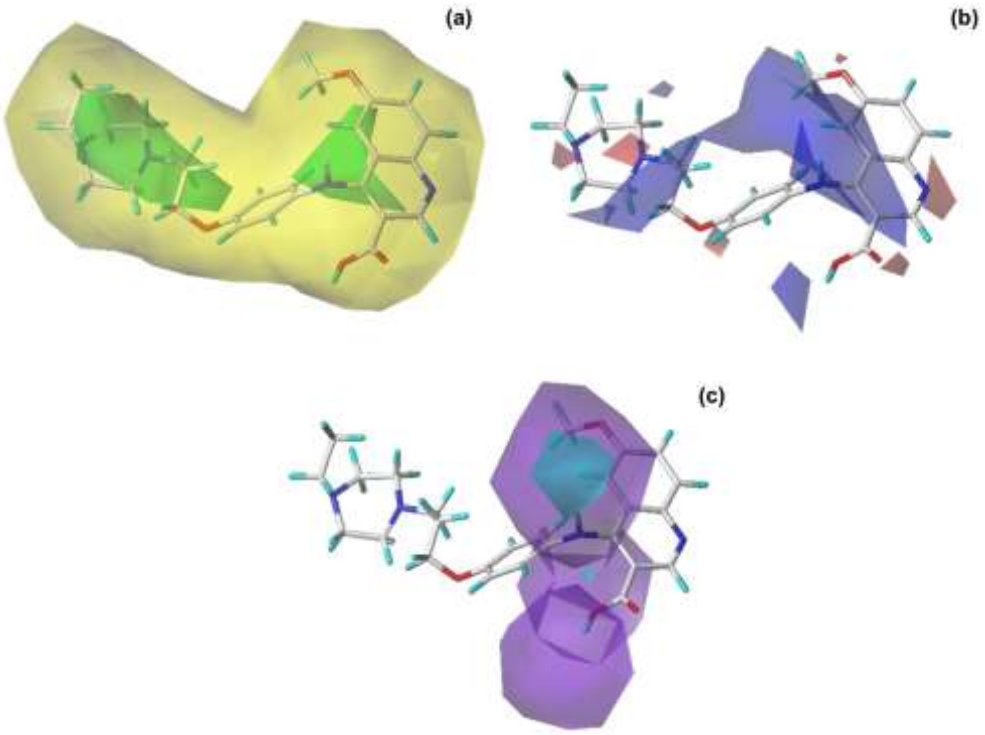

Figure 4.33 Steric (a), Electrostatic (b), and Hydrogen donor (c) CoMSIA contours in combination with compound 39.

From Figure 4.31, in this case the CoMSIA model showed big contours map of steric and hydrogen donor fields. Therefore, CoMSIA contour maps in this case can do not explain the structural requirement obtained from CoMSIA model to improve the biological activity against GyrB.

Electrostatic contour map has high contribution of 37.50% than steric and hydrogen donor fields, red contour appeared at the oxygen atom of carbonyl (C=O) group and nitrogen atom of quinoline ring indicated that electron withdrawing group of this fragment was required. At R substituent has the blue contour indicated that electron donating group of this fragment was required. For example compound **18** ($\log(1/IC_{50})$ = 4.68) showed the biological activity lower than compound **16** ($\log(1/IC_{50})$ = 6.01) due to compound **16** has hydrogen atom showing more electron donating group than fluoro (-F) group of compound **18**, respectively. For the X substituent has the small red contour indicated that electron withdrawing group of this position. For example compound **15** ($\log(1/IC_{50})$ = 5.05) showed the biological

activity lower than compound **11** ($\log(1/IC_{50})$ = 6.01) due to compound **11** has oxygen atom at X position showing more electron withdrawing group than amide (-NH-) of compound **15**, respectively. It indicates that positive charge properties referred to electron donating substituent at R position was required to design new and more potent activity of GyrB inhibitor as anti-tuberculosis agents.

4.2.3.4 The structural requirement obtained from CoMSIA model to improve the biological activity against GyrB should be as following;

(1) At the oxygen atom of carbonyl (C=O) group and nitrogen atom of quinoline ring, electron withdrawing group of this fragment was required.

(2) At R substituent, the electron donating group of this fragment was required.

(3) At X substituent, the electron withdrawing group of this fragment was required.

From these results can be concluded that the structural requirements of 4-aminoquinoline derivatives that favor for binding interactions in the GyrB binding pocket and aid to design new and more potent 4-aminoquinoline derivatives as anti-tuberculosis agents.

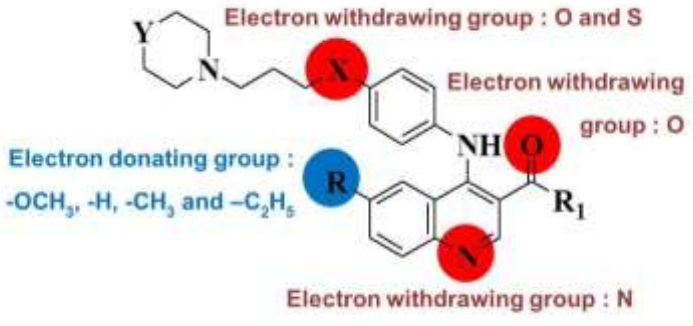

Figure 4.34 The structural requirement of 4-aminoquinoline derivatives in binding pocket obtained from 3D-QSAR study.

4.2.4 The structural concept of 4-aminoquinoline derivatives based on the integrated results from molecular dynamics simulations and 3D-QSAR CoMSIA model

Based on the molecular dynamics simulations and 3D-QSAR CoMSIA model results, structural concept of 4-aminoquinoline derivatives is summarized in Figure 4.35. At the oxygen atom of carbonyl (C=O) group and nitrogen atom of quinoline ring, electron withdrawing group. R substituent has blue contour indicated that electron donating group of this fragment was required. The position of R_1 substituent has hydrogen bond interactions with Ala53A, Asp5A, Glu56A and Asp79A, hydrophobic interaction with Met100A. The X substituent has the small red contour indicated that electron withdrawing group of this position.

Figure 4.35 Structural concept of 4-aminoquinoline derivatives derivatives summarized from molecular dynamics simulations and 3D-QSAR CoMSIA model.

CHAPTER 5
CONCLUSIONS

Computer aided molecular design is successfully applied on heteroaryl benzamide derivatives and 4-aminoquinoline derivatives against *M. tuberculosis* InhA and GyrB, repectively. The obtained results can be concluded as follows.

5.1 Enoyl-ACP reductase (InhA) inhibitors

The InhA inhibitor using molecular docking calculations provide a better understanding of the crucial interactions for binding affinity of heteroaryl benzamide derivatives in the InhA binding pocket. The obtained results indicate that hydrogen bond interactions play an important role on InhA binding pocket, especially. Hydrogen bonds interaction between hydrogen atoms of amide (-NH-) group in heteroaryl benzamide derivatives with oxygen atom of backbone of Met98 residue in the InhA binding pocket were reported and hydrogen bond interactions could be formed between nitrogen atom (N) of 3,5-dimethyl-1*H*-pyrazol-1-yl ring and pyridine ring with NAD^+ cofactor. Moreover, π-π interaction between 3,5-dimethyl-1*H*-pyrazol-1-yl ring and pyridine ring with aromatic ring of NAD^+ cofactor and hydrophobic interactions between heteroaryl benzamide derivatives with InhA residues in 4 angstrom could be observed. The dynamic behavior in structural information in term of structure flexibility, binding mode and binding interaction MD simulations were applied. MD trajectories evaluate the reliable stability the RMSDs for all atoms of InhA, NAD^+ cofactor and selected heteroaryl benzamide derivatives reach equilibrium at an early time point, whereas InhA reaches the equilibrium state after 5 ns. The binding modes and binding interaction of inhibitors in the InhA binding pocket obtained from MD simulations were analyzed. The hydrogen bond interaction between hydrogen atoms of amide (-NH-) group in heteroaryl benzamide derivatives with oxygen atom of backbone of Met98 residue in the InhA binding pocket was observed. The hydrogen bond interactions could be formed between nitrogen (N) atom of 3,5-dimethyl-1*H*-pyrazol-1-yl ring and pyridine ring with NAD^+ cofactor. This result

obtained from MD simulations corresponded well to molecular docking result as discussion. Met98 residue is a key interaction for binding of heteroaryl benzamide derivatives in InhA binding pocket. Therefore, the results obtained from this study should be beneficially for further modification of heteroaryl benzamide derivatives for rational design as potent InhA inhibitors against *M. tuberculosis*. The 3D-QSAR study can be beneficial to understand the structural requirements of heteroaryl benzamide derivatives were selected. The best of CoMSIA model showed highly prediction with r_{cv}^2 and r^2 of 0.50 and 0.96, respectively. The CoMSIA model shown the big contours map of steric and hydrophobic fields because the r_{cv}^2 is lower than 0.60. Therefore, CoMSIA contour maps in this case cannot explain the structural requirement of steric hydrophobic and hydrogen bond acceptor fields to improve the biological activity against InhA.

5.2 DNA gyras subunit B (GyrB) inhibitors

The GyrB inhibitor using molecular docking calculation was successfully applied to predict binding mode of 4-aminoquinoline derivatives in GyrB binding pocket. The obtained results demonstrate that hydrogen bond interactions play an important role in the binding in GyrB, especially on the hydrogen bonds of R and R_1 substituents part. The hydrogen bond interactions show with Asp79A, Thr169A and Tyr114A. The quinolone ring has the σ-π interaction with residues of Lys108A. Moreover, the hydrophobic interactions between 4-aminoquinoline derivatives with GyrB residues in 4 angstrom could be observed. The dynamic behavior in term of flexibility, conformation and the inhibitor enzyme interaction of 4-aminoquinoline derivatives in the GyrB binding pocket was successfully explained by MD simulations. The system of 4-aminoquinoline derivatives reach equilibrium at an early time point, whereas GyrB reaches the equilibrium state after 5 ns. In the case of compound **09**, **24**, **31**, **38**, **39**, **40**, **41** and **43**, MD systems reache equilibrium after 30, 45, 30, 40, 30, 30, 20 and 35 ns, respectively. The hydrogen bond interaction between hydrogen atoms of amide (-NH-) group in 4-aminoquinoline derivatives with oxygen atom of backbone of Asn52A residue in the GyrB binding pocket was observed. The hydrogen bonds of R_1 substituents with Ala53A, Asp55A, Glu56A and Asp79A were found. This result obtained from MD simulations corresponded well to molecular docking result as

discussion. Therefore, Met98 residue is a key interaction for binding of 4-aminoquinoline derivatives in GyrB binding pocket. For the CoMSIA model showed highly prediction with r_{cv}^2 and r^2 of 0.68 and 0.98, respectively. The CoMSIA model showed big contours map of steric and hydrogen bond donor fields, it can not explain the structural requirement of steric and hydrogen donor fields to improve the biological activity against GyrB. Therefore, the results obtained from this study should be beneficially for further modification of 4-aminoquinoline derivatives for rational design as potent GyrB inhibitors against *M. tuberculosis*.

Therefore, molecular modeling and computer aided molecular design approaches in this study provide an insight into the crucial interactions of inhibitor to exhibit enhanced inhibitory activity against InhA enzyme and GyrB enzyme. Successfully, predicted binding mode and binding interactions of anti-tuberculosis agents were obtained.

REFERENCE

REFERENCE

Abdel-Meguid, S. S., Murthy, H. M. K. and Steitz, T. A. "Preliminary X-ray diffraction studies of the putative catalytic domain of resolvase from *E. coli*", **The Journal of Biological Chemistry**. 261(34): 15934-15935; December, 1986.

Ahmad, Z., Sharma, S. and Khuller, G.K. "In vitro and ex vivo antimycobacterial potential of azole drugs against *Mycobacterium tuberculosis* H37Rv", **FEMS Microbiology Letters**. 251(1): 19-22; October, 2005.

Ahmad, Z. et al., "Anitimycobacterial activity of econazole against multidrug-resistant strains of *Mycobacterium tuberculosis*", **The International Journal Antimicrobial Agents**. 28(6): 543-544; December, 2006.

Ahmad, Z., Sharma, S. and Khuller, G. K. "Azole antifungals a novel chemotherapeutic agents aginst murine tuberculosis", **FEMS Microbiology Letters**. 261(2): 181-186; August, 2006.

Ahmad, Z., Sharma, S. and Khuller, G. K. "The potential of azole antifungals against latent/persistent tuberculosis", **FEMS Microbiology Letters**. 258(2): 200-203; May, 2006.

Akib, M. K. et al., "Multiple Receptor Conformers based Molecular Docking study of Fluorine Enhanced Ethionamide with Mycobacterium Enoyl ACP Reductase (InhA)", **Journal of Molecular Graphics and Modelling**. 77: 386-398; October, 2017.

am Ende, C. W. et al., "Synthesis and in vitro antimycobacterial activity of B-ring modified diaryl ether InhA inhibitors", **Bioorganic & Medicinal Chemistry Letters**. 18(10): 3029-3033; May, 2008.

Amit, P. et al., "First report on 3D-QSAR and molecular dynamics based docking studies of GCPII inhibitors for targeted drug delivery applications", **Journal of Molecular Structure**. 1159: 179-192; May, 2018.

Annaik, Q. et al., "Binding of catalase-peroxidase-activated isoniazid to wild-type and mutant *Mycobacterium tuberculosis* enoyl-ACP reductases", **Journal of the American Chemical Society**. 118(6): 8235-8241; February, 1996.

REFERENCE (CONTINUED)

Banerjee, A. et al., "inhA, a gene encoding a target for isoniazid and ethionamide in *Mycobacterium tuberculosis*", **Science**. 263(5144): 227-230; January, 1994.

Baulard, A. R. et al., "Activation of the Pro-drug Ethionamide Is Regulated in Mycobacteria", **The Journal of Biological Chemistry**. 275(36): 28326-28331; September, 2000.

Brown, P. O., Peebles, C. L. and Cozzarelli, N. R. "A topoisomerase from Escherichia coli related to DNA gyrase", **Proceedings of the National Academy of Sciences of the United States of America**. 79(12): 6110-6114; December, 1979.

Bruno, C. G. et al., "New insights into the SAR and drug combination synergy of 2-(quinolin-4-yloxy)acetamides against *Mycobacterium tuberculosis*", **European Journal of Medicinal Chemistry**. 126: 491-501; January, 2017.

Boyne, M. E. et al., "Targeting fatty acid biosynthesis for the development of novel chemotherapeutics against *Mycobacterium tuberculosis*: evaluation of A-ring-modified diphenyl ethers as high-affinity InhA inhibitors", **Antimicrobial Agents and Chemotherapy**. 51(10): 3562-3567; October, 2007.

Christophe, M. et al., "Chemical synthesis and biological evaluation of triazole derivatives as inhibitors of InhA and antituberculosis agents", **European Journal of Medicinal Chemistry**. 52: 275-283; June, 2012.

Comstock, G. W. "Epidemiology of tuberculosis", **American Review of Respiratory Disease**. 125(3): 8-15; March, 1982.

Coutinho, E. et al., "3D-QSAR study of ring-substituted quinoline class of anti-tuberculosis agents", **Bioorganic & Medicinal Chemistry**. 14(3): 847-856; February, 2006.

De, L. I. and Morbidoni, H. R. "Mechanisms of action of and resistance to rifampicin and isoniazid in *Mycobacterium tuberculosis*: New information on old friends", **Revista Argentina De Microbiologia**. 38(2): 97-109; June, 2006.

Erik, R. L. "Molecular Dynamics Simulations", **Molecular Modeling of Proteins**. 443: 3-23, 2015.

REFERENCE (CONTINUED)

Fangfang, W. et al., "Toward the identification of a reliable 3D-QSAR model for the protein tyrosine phosphatase 1B inhibitors", **Journal of Molecular Structure**. 1158: 75-87; April, 2018.

Freundlich, J.S. et al., "Triclosan derivatives: Towards potent inhibitors of drug-sensitive and drug-resistant *Mycobacterium tuberculosis*", **Chem. Med. Chem**. 4(2): 241-248; February, 2009.

Ganesh, S. P. et al., "Development of 2-(4-oxoquinazolin-3(4*H*)-yl)acetamide derivatives as novel enoyl-acyl carrier protein reductase (InhA) inhibitors for the treatment of tuberculosis", **European Journal of Medicinal Chemistry**. 86(30): 613-627; October, 2014.

Ganesh, S. P. et al., "Development of benzo[*d*]oxazol-2(3*H*)-ones derivatives as novel inhibitors of *Mycobacterium tuberculosis* InhA", **Bioorganic & Medicinal Chemistry**. 22(21): 6134-6145; November, 2014.

Gellert, M., Fisher, L. M. and O'Dea, M. H. "DNA gyrase: purification and catalytic properties of a fragment of gyrase B protein", **Proceedings of the National Academy of Sciences of the United States of America**. 76(12): 6289-6293; December, 1979.

Glikin, G. C., Ruberti, I. and Worcel, A. "Chromatin assembly in Xenopus oocytes: In vitro studies", **Cell**. 37(1): 33-41; May, 1984.

Global Tuberculosis Report; World Health Organization: Geneva, 2017. http://www.who.int/tb/publications/global_report/en/. April 26, 2017.

Graham, A. W. et al., "Immune responses to tuberculosis in developing countries: implications for new vaccines", **Nature Reviews Immunology published**. 5(8): 661-667; August, 2005.

Guardia, A. et al., "N-Benzyl-4-((heteroaryl)methyl)benzamides: A New Class of Direct NADH-Dependent 2-trans Enoyl–Acyl Carrier Protein Reductase (InhA) Inhibitors with Antitubercular Activity", **ChemMedChem**. 11(7): 687-701; April, 2016.

REFERENCE (CONTINUED)

He, X., Alian, A., and Ortiz de Montellano P. R. "Inhibition of the *Mycobacterium tuberculosis* enoyl acyl carrier protein reductase InhA by arylamides", **Bioorganic & Medicinal Chemistry**. 15(21): 6649-6658; November, 2007.

He, X. et al., "Pyrrolidine carboxamides as a novel class of inhibitors of enoyl acyl carrier protein reductase from *Mycobacterium tuberculosis*", **Journal of Medicinal Chemistry**, 49(21): 6308-6323; October, 2006.

Hou, T. et al., "Assessing the Performance of the MM/PBSA and MM/GBSA Methods. 1. The Accuracy of Binding Free Energy Calculations Based on Molecular Dynamics Simulations", **Journal of Chemical Information and Modeling**. 51(1): 69-82; January, 2011.

Jeankumar, V. U. et al., "Engineering another class of anti-tubercular lead: Hit to lead optimization of an intriguing class of gyrase ATPase inhibitors", **European Journal of Medicinal Chemistry**. 122: 216-231; October, 2016.

Kai, J. and Peter, G. S. "Mechanistic Studies of the Oxidation of Isoniazid by the Catalase Peroxidase from *Mycobscterium tuberculosis*", **American Chemical Society**. 116(16): 7425-7426; August, 1994.

Kaledin, M. et al., "Normal Mode Analysis Using the Driven Molecular Dynamics Method. Ii. An Application to Biological Macromolecules", **The Journal of Chemical Physics**. 121(12): 5646-5653; June, 2004.

Kenneth, T. "Tubercolosis", **Todar's Online Texthbook of Bacteriology**. http://www.textbookofbacteriology.net. (accessed May 01, 2018)

Kirchhausen, T., Wang, J. C. and Harrison, S. C. "DNA gyrase and its complexes with DNA: direct observation by electron microscopy", **Cell**. 41(3): 933-943; July, 1985.

Kitchen, D. B. et al., "Docking and scoring in virtual screening for drug discovery: methods and applications", **Nature reviews. Drug discovery**. 3(11): 935-949; November, 2004.

REFERENCE (CONTINUED)

Krishna, K. M. et al., "Design, synthesis and 3D-QSAR studies of new diphenylamine containing 1,2,4-triazoles as potential antitubercular agents", **European Journal of Medicinal Chemistry**. 84(12): 516-529; September, 2014.

Krueger, S. et al., "Neutron and light-scattering studies of DNA gyrase and its complex with DNA", **Journal of Molecular Biology**. 211(1): 211-220; January, 1990.

Kubinyi, H. **QSAR: Hansch Analysis and Related Approaches**. Weinheim, New York, Basil, Cambridge, Tokyo: VCH; 1993(a).

Kummetha, I. R. et al., "An efficient synthesis and biological screening of benzofuran and benzo[d]isothiazole derivatives for *Mycobacterium tuberculosis* DNA GyrB inhibition**", Bioorganic & Medicinal Chemistry**. 22(23): 6552-6563; December, 2014.

Kuo, M. R. et al., "Targeting tuberculosis and malaria through inhibition of Enoyl reductase: compound activity and structural data", **The Journal of Biological Chemistry**. 278(23): 20851-20859; June, 2003.

Lebeau, L. et al., "Two-dimensional crystallization of DNA gyrase B subunit on specifically designed lipid monolayen", **FEBS Letters**. 267(1): 38-42; July, 1990.

Lei, B., Wei, C. J. and Tu, S. C. "Action mechanism of antitubercular isoniazid. Activation by *Mycrobacterium tuberculosis* KatG, isolation, and characterization of inha inhibitor", **The Journal of Biological Chemistry**. 275(4): 2520-2526; January, 2000.

Lu, X., Huang, K. and You, Q. "Enoyl acyl carrier protein reductase inhibitors: a patent review (2006-2010)", **Expert Opinion on Therapeutic Patents**. 21(7): 1007-1002; July, 2011.

Manaf, A. et al., "Novel compounds targeting InhA for TB therapy", **Pharmacological Reports**. 70(2): 217-226; April, 2018.

Mario, C. R. et al., "XDR Tuberculosis-Implications for Global Public Health", **The New England Journal of Medicine**. 356: 656-659; February, 2007.

REFERENCE (CONTINUED)

Maxwell, A., "DNA Gyrase as a drug target", **Portland Press Limited**. 27(2): 48-53; February, 1999.

Maxwell, A. and Gellert, M. "Mechanistic aspects of DNA topoisomerases", **Advances in Protein Chemistry**. 38: 69-107, 1986.

Medapi, B. et al., "4-Aminoquinoline derivatives as novel *Mycobacterium tuberculosis* GyrB inhibitors: Structural optimization, synthesis and biological evaluation", **Journal of Medicinal Chemistry**. 103: 1-16; October, 2015.

More, U. A. et al., "Design, synthesis, molecular docking and 3D-QSAR studies of potent inhibitors of enoyl-acyl carrier protein reductase as potential antimycobacterial agents", **European Journal of Medicinal Chemistry**. 71: 199-218; January, 2014.

Morris, G. M. et al., "AutoDock", **User Guide**. http://chemistry.umeche.maine. edu/ Manuals/Autodock. April 12, 2018.

Morris, G. M. et al., "AutoDock Version 4.2", **User Guide**. http://autodock. scripps.edu/faqs-help/manual/autodock-4-2-user-guide/AutoDock4.2_User Guide.pdf. April 12, 2018.

Nadine, H. and Holger, G. "Free Energy Calculations by the Molecular Mechanics Poisson-Boltzmann Surface Area Method", **Molecular Informatics**. 31: 114-122, 2012.

Nayyar, A. et al., "synthesis, anti-tuberculosis activity, and 3D-QSAR study of ring-substituted-2/4-quinolinecarbaldehyde derivatives", **Bioorganic & Medicinal Chemistry**. 14(21): 7302-7310; November, 2006.

Ohta, T. and Hirose, S. "Purification of a DNA supercoiling factor from the posterior silk gland of Bombyx mori", **Proceedings of the National Academy of Sciences of the United States of America**. 87(14): 1307-1311; July, 1990.

Ramaswamy, S. V. et al., "Single Nucleotide Polymorphisms in Genes Associated with Isoniazid Resistance in *Mycobacterium tuberculosis*", **Antimicrobial Agents and Chemotherapy**. 47(4): 1241-1250; April, 2003.

REFERENCE (CONTINUED)

Patrice, L. J. et al., "Enaminones 8: CoMFA and CoMSIA studies on some anticonvulsant enaminones", **Bioorganic & Medicinal Chemistry**. 17: 133-140; January, 2009.

Pravin, S. et al., "Aminopyrazinamides: Novel and Specific GyrB Inhibitors that Kill Replicating and Nonreplicating *Mycobacterium tuberculosis*", **American Chemical Society Chemical Biology**. 8(3): 519-523; December, 2013.

Punkvang, A. **Computer-aided molecular design of mycobacterium tuberculosis enoyl-ACP reductase inhibitors as anti-tuberculosis agents**. Doctor's Thesis: Ubon Ratchathani University, 2010.

Punkvang, A. et al., "Elucidating Drug-Enzyme Interactions and Their Structural Basis for Improving the Affinity and Potency of Isoniazid and Its Derivatives Based on Computer Modeling Approaches", **Molecules**. 15(4): 2791-2813; April, 2010.

Rau, D. C. et al., "Structure of the DNA gyrase-DNA complex as revealed by transient electric dichroism", **Journal of Molecular Biology**. 193(3): 555-569; February, 1987.

Raviglione, M. C. and Uplekar, M. W. "WHO's new stop TB strategy", **The Lancet**. 367: 952-955; March, 2006.

Rhoda, D. and Mug, A. "Helical periodicity of DNA determined by enzyme digestion", **Nature**. 286: 573-578; August, 1980.

Richard, J. R. and Anthony, M. "DNA Gyrase: Structure and Function", **Critical Reviews in Biochemistry and Molecular Biology**. 26: 335-375, 1991.

Rozwarski, D. A. et al., "Modification of the NADH of the Isoniazid Target (InhA) from *Mycobacterium tuberculosis*", **Science**. 279(53747): 98-102; January, 1998.

Rozwarski, D. A. et al., "Crystal structure of the *Mycobacterium tuberculosis* enoyl-ACP reductase, InhA, in complex with NAD^+ and a C16 fatty acyl substrate", **The Journal of Biological Chemistry**. 274(22): 15582-15589; May, 1999.

REFERENCE (CONTINUED)

Ryoji, M. and Worcel, A. "Chromatin assembly in Xenopus oocytes: In vivo studies", **Cell**. 37(1): 21-32; May, 1984.

Saint-Joanis, B. et al., "Use of site-directed mutagenesis to probe the structure, function and isoniazid activation of the catalase/peroxidase, KatG, from *Mycrobacterium tuberculosis*", **Biochemical Journal**. 338(3): 753-760; March, 1999.

Shalini, S. et al., "Development of 2-amino-5-phenylthiophene-3-carboxamide derivatives as novel inhibitors of *Mycobacterium tuberculosis* DNA GyrB domain", **Bioorganic & Medicinal Chemistry**. 23(7): 1402-1412; April, 2015.

Shen, L. L., Baranowski, J. and Pernet, A. G. "Mechanism of inhibition of DNA gyrase by quinolone antibacterial agents; specificity and cooperativity of drug binding", **Biochemistry**. 28(9): 3879-3885, 1989.

Shrinivas, D. J. et al., "Chemical synthesis and in *silico* molecular modeling of novel pyrrolyl benzohydrazide derivatives: Their biological evaluation against enoyl ACP reductase (InhA) and *Mycobacterium tuberculosis*", **Bioorganic Chemistry**. 75: 181-200; December, 2017.

Soolingen, D. et al., "A novel pathogenic taxon of the *Mycobacterium tuberculosis* complex, Canetti: characterization of an exceptional isolate from Africa", **International Journal of Systematic Bacteriology**. 47(4): 1236-1245; October, 1997.

Srilata, B. et al., "Rational design of methicillin resistance staphylococcus aureus inhibitors through 3D-QSAR, molecular docking and molecular dynamics simulations", **Computational Biology and Chemistry**. 73: 95-104; April, 2018.

Stane, P. et al., "New direct inhibitors of InhA with antimycobacterial activity based on a tetrahydropyran scaffold", **European Journal of Medicinal Chemistry**. 112(13): 252-257; April, 2016.

REFERENCE (CONTINUED)

Sullivan, T. J. et al., "High affinity InhA inhibitors with activity against drug-resistant strains of *Mycobacterium tuberculosis*", **ACS Chemical Biology**. 1(1): 43-53; February, 2006.

Tihomir, T. et al., "Design, synthesis and biological evaluation of 4,5-dibromo-*N*-(thiazol-2-yl)-1H-pyrrole-2-carboxamide derivatives as novel DNA gyrase inhibitors", **Bioorganic & Medicinal Chemistry**. 25(1): 338-349; November, 2017.

Totrow, M. and Abagyan, R. "Flexible ligand docking to multiple receptor conformations: a practical alternative", **Current Opinion in Structural Biology**. 18(2): 178-184; April, 2008.

Variam, U. J. et al., "Development of novel *N*-linked aminopiperidine-based mycobacterialDNA gyrase B inhibitors: Scaffold hopping from known antibacterialleads", **International Journal of Antimicrobial Agents**. 43(3): 269-278; March, 2014.

Variam, U. J. et al., "Thiazole-aminopiperidine hybrid analogues: Design and synthesis of novel *Mycobacterium tuberculosis* GyrB inhibitors", **European Journal of Medicinal Chemistry**. 70: 143-153; December, 2013.

Wahab, H. A. et al., "Binding of the tautomeric forms of isoniazid-NAD adducts to the active site of the *Mycobacterium tuberculosis* enoyl-ACP reductase (InhA): A theoretical approach", **Journal of Molecular Graphics and Modelling**. 27(4): 536-545; November, 2008.

Wang, J. et al., "Recent Advances in Free Energy Calculations with a Combination of Molecular Mechanics and Continuum Models", **Current Computer-Aided Drug Design**. 2(3): 287-306; December, 2006.

Wang, J. et al., "Use of Mm-Pbsa in Reproducing the Binding Free Energies to Hiv-1 Rt of Tibo Derivatives and Predicting the Binding Mode to HIV-1 RT of Efavirenz by Docking and MM-PBSA", **Journal of the American Chemical Society**. 123(22): 5221-5230; June, 2001.

White, J. H., Cozzarelli, N. R. and Bauer, W. R., "Helical repeat and linking number of surface wrapped DNA", **Science**. 241(4863): 323-327; July, 1988.

REFERENCE (CONTINUED)

World Health Organization. **Treatment of Tuberculosis: guideline**. 4th ed. Geneva: World Health Organization, 2010.

_____. **Global Tuberculosis Report; Geneva**, 2017. http://www.who.int/tb/publications/global_report/en/. April 26, 2017.

Xiao-Yun, L. et al., "Discovery of potential new InhA direct inhibitors based on pharmacophore and 3D-QSAR analysis followed by in silico screening", **European Journal of Medicinal Chemistry**. 44(9): 3718-3730; September, 2009.

Zhao, X. et al., " Hydrogen peroxide-mediated isoniazid activation catalyzed by *Mycrobacterium tuberculosis* catalase-peroxidase (KatG) and its S315T mutant", **Biochemistry**. 45(1): 4131-4140; March, 2006.

Zhipeng, K. et al., "3D-QSAR and molecular fragment replacement study on diaminopyrimidine and pyrrolotriazine ALK inhibitors", **Journal of Molecular Structure**. 1067: 127-137; June, 2014.

Ziga, J. et al., "Discovery of substituted oxadiazoles as a novel scaffold for DNA gyrase inhibitors", **European Journal of Medicinal Chemistry**. 130: 171-184; April, 2017.

Zsoldos, Z. et al., "eHiTS: A new fast, exhaustive flexible ligand docking system", **Journal of Molecular Graphics and Modelling**. 26(1): 198-212; July, 2007.

APPENDIX

CONFERENCES

Publication

National proceeding

1. **N. Phusi**, C. Hanwarinroj, K. Chayaras, P. Kamsri, A. Punkvang,P. Saparpakorn, S. Hannongbua, K. Suttisintong, N. Suttipanta, R. Takeda,I. Kobayashi, N. Kurita, P. Pungpo, "**Structure based inhibitor design of novel anti-tuberculosis agents of 4-aminoquinoline derivatives in DNA gyrase b subunit (Gyrb) using molecular docking study**", Proceedings of The 42nd Congress on Science and Technology of Thailand (STT 42), Bangkok, Thailand, 2016, 258-262.

International proceeding

1. **N. Phusi**, B. Tharat, C. Hanwarinroj, K. Chayajaras, N. Suttipanta, P. Kamsri, A. Punkvang, P. Saparpakorn, S. Hannongbua, K. Suttisintong, P. Pungpo, "**Insight into the crucial binding mode and binding interaction of 4-aminoquinoline derivatives with *M. tuberculosis* GyrB using MD simulation and binding free energy calculation**", Proceedings of The 8th Thailand-Japan International Academic Conference 2016, Tokyo, Japan, 101-105.
2. **N. Phusi**, P. Kamsri, A. Punkvang, P. Saparpakorn, S. Hannongbua, Z. Chen, W. Zhu, S. Sureram, P. Kittakoop, N. Suttipanta, K. Chayajaras, P. Pungpo, "**Discovery of New of PknG Inhibitors from the Endophytic Fungus Dothideomycete sp.: In Silico based Drug Design**", Abstract of The 1st International Conference on Natural Medicine : From Local Wisdom to International Reseach, Bangkok, Thailand, 2017, 96.

National paper

1. **N. Phusi**, C. Hanwarinroj, K. Chayajaras, N. Suttipanta, P. Kamsri, A. Punkvang, K. Suttisintong, P. Saparpakorn, S. Hannongbua, P. Kittakoop, J. Spencer, A. Mulholland, P. Pungpo, "**Structure based drug design of 4-aminoquinilone derivatives in DNA Gyrase B subunit for anti-tuberculosis agents using molecular dynamics simulations**", Proceedings of the 21st International Annual Symposium on Computational Science and Engineering (ANSCSE21), Journal of Science and Technology Ubon Ratchathani University, Special Issue November, 2017, 31-35

C4_238_PF: STRUCTURE BASED INHIBITOR DESIGN OF NOVEL ANTI-TUBERCULOSIS AGENTS OF 4-AMINOQUINOLINE DERIVATIVES IN DNA GYRASE B SUBUNIT (GyrB) USING MOLECULAR DOCKING STUDY

Naruedon Phusi,[1] Chayanin Hanwarinroj,[1] Kampanart Chayaras,[1] Pharit Kamsri,[2] Auradee Punkvang,[2] Patchareenart Saparpakorn,[3] Supa Hannongbua,[3] Khomson Suttisintong,[4] Nitima Suttipanta,[5] Ryosuke Takeda,[6] Ittettsu Kobayashi,[6] Noriyuki Kurita,[6] and Pornpan Pungpo[1,*]

[1] Department of Chemistry, Faculty of Science, Ubon Ratchathani University, 85 Sthollmark Rd.,Warinchamrap, Ubonratchathani, 34190, Thailand

[2] Faculty of Science, Nakhon Phanom University, Nakhon Phanom, 48000, Thailand

[3] Department of Chemistry, Faculty of Science, Kasetsart University, Chatuchak, Bangkok, 10900, Thailand

[4] National Nanotechnology Center, 114 Thailand Science Park, Pathumthani, Thailand

[5] Faculty of Pharmaceutical Science, Ubon Ratchathani University, 85 Sthollmark Rd., Warinchamrap, Ubonratchathani, 34190, Thailand

[6] Department of Computer Science and Engineering, Toyohashi University of Technology, Tempaku-cho, Toyohashi, Aichi, 441-8580, Japan

*E-mail: pornpan_ubu@yahoo.com

Abstract: Mycobacterial DNA gyrase B subunit has been identified to be one of the potentially underexploited drug targets in the field of anti-tuberculosis drug discovery. This research, molecular docking calculations using Autodock 4.2 program was used to study the binding interactions between 4-aminoquinoline derivatives and DNA gyrase B subunit. The obtained results showed that the molecular docking calculation was reliable to predict the binding mode and binding interactions with RMSD of 0.84 angstrom. The crucial interactions of 4-aminoquinoline derivatives in the binding pocket are hydrogen bond interaction between methoxyl (-OCH_3) at R substituent with Val13 and Ile115 of DNA gyrase B subunit, hydroxyl at R_1 substituent with Glu20. Two hydrogen bond interactions could be formed between carbonyl oxygen of carboxylic functional on quinoline with Ile48 and Thr113. Moreover, R, R_1, X and Y substituents were benefit to hydrophobic interactions leading to increasing of DNA gyrase B subunit inhibitory activity. Therefore, molecular docking aids to a better understand the structural basis of 4-aminoquinoline derivatives to rational design more potent DNA gyrase B subunit inhibitors as potential anti-tuberculosis agents.

Introduction: Tuberculosis (TB), caused by *Mycobacterium tuberculosis* (*M. tuberculosis*), remains a major global health problem. In 2014, an estimated 9.0 million people developed TB and 1.5 million died from the disease [1]. Multidrug resistant tuberculosis (MDR-TB), widespread extensive drug-resistance TB (XDR-TB), and co-infection between *M. tuberculosis* and HIV (TB/HIV) are major problems of tuberculosis treatment [2,3]. The proportion of new cases with MDR-TB was 3.5% in 2015 [1]. The clinical efficacy of fluoroquinolone drugs demonstrated over the past 20-30 years has validated DNA gyrase as a target in the area of broad-spectrum antibacterials[4]. Gyrase A subunit has been facing a major hurdle of their resistance developed by *M. tuberculosis* which makes gyrase B subunit a drug able target for discovery of potent anti-tuberculosis agents. DNA gyrase B subunit is involved in the process of ATP hydrolysis which in turn provides energy to gyrase A subunit for maintaining the DNA topological state [5]. Therefore, GyrB has been genetically demonstrated to be a bactericidal drug target in *M. tuberculosis*, but there have not been any effective therapeutics developed against this target for TB [6]. Recently, 4-aminoquinoline derivatives have been developed as anti-tuberculosis agents with moderate biological activities against *M. tuberculosis* and XDR *M. tuberculosis* [7]. Therefore, molecular docking calculations approaches have been used to understand the structural basis of these derivatives to develop new highly anti-tuberculosis agents. The obtained results aid to design new and more potent anti-tuberculosis agents.

Methodology: Eight chemical structures and their experimental biological activities of 4-aminoquinoline derivatives were selected from the literature as presented in Table 1[7]. The biological activities of these compounds were expressed in terms of *Msm*GyrB assay (IC_{50} in μM) values. All chemical structures of these inhibitors were constructed using the standard tools available in GaussView 3.07 program and were then fully optimized using the HF/6-31G* method implemented in

Gaussian 09 program. Molecular docking calculations using Autodock 4.2 program was performed to predict the potent inhibitors in the GyrB binding pocket (PDB Code: 4B6C)

Table 1. Eight chemical structures and their *Msm*Gyr B assay (IC_{50} in μM) values of 4-aminoquinoline derivatives.

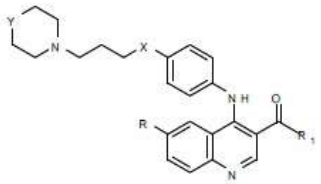

Cpd.	R	R_1	X	Y	MsmGyr B assay (IC_{50} in μM)
1	OCH_3	OH	O	NC_2H_5	0.86
2	H	OH	O	NC_2H_5	21.66
3	F	OH	O	NC_2H_5	6.82
4	CF_3	OH	O	NC_2H_5	7.91
5	OCH_3	OC_2H_5	O	NC_2H_5	15.92
6	OCH_3	$NHNH_2$	O	NC_2H_5	12.63
7	OCH_3	OH	NH	NC_2H_5	1.32
8	OCH_3	OH	O	O	20.56

Results and Discussion: This research, molecular docking calculations using Autodock 4.2 program were performed to study the binding interactions between 4-aminoquinoline derivatives and DNA gyrase B subunit. The obtained results show that the molecular docking calculation was reliable to predict the binding mode and binding interactions with RMSD of 0.84 angstrom as shown in Figure 1.

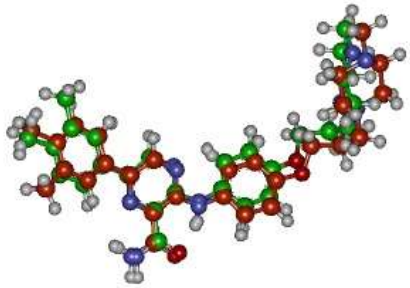

Figure 1. The x-ray ligand (green) and calculation ligand (orange) in DNA gyrase B subunit biding pocket.

High GyrB inhibition (compound 1): The interactions compound **1** (IC_{50} of 0.86 μM) with of amino acid surrounding the binding pocket of GyrB enzyme was shown in Figure 2. Hydrogen bond interactions were found as the crucial interactions for binding in GyrB binding site. An oxygen atom of methoxy (–OCH_3) R substituent, hydrogen bond interactions of this substituent with Val13 and Ile115 in the GyrB binding pocket were reported. Hydroxyl (–OH) at R_1 substituent interacted with Glu20 *via* hydrogen bond interaction. Moreover, hydrogen bond interactions could be formed between carbonyl oxygen (C=O), quinoline (N) with Ile48 and Thr113, respectively. Moreover, hydrophobic interactions with Ala17, Met64, Val69 and Ser70 were observed as shown in Figure 2.

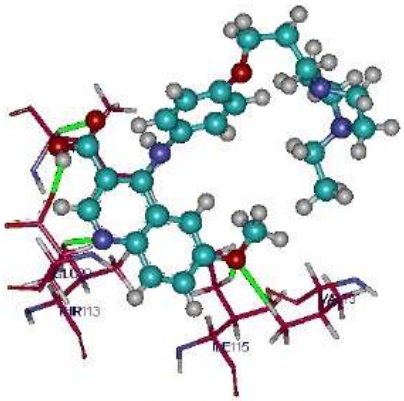

Figure 2. The binding mode of compound **1** in the GyrB binding pocket.

The effects of R substituent: The interactions compound **2** (IC_{50} of 21.66 µM), compound **3** (IC_{50} of 6.82 µM) and compound **4** (IC_{50} of 7.91 µM) with of amino acid surrounding the binding pocket of GyrB enzyme were investigated to study the effect of R substituent. Compound **2** at R substituent (-H) hydrogen bond interaction was not found. Whereas, hydrogen interactions of fluoro (-F) R substituent of compound **3** with Val13 and Ile115 were found. For compound **4**, trifluoromethyl ($-CF_3$) substituent formed hydrogen interaction with Ile48. Moreover, hydrogen bond interactions could be formed between carbonyl oxygen (C=O), quinoline (N) with Ile48, Pro49 and Thr113, respectively. Additional hydrophilic interactions with Val63, Met64 and Ser70 can be found were shown in Figure 3.

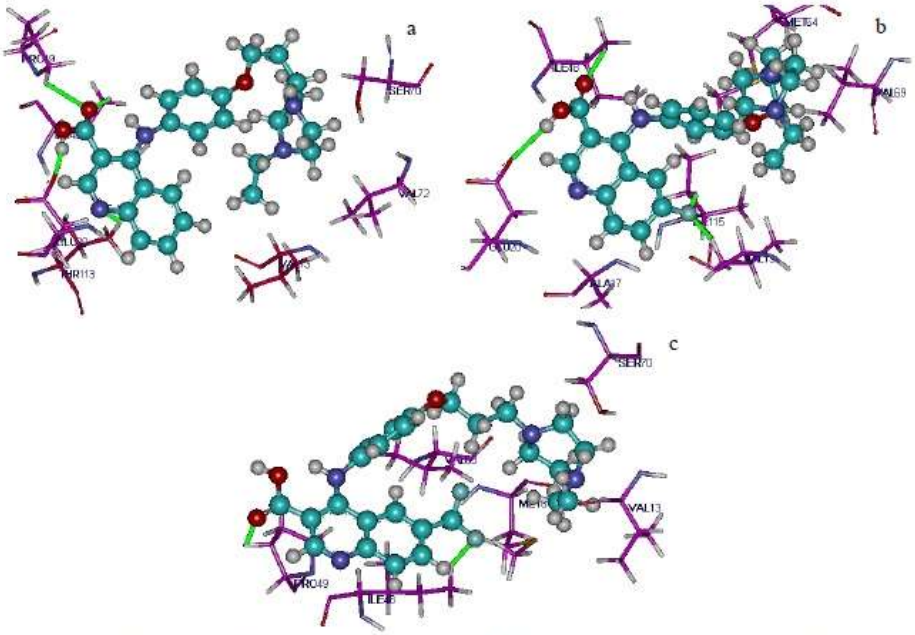

Figure 3. The binding mode of (a) compound **2**, (b) compound **3** and (c) compound **4** in the GyrB binding pocket.

The effects of R_1 substituent: The ethoxy ($-OC_2H_5$) R_1 substituent of compound **5** (IC_{50} of 15.92 µM) formed hydrogen interactions with Glu20 and Ile48 amino acid surrounding the binding pocket of GyrB enzyme. Hydrazine ($-NHNH_2$) R_1 substituent of compound **6** (IC_{50} of 12.63 µM) bound with Glu20 and Gly47 in the GyrB binding pocket *via* hydrogen bond interactions. Moreover, hydrophilic interactions with Ala17, Pro49, Val63 and Met64 were found to improve the biological activity as shown in Figure 4.

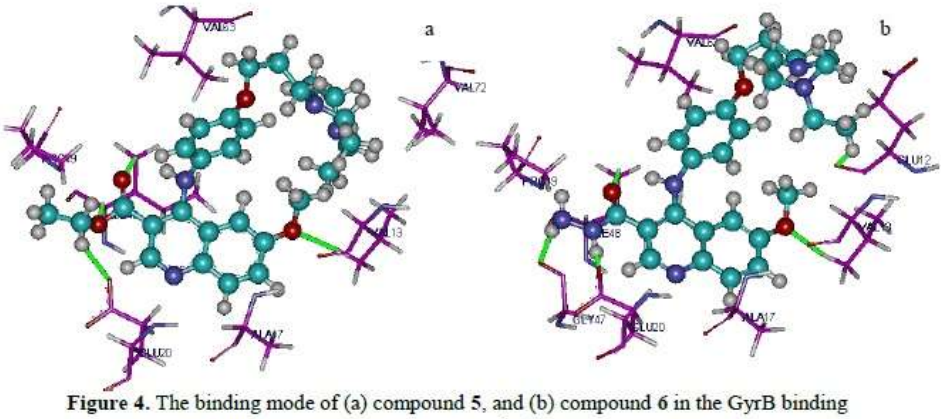

Figure 4. The binding mode of (a) compound **5**, and (b) compound **6** in the GyrB binding pocket.

The effects of X and Y substituent: The interactions of compound **7** (IC_{50} of 1.32 µM) with amino acid surrounding the binding pocket of GyrB enzyme were studied. The crucial interaction with amino acid of NH at X substituent was not found. Whereas, compound **8** (IC_{50} of 20.56 µM), oxygen atom (-O) at Y substituent with Val72 in the binding pocket *via* bound hydrogen interaction. Moreover, hydrogen bond interactions with Asn16 and Ser70 were reported. Additional hydrophilic interactions with Val13, Ala17, Val63 and Met64 were found as shown in Figure 5.

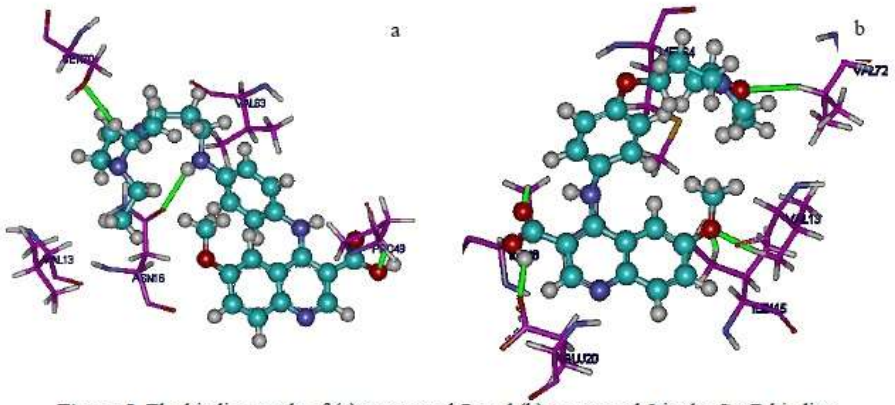

Figure 5. The binding mode of (a) compound **7**, and (b) compound **8** in the GyrB binding pocket.

Key binding for improving biological activity: At R position when compare with compound **3** and compound 4 the result indicated that compound **3** is more hydrophobic in interactions than compound **4**. The R_1 position compound **6** is highly active compound more than compound 5 because compound **6**

have more hydrogen bonds and hydrophilic interactions than compound **5**. At Y position large substituent and polarity were required to improve the biological activity. Therefore, new design compounds should be contained the substituent that they can interacted with amino acid surrounding GyrB binding pocket *via* structural basis derived from molecular docking calculations.

Conclusion: Molecular docking calculations were successfully applied to investigate the key structural for binding of 4-aminoquinoline derivatives in the binding site of DNA gyrase B subunit. Hydrogen bond and hydrophobic interactions are crucial interactions for binding of 4-aminoquinoline derivatives in GyrB derived from molecular docking calculations. The information derived from this study guided to design new and more potent GyrB inhibitors against *M. tuberculosis*.

References:

1. World Health Organization, Global tuberculosis report 2015, http://www.who.int /tb/publications/global_report/gtbr15_main_text.pdf
2. M. A. Aziz, A. Wright, L A.aszlo, A. De Muynck, F. Portaels, A. Van Deun, C. Wells, P. Nunn, L. Blanc, M. Raviglione, "Epidemiology of antituberculosis drug resistance (the Global Project on Anti-tuberculosis Drug Resistance Surveillance): an updated analysis". j.Lancet 2006, 368, 2142–2154.
3. M. C. Raviglione, I. M. Smith, N Engl. "XDR Tuberculosis-Implications for Global Public Health", N. Engl. J. Med. 2007, 356, 656–659.
4. A. Maxwell, "DNA gyrase as a drug target", Trends Microbiol.5: 1997, 5, 102-109.
5. R.J. Lewis, O.M. Singh, C.V. Smith, T. Skarzynski, A. Maxwell, A.J. Wonacott, D.B. Wigley, "The nature of inhibition of DNA gyrase by the coumarins and the cyclothialidines revealed by X-ray crystallography", EMBO.J., 1996, 15, 1412-1420.
6. P. Kaur, S. Agarwal, S. Datta, "Delineating Bacteriostatic and Bactericidal Targets in Mycobacteria Using IPTG Inducible Antisense Expression", PLoS One 4, 2009, 5923.
7. B. Medapi, P. Suryadevara, J. Renuka, J. P. Sridevi, P. Yogeeswari, D. Sriram, "4-Aminoquinoline derivatives as novel *Mycobacterium tuberculosis* GyrB inhibitors: Structural optimization, synthesis and biological evaluation", Eur. J. Med.Chem., 2015, 103,1-16.

Acknowledgements: This research has been supported by the Thailand Research Fund (RSA5980057 and MRG5980152), the National Research Council of Thailand, Center of Excellence for Innovation in Chemistry: PERCH-CIC and Higher Education Research Promotion. Faculty of Science, Ubon Ratchathani University, Kasetsart University and NECTEC are gratefully acknowledged for supporting this research.

Conference Proceedings
The 8th Thailand-Japan International Academic Conference 2016

Insight into the crucial binding mode and binding interaction of 4-aminoquinoline derivatives with *M. tuberculosis* GyrB using MD simulation and binding free energy calculation

Naruedon Phusi[1], Bunrat Tharat[1], Chayanin Hanwarinroj[1], Kampanart Chayajaras[1], Nitima Suttipanta[2], Pharit Kamsri[3], Auradee Punkvang[3], Patchareenart Saparpakorn[4], Supa Hannongbua[4], Khomson Suttisintong[5] and Pornpan Pungpo[1,a]

1 Department of Chemistry, Faculty of Science, Ubon Ratchathani University,85 Sthollmark Rd., Warinchamrap, Ubonratchathani, 34190, Thailand
2 Faculty of Pharmaceutical Science, Ubon Ratchathani University,85 Sthollmark Rd., Warinchamrap, Ubonratchathani, 34190, Thailand
3 Faculty of Science, Nakhon Phanom University, Nakhon Phanom, 48000, Thailand
4 Department of Chemistry, Faculty of Science, Kasetsart University, Chatuchak, Bangkok, 10900, Thailand
5 National Nanotechnology Center, 114 Thailand Science Park, Pathumthani, Thailand
E-mail: [a]pornpan_ubu@yahoo.com

Abstract. Mycobacterial DNA gyrase B subunit has been identified to be one of the potentially underexploited drug targets in the field of antitubercular drug discovery. A series of novel 4-aminoquinoline derivatives were developed as potential GyrB inhibitors. In the present study, we applied MD simulations to elucidate the binding site of 4-aminoquinoline derivatives in the GyrB pocket. Based on the obtained MD simulations, the results indicate that compound 1, the highest active compound, could form hydrogen bond interactions with residues Asn52 in the GyrB pocket as compared to other compounds. Moreover, electrostatic and hydrophobic interactions are also important for binding affinities. Based on rational design novel 4-aminoquinoline derivatives, design compounds showed strong hydrogen bond interactions with amino acids in GyrB binding pocket. Consequently, the obtained results from this study provide informative structural concept for designing of novel 4-aminoquinoline derivatives with better potency against GyrB.

Keywords: 4-Aminoquinoline derivatives, GyrB, anti-TB agents, MD simulations

1. Introduction

Tuberculosis (TB), caused by *Mycobacterium tuberculosis* (*M. tuberculosis*), remains a major global health problem. In 2015, an estimated 9.0 million people developed TB and 1.5 million died from the disease [1]. Multidrug resistant tuberculosis (MDR-TB), widespread extensive drug-resistance TB (XDR-TB), and co-infection between *M. tuberculosis* and HIV (TB/HIV) are major problem of tuberculosis treatment [2,3]. The proportion of new cases with MDR-TB was 3.5% in 2015 [1]. The clinical efficacy of fluoroquinolone drugs demonstrated over the past 20-30 years has validated DNA gyrase as a target in the area of broad-spectrum antibacterials [4]. Gyrase A subunit has been facing a major hurdle of their resistance developed by *M. tuberculosis* which makes gyrase B subunit a drug able target for discovery of potent anti-tuberculosis agents. DNA gyrase B subunit is involved in the process of ATP hydrolysis which in turn provides energy to gyrase A subunit for maintaining the DNA topological state [5]. So, GyrB has been genetically demonstrated to be a bactericidal drug target in *M. tuberculosis*, but there have not been any effective therapeutics developed against this target for TB

[6]. Recently 4-aminoquinoline derivatives have been developed as anti-tuberculosis agents with moderate biological activities against *M. tuberculosis* and XDR *M. tuberculosis* [7]. Therefore, MD simulations approaches have been used to understand dynamic be heavier and the structural requirements of these derivatives. The obtained results showed aid to design new and more potent anti-tuberculosis agents.

2. Materials and Methods

Three chemical structures and their experimental biological activities of 4-Aminoquinoline derivatives were selected from the literature, presented in Table 1, where they are described to be determined under the same experimental conditions [7]. The biological activities of these compounds were expressed in terms of MsmGyrB assay (IC_{50} in μM) values. All chemical structures of these inhibitors were constructed using the standard tools available in GaussView 3.07 program and were then fully optimized using the HF/6-31G* method implemented in Gaussian 09 program. The initial coordinates for MD simulations of the complexes was obtained from molecular docking calculations using Autodock 3.05 program. MD simulations were performed to predict the inhibitors in the GyrB binding pocket (PDB Code: 4B6C). TIP3P water model and Na^+ were chosen to represent water for salvation and ion for neutralize system. The root-mean square deviations (RMSDs) of the GyrB enzyme and the inhibitors, binding interactions were analyzed based on the equilibrium state obtained. The binding free energies were calculated to evaluate the binding affinities of inhibitors in GyrB binding pocket using the Molecular Mechanics Poisson-Boltzmann Surface Area (MM-PBSA) [8-11] and Normal-mode [12] methods.

Table 1 Three chemical structures and their MsmGyr B assay (IC_{50} in μM) values of 4-Aminoquinoline derivatives.

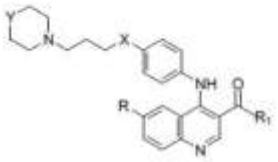

Cpd.	R	R_1	X	Y	MsmGyr B assay (IC_{50} in μM)
1	OCH_3	OH	NH	NC_2H_5	1.32
2	F	OH	O	NC_2H_5	6.82
3	CF_3	OH	O	NC_2H_5	7.91

3. Results and Discussion

Structural stability during MD simulations and binding free energy calculations

In order to determine structural stability during MD simulation of compounds **1**, **2** and **3** in GyrB binding pocket, the RMSDs for all atoms of solute species (GyrB enzyme and inhibitor) relative to the initial structure over the 15 ns of simulation times were calculated and plotted in Figure 1. The plateau characteristic of the RMSD plot over the simulation time is the criteria to indicate the equilibrium state of each solute species. Convergent RMSD plots indicate that the equilibrium state of compounds **1**, **2** and **3** was reached after 2 ns, 5ns and 2ns, respectively. The obtained results from the last 5 ns were mainly analyzed in more details of binding free energy and binding interactions.

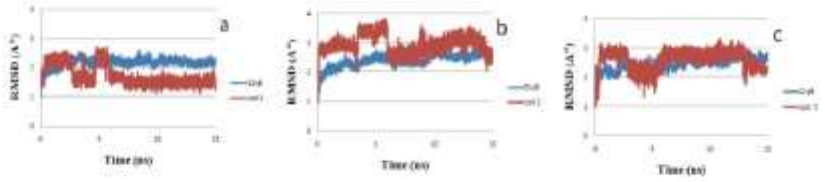

Fig.1 RMSD plots of compounds **1** (a), **2** (b), and **3** (c) complexed with GyrB

Binding mode and binding interactions of compounds

The crucial interactions of compound 1, the highest active compound, with amino acids surrounding the binding pocket of GyrB enzyme was analyzed, shown in Figure 2 (a). The major interactions in the GyrB binding pocket are hydrogen bond interactions as following details: A strong hydrogen bond interaction between -OCH_3 at R substituent of compound 1 with Asn52 (2.120 Å) can be observed. Electrostatic interaction between carboxylic and guanidinium group of Arg82 and Arg121 were observed. Additional hydrophobic interaction between quinoline with amino acid residue in their binding pocket can be found. In contrast, for compounds 2 and 3 showing less active compounds, important interactions of the inhibitors were significantly reduced. As compared to compound 1, stronger hydrogen bond interaction between R substituent of compound 2 with Gln102 (2.046 Å) and hydrogen bond interaction of nitrogen atom (N) on piperazine ring of compound 3 and NH_2 of Gln102 (1.957 Å) were found. As compared the hydrogen bond interaction and hydrophobic interaction of inhibitors in GyrB binding site, it can be seen that these interactions in compound 1 are high than compound 2 and compound 3. To gain quantitative insights into the affinity for binding of aminoquinoline inhibitors in the GyrB binding site, the binding free energies of aminoquinolines/GyrB complexes were calculated by the MM-PBSA method, reported in Table 2. It is notable that the calculated free binding energies of inhibitors are in the correct order as compared with the IC_{50} values. The obtained results could be successfully used to validate the MD procedure in this study.

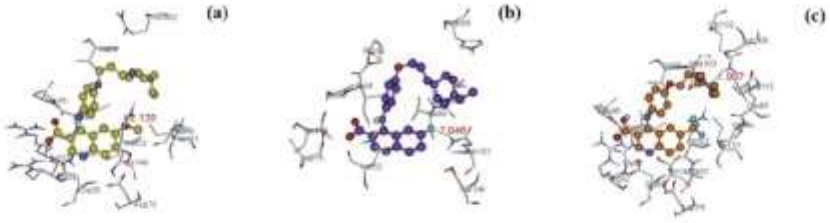

Fig. 2 Binding mode of compound 1 (a), compound 2 (b) and compound 3 (c) in GyrB binding pocket derived from MD simulations.

Table 2 The calculated binding free energies (kcal/mol) of 4-Aminoquinoline inhibitors calculated by MM-PBSA method.

Cpd.	Energies (kcal/mol)			
	ΔH	-TΔS	$\Delta G_{cal.}$	$\Delta G_{exp.}$
1	-38.00	-29.60	-8.40	-8.07
2	-20.58	-14.21	-6.37	-7.09
3	-43.39	-27.48	-6.91	-7.01

Rational design of new 4-aminoquinoline derivatives

Based on MD simulations results, the key structural basis of 4-aminoquinoline derivatives were obtained. The binding mode and binding interactions of compound **1** was considered to design new compounds. All functional groups of compound **1** was kept. Weak hydrogen bond interaction of hydrogen atom at 8 position on quinoline of compound **1** with carboxylate functional of Asp79 was considered. To improve the binding interaction with this position, hydrogen bond donor groups such as OH and NH_2 were introduced on this position. Based on molecular docking, we found that introduced hydrogen bond donor groups increased number of hydrogen bond interaction in GyrB binding pocket. For example, hydrogen bond network between HO functional on 8 position of quinolone ring of design compound with Asp79 (2.088 Å) and Thr149 (2.010 Å). Other hydrogen bond network, carboxylic function on 3 position of quinoline ring with Val49 (1.963 Å) and Gln52 (2.194 Å) were found. In addition, hydrogen bond interaction of nitrogen atom on piperazine ring with NH_2 group of Asn52 (2.482 Å) was obtained. Sigma-pi interactions between Ile84 side chain and quinoline was found. Based on this results, we can be concluded that our designed compounds based on MD simulations results should be more active than 4-aminoquinoline derivatives in this study.

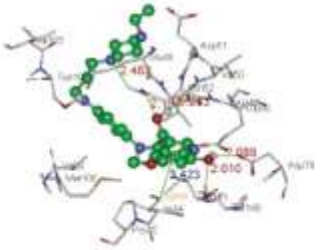

Fig. 3 Binding mode and binding interactions of new design compounds

4. Conclusions

MD simulations were successful to model the reliable binding modes inhibitor-enzyme interactions and binding free energies of aminoquinoline derivatives in the GyrB binding pocket. Hydrogen bond and hydrophilic interactions play important role in binding affinities of aminoquinoline derivatives. Rational design compounds of 4-aminoquinoline derivatives can be found that new designed compounds should be active against GyrB. Accordingly, the structural and dynamical concepts are fruitful to design new and more potent GyrB inhibitors against *M. tuberculosis*.

5. Acknowledgements

This research has been supported by the Thailand Research Fund (RSA5980057 and MRG5980152), the National Research Council of Thailand, Center of Excellence for Innovation in Chemistry: PERCH-CIC and Higher Education Research Promotion. Faculty of Science, Ubon Ratchathani University, Kasetsart University and NECTEC are gratefully acknowledged for supporting this.

References

[1] World Health Organization, Global tuberculosis report 2015, http://www.who.int/tb/publications/global_report/gtbr15_main_text.pdf

[2] M. A.Aziz, A.Wright, L. A.aszlo, A.De Muynck, F.Portaels, A.Van Deun, C.Wells, P.Nunn,L.Blanc, M. Raviglione, "Epidemiology of antituberculosis drug resistance (the Global Project on Anti-tuberculosis Drug Resistance Surveillance): an updated analysis", *j.Lancet*.,368, 2142–2154, 2006.

[3] M. C.Raviglione, I. M.Smith, N Engl. "XDR Tuberculosis-Implications for Global Public Health", *J. Med*., 356, 656–659, 2007.

[4] MaxwellA.1997. DNA gyrase as a drug target. Trends Microbiol.5:102-109. http://dx.doi.org/10.1016/S0966-842X(96)10085-8.

[5] R.J. Lewis, O.M. Singh, C.V. Smith, T. Skarzynski, A. Maxwell, A.J. Wonacott, D.B. Wigley, "The nature of inhibition of DNA gyrase by the coumarins and the cyclothialidines revealed by X-ray crystallography", *J.EMBO*., 15, 1412-1420, 1996.

[6] P. Kaur, S. Agarwal, S. Datta, *"Delineating Bacteriostatic and Bactericidal Targets in Mycobacteria Using IPTG Inducible Antisense Expression", PLoS One 4*, 5923, 2009.

[7] B.Medapi, P.Suryadevara, J.Renuka, J. P.Sridevi, P.Yogeeswari, D.Sriram, "4-Aminoquinoline derivatives as novelMycobacterium tuberculosis GyrB inhibitors: Structural optimization, synthesis and biological evaluation", *J.Med.Chem*., 103,1-16, 2015.

[8] N. Homeyer, H. Gohlke, "Free Energy Calculations by the Molecular Mechanics Poisson−Boltzmann Surface Area Method", *Mol. Inf*., 31,114–122, 2012.

[9] J. Wang, T. Hou, X. Xu, "Recent advances in free energy calculations with a combination of molecular mechanics and continuum models", Curr Comput Aided Drug Des, 2, 95-103, 2006.

[10] J. Wang, P. Morin, W. Wang, P.A. Kollman, "Use of MM-PBSA in reproducing the binding free energies to HIV1 RT of TIBO derivatives and predicting the binding mode to HIV1 RT of Efavirenz by docking and MM-PBSA", *J. Am Chem Soc*., 123, 5221-5230, 2001.

[11] T. Hou, J. Wang, Y. Li, W. Wang, "Assessing the performance of the MM/PBSA and MM/GBSA Methods. 1. The accuracy of binding free energy calculations based on molecular dynamics simulations", *J. Chem Inf Model*, 51, 69–82, 2011.

[12] M. Kaledin, A. Brown, A.L. Kaledin, J.M. Bowman, "Normal mode analysis using the driven molecular dynamics method. II. An application to biological macromolecules", *J. Chem Phys*, 121, 5646-5653, 2004.

Journal of Science and Technology Ubon Ratchathani University : Special Issue November 2017

Structure based drug design of 4-aminoquinilone derivatives in DNA Gyrase B subunit for anti-tuberculosis agents using molecular dynamics simulations

Naruedon Phusi[1], Chayanin Hanwarinroj[1], Kampanart Chayajaras[1], Nitima Suttipanta[2], Pharit Kamsri[3], Auradee Punkvang[3], Khomson Suttisintong[4], Patchareenart Saparpakorn[5], Supa Hannongbua[6], Prasat Kittakoop[6], James Spencer[7], Adrian Mulholland[8] and Pornpan Pungpo*[1]

[1] Department of Chemistry, Faculty of Science, Ubon Ratchathani University,85 Sthollmark Rd., Warinchamrap, Ubonratchathani, 34190, Thailand

[2] Faculty of Pharmaceutical Science, Ubon Ratchathani University, 85 Sthollmark Rd., Warinchamrap, Ubonratchathani, 34190, Thailand

[3] Faculty of Science, Nakhon Phanom University, Nakhon Phanom, 48000, Thailand

[4] National Nanotechnology Center, 114 Thailand Science Park, Pathumthani, Thailand

[5] Department of Chemistry, Faculty of Science, Kasetsart University, Chatuchak, Bangkok, 10900, Thailand

[6] Chulabhorn Research Institute and Chulabhorn Graduate Institute, Vipavadee-Rangsit Highway, Bangkok, 10210, Thailand

[7] School of Cellular and Molecular Medicine, Biomedical Sciences Building, University of Bristol, Bristol, BS8 1TD, United Kingdom

[8] Centre for Computational Chemistry, School of Chemistry, University of Bristol, Bristol, BS8 1TS, United Kingdom

*E-mail: pornpan_ubu@yahoo.com

Abstract

Mycobacterial DNA gyrase B subunit, GyrB has been identified to be one of the potentially underexploited drug targets in the field of antitubercular drug discovery. 4-aminoquinoline derivatives were developed as potential GyrB inhibitors. In the present study, we applied molecular dynamics simulations to elucidate the binding mode and the key interactions of 4-aminoquinoline derivatives in the GyrB pocket. The obtained results indicated that the crucial interactions of the highest active compound were hydrogen bond interactions with Met93(A) and electrostatic interactions of carboxylic group with Arg185(B) sidechain in the GyrB pocket. This interaction absented in other compounds. Moreover, hydrophobic interactions are also important for binding affinities in GyrB binding site of 4-aminoquinoline derivatives. Therefore, the obtained results from this study provide informative structural concept for designing of novel 4-aminoquinoline derivatives with better potency of GyrB inhibitors against *Mycobacterial tuberculosis*.

Keywords : 4-Aminoquinoline derivatives, GyrB, anti-TB agents, molecular dynamics simulations

Introduction

Tuberculosis (TB) , caused by *Mycobacterium tuberculosis* (*M. tuberculosis*) , remains a major global health problem. In 2015, an estimated 9.6 million people developed TB and 1.8 million died from the disease[1]. The clinical efficacy of fluoroquinolone drugs demonstrated over the past 20-30 years has validated DNA gyrase as a target in the area of broad-spectrum antibacterials [2]. Gyrase A subunit, GyrA has been facing a major hurdle of their resistance developed by

M. tuberculosis which makes gyrase B subunit a drug able target for discovery of potent anti- tuberculosis agents. DNA gyrase B subunit, GyrB is involved in the process of ATP hydrolysis which in turn provides energy to gyrase A subunit for maintaining the DNA topological state[3]. So, GyrB has been genetically demonstrated to be a bactericidal drug target in *M. tuberculosis*, but there have not been any effective therapeutics developed against this target for TB [4]. Recently, 4-aminoquinoline derivatives have been developed as anti- tuberculosis agents with moderate biological activities against *M. tuberculosis* and XDR *M. tuberculosis* [5]. These compounds were tested against *Msm*GyrB with moderate activities based on ATPase assay and DNA supercoiling assay. To develop these derivatives as highly potent GyrB inhibitors, the key interactions for binding of 4- aminoquinoline derivatives in GyrB binding site are required. Therefore, molecular dynamics simulations approaches have been used to understand dynamic behaviour, the binding mode and key binding interactions of these derivatives. The obtained results derived from this work aid to rational design of new potential GyrB inhibitors as anti-tuberculosis agents.

Propose approach

Two inhibitors, the highest active compound **1** and the lowest active compound **2** (**Figure 1**) were selected to model the binding mode and key binding interactions in this work. The chemical structures and their experimental biological activities of 4- aminoquinoline derivatives were selected from the literature [5].

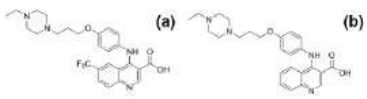

Figure 1 The structures of 4-aminoquinoline derivatives (a) compound **1** (IC_{50} 7.89 μM) and (b) compound **2** (IC_{50} 11.33 μM)

The biological activities of these compounds were expressed in terms of *Msm*GyrB assay (IC_{50} in μM) values. The chemical structures of these inhibitors were constructed using the standard tools available in GaussView 3.07 program and were then fully optimized using the M062X/ 6- 31G* * method implemented in Gaussian 09 program. The initial coordinates for molecular dynamics simulations of the complexes was obtained from molecular docking calculations using Autodock 4.02 program. GyrB structure for docking was downloaded from protein databank (PDB Code: 4B6C). Molecular dynamics simulations were performed to predict the inhibitors in the GyrB binding pocket. TIP3P water model and Na^+ were chosen to represent water for salvation and ions for neutralize system. To reduce the bad steric interactions of solvate water molecules and Na^+ ions of each system, the inhibitor- GyrB complex was first minimized by 1,000 steps with atomic positions of solute species restraint with using force constant of 500 kcal/mol $Å^2$. Non-bonded cut-off was set to 8 Å. The threshold value of the energy- gradient foe the convergence was set as 0.001 kcal/mol/ Å. Then, the whole system was minimized by 1,500 steps as the same conditions of water and ions minimization without restraining condition. Next, the systems were gradually warmed up from 0 to 300 K in the first 20 ps followed by maintaining the temperature at 300 K in the last 10 ps with 2 fs time simulation steps in a constant volume

boundary. The solute species were restrained to their initial coordinate structures with a weak force constant of 10 kcal/mol Å^2 during the temperature warming. This was followed by 70 ps of the position- restrained dynamics simulation with a restrain weight of 2 kcal/mol Å^2 at 300 K under an isobaric condition. Finally, 15 ns molecular dynamics simulations without any restraints were performed using the same conditions. The root-mean square deviations (RMSDs) of the GyrB enzyme and the inhibitors, binding interactions were analysed based on the equilibrium state obtained. The binding free energies were calculated to evaluate the binding affinities of inhibitors in GyrB binding pocket using the Molecular Mechanics Poisson- Boltzmann Surface Area (MM-PBSA) [6-9] and Normal-mode [10] methods. 10 snapshots were used to calculate the binding free energy in this work. The single snapshot that showed the calculated binding free energy closed to experimental binding free energy was selected to analyze the binding mode and binding interactions.

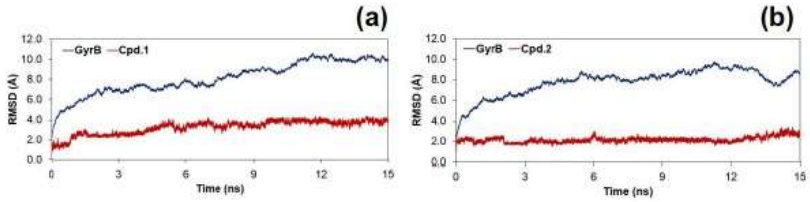

Figure 2. RMSD plots of (a) compounds **1** and (b) compound **2** complexed with GyrB

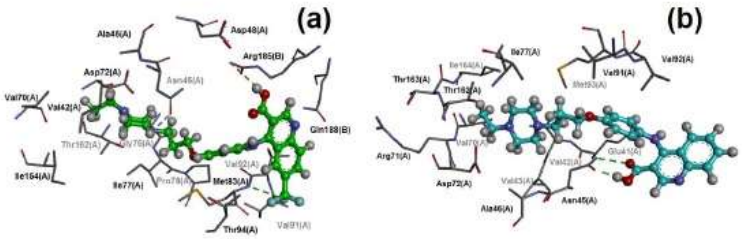

Figure 3. Binding mode of (a) compound **1** and (b) compound **2** in GyrB binding pocket derived from molecular dynamics simulations.

Table 1. The calculated binding free energies (kcal/mol) of 4-aminoquinoline inhibitors calculated by MM-PBSA method.

Cpd.	Energy contribution (kcal/mol)							
	ΔE_{MM}	ΔG_{polar}	ΔG_{non}	ΔG_{solv}	ΔH	$-T\Delta S$	$\Delta G_{cal.}$	$\Delta G_{exp.}$
1	-51.93	19.83	-48.61	23.15	-28.78	13.46	-15.30	-8.07
2	-48.51	19.87	-42.72	25.66	-22.85	13.30	-9.55	-7.01

RESULTS AND DISCUSSION

Structural stability during MD simulations and binding free energy calculations

In order to determine structural stability during molecular dynamics simulations of the highest active compound **1** and less active compound **2** in GyrB binding pocket, the RMSDs for all atoms of solute species relative to the initial structure over the 15 ns of simulation times were calculated and plotted in **Figure 2**. The plateau characteristic of the RMSD plot over the simulation time is the criteria to indicate the equilibrium state of each solute species. Convergent RMSD plots indicate that the equilibrium state of the highest active (Cpd. **1**) and the less active (Cpd. **2**) compound was reached after 12 ns. The obtained results from the last 3 ns were mainly analysed in more details of binding free energy and binding interactions.

Binding mode and binding interactions of compounds

The crucial interactions of compounds, the highest active compound **1**, with amino acids surrounding the binding pocket of GyrB enzyme was analysed as shown in **Figure 3** (a). The major interactions in the GyrB binding pocket is electrostatic interaction between carboxylic group (COOH) to nitrogen atom of Arg185(B) sidechain of DNA gyrase B subunit. Hydrogen bond interactions of trifluoromethyl with NH sidechain of Met93(A) was obtained. Moreover, hydrophobic interactions with Val42(A), Val70(A) and Val93(A) sidechain of DNA gyrase B were found as an additional contribution for binding in GyrB binding site. The binding mode of the less active compound **2** bound with GyrB pocket observed from the molecular dynamics simulations are shown in **Figure 3** (b). The major interaction in the GyrB binding pocket is the crucial hydrogen bond interaction of carboxylic group of compound **2** with amide sidechain of Asn45(A) of DNA gyrase B subunit. Moreover, hydrophobic interactions of this compound with Val42(A), Val70(A), Val92(A), Ile164(A) sidechains were observed. To gain quantitative insights into the affinity for binding of 4-aminoquinoline inhibitors in the GyrB binding site, the binding free energies of 4-aminoquinoline/ GyrB complexed were calculated by the MM-PBSA method as shown in **Table 1**. The obtained results showed that the calculated binding free energy of compound **1** and compound **2** are -15.32 kcal/mol and -9.55 kcal/mol, respectively. The obtained result indicated that binding free energy calculations based on MM-PBSA method produced good value and closed to experimental binding free energy of compound **1** and compound **2**, -8.07 kcal/mol and -7.01 kcal/mol respectively. It is notable that the calculated free binding energies of inhibitor are in the correct order as compared with the IC_{50} (experimented binding free energy) values. The obtained results could be successfully used to validate the molecular dynamics simulations procedure in this study. The obtained results in this work are reliable.

Conclusion

Molecular dynamics simulations were successfully applied to model the reliable binding modes, inhibitor-enzyme interactions and binding free energies of 4-aminoquinoline derivatives in the GyrB binding pocket. Hydrogen bond, electrostatic and hydrophilic interactions play the important role for binding of 4-aminoquinoline derivatives. Accordingly, the key structural for binding and dynamical concepts are fruitful to design new potential GyrB inhibitors against *M. tuberculosis*.

Acknowledgments

This research was supported by the Thailand Research Fund (RSA5980057 and MRG5980152), the National Research Council of Thailand, Higher Education Research Promotion and the Center of Excellence for Innovation in Chemistry (PERCH-CIC). Faculty of Science, Ubon Ratchathani University, University of Bristol and NECTEC are gratefully acknowledged.

References

[1] Organization, W. H. 2015. **Global Tuberculosis Report.** http://www.who.int/tb/publications/global_report/en/ (accessed 26 October).

[2] Maxwell, A., DNA Gyrase as a Drug Target. Portland Press Limited: 1999.

[3] Lewis, R. J. et al., 1996. "The Nature of Inhibition of DNA Gyrase by the Coumarins and the Cyclothialidines Revealed by X- Ray Crystallography". **The EMBO Journal.** 15: 1412-1420.

[4] Kaur, P. et al., 2009. "Delineating Bacteriostatic and Bactericidal Targets in Mycobacteria Using Iptg Inducible Antisense Expression". **PLoS ONE.** 4: e5923.

[5] Medapi, B. et al., 2015. "4-Aminoquinoline Derivatives as Novel *Mycobacterium Tuberculosis* Gyrb Inhibitors: Structural Optimization, Synthesis and Biological Evaluation". **European Journal of Medicinal Chemistry.** 103: 1-16.

[6] Homeyer, N.; Gohlke, H., 2012. "Free Energy Calculations by the Molecular Mechanics Poisson-Boltzmann Surface Area Method". **Molecular Informatics.** 31: 114-122.

[7] Hou, T. et al., 2011. "Assessing the Performance of the MM/PBSA and MM/GBSA Methods. 1. The Accuracy of Binding Free Energy Calculations Based on Molecular Dynamics Simulations". **Journal of Chemical Information and Modeling.** 51: 69-82.

[8] Wang, J. et al., 2006. "Recent Advances in Free Energy Calculations with a Combination of Molecular Mechanics and Continuum Models". **Current Computer-Aided Drug Design.** 2: 287-306.

[9] Wang, J. et al., 2001. "Use of Mm-Pbsa in Reproducing the Binding Free Energies to Hiv-1 Rt of Tibo Derivatives and Predicting the Binding Mode to HIV-1 RT of Efavirenz by Docking and MM-PBSA". **Journal of the American Chemical Society.** 123: 5221-5230.

[10] Kaledin, M. et al., 2004. "Normal Mode Analysis Using the Driven Molecular Dynamics Method. Ii. An Application to Biological Macromolecules". **The Journal of Chemical Physics.** 121: 5646-5653.

CURRICULUM VITAE

NAME	Mr. Naruedon Phusi
EDUCATION	2012-2015, Bachelor of Science (Chemistry), Department of Chemistry, Faculty of Science, Ubon Ratchathani University, Ubon Ratchathani, Thailand.
GRANT	Center of Excellencefor for Innovation in Chemistry (PERCH-CIC)
VISITTINGS	June 18-July 31, 2017. Centre for Computational Chemistry (CCC), School of Chemistry, University of Bristol, Bristol, United Kingdom (Prof. Dr. Adrian Mulholland) October 1, 2017-January 31, 2018. Quantum Biology Laboratory, Department of Computer Science and Engineering, Toyohashi University of Technology, Toyohashi, Japan (Assoc. Prof. Noriyuki Kurita)